POLITECNICO DI TORINO

Corso di Laurea Magistrale
in Ingegneria Aerospaziale

Tesi di Laurea Magistrale

Analysis and Optimization of Chill-down Processes in Cryogenic Liquid Propellant Rocket Engines

Relatore Accademico
Prof. Lorenzo Casalino
Relatore Aziendale
Ing. Riccardo Pellicanò
firma dei relatori

. . . . . .
. . . . . .

Candidato
Agnese Raia
288972

firma del candidato

. . . . . .

Anno Accademico 2022-2023

*Alla mia **famiglia**,*

*l'**amore** che mi ha dato*
__forza__ in ogni
circostanza,

*il **calore** che mi ha*
riscaldato quando ero
sola ad affrontare il
mondo fuori,

*la **luce** che mi ha guidato*
nei momenti più bui.

Summary

For Liquid Rocket Engines (LREs) which employs cryogenic fluids, chill-down process represents a fundamental phase before turbopumps operation. The propellant, before being sent to the combustion chamber, is employed to perform cooling function of both fuel and oxidizer fluidic transfer lines. In this manner, no pumps cavitation and correct ignition during engine operation are ensured.
This thesis, carried out at the Avio Company based in Colleferro, has the main objective of analysing and optimizing chill-down processes in cryogenic LREs, using EcosimPro software.
The thermal conditioning process of cryogenic propellant transfer lines is essential due to the high temperature difference existing between the cryogenic liquid in the storage tanks and the wall of ducts at the ambient temperature. The chill-down process requires an amount of propellant which will cool the solid walls of the pipes, bringing them to the same temperature of the liquid fluid and establishing a continuous cryogenic propellant flow in liquid phase. Important parameters of this process are chill-down time, defined as the time required to complete the desired cooling of the feeding lines, and propellant consumption, which must be minimized because unusable for propulsive purposes.
Following the exposition in chapter 1 of the general principles on cryogenic LREs, in ch. 2 the generalities on the chill-down process are described and the behaviour of the cryogenic fluid in the feed lines is explained. Moreover, the influence of the main parameters, such as the inlet driving pressure and the gravity acceleration, as well as the various possible methodologies suitable to successfully complete chill-down process, are detailed.
To pursue the main objective of this thesis, a preliminary analysis of several chill-down techniques, going deeper in each strategy advantages and drawbacks understanding, is performed, and subsequently analyzed with the EcosimPro software. For this reason, the goal of ch. 3 is to realize an initial sorting of different chill-down methods to evaluate a preliminary trade-off, as compromise between low propellant consumption and low cooling time.
In ch. 4, the focus is to reproduce, simulate and analyse various experimental test cases on chill-down process, available in literature, to validate EcosimPro models and to identify software weakness points in the simulation of this kind of phenomena. This activity leads to the conclusion that the software is not able to correctly simulate the chill-down, therefore appropriate margins shall be considered in the results employing standard components of ESPSS EcosimPro Library.

In ch. 5, let's get to the heart of the experimental work of this thesis, in which the objective pursued is the analysis and optimization of the open loop full flush flow chill-down technique for the cryogenic oxidant feed line, for application in the framework of VEGA-E program. The aim is to ensure, assigned the boundary conditions, the cooling of the lines within a certain target time, with the lowest propellant consumption.
Eventually, in ch. 6, the design of a closed-loop chill-down method follows for the recovery of the propellant used in the lines cooling, which otherwise would be expelled into the environment and therefore lost. It is an innovative design, currently not yet used in present main launchers, for reasons related to the costs, complexity, and feasibility of the process. However, this is a topic that will largely find its way into future developments. Indeed, launcher mass budget reduction leads to a further increase in the payload mass.

Contents

List of Tables

List of Figures

"Space is not a void, but a volume, and it is the volume of space that gives meaning to any motion we make."
[Steven Soter]

Chapter 1

Generalities on liquid propellant rocket engines

In the field of chemical space propulsion, liquid rocket engines (LREs) are considered to be the most dominant technology and are continuously studied to develop innovative solutions that can enhance their performance and capabilities, ensuring continuous progress in the current space scenario.
Despite being more complex in design and having a higher number of components compared to other types of chemical engines currently available, LREs offer numerous advantages that make them indispensable for certain applications and mission types. For instance, LREs offer higher specific impulses I_{sp} (possibility of higher thrust levels, with the same propellant consumption or lower propellant consumption, with the same thrust level), greater propulsive efficiency, and the ability to adjust the thrust level by regulating the propellant flow rate and pressure level in the combustion chamber. They can also be switched on/off multiple times during a mission and can reusable. In addition, LREs can be more environmentally friendly compared to solid rocket motors (SRMs). While the construction complexity of LREs may lead to higher costs, weight, and reduced system reliability, their advantages clearly outweigh these drawbacks.

1.1 General principles on LREs

Liquid Rocket Engines, also known as LREs, differ from Solid Rocket Motors (SRMs) and Hybrid Rocket Engines (HREs) primarily because they use propellants in liquid state of matter instead of solid or hybrid ones.This difference in propellant state leads to a more complex structure for the engine and entire propulsion system.
The structure of a LRE has been illustrated in the following figure.

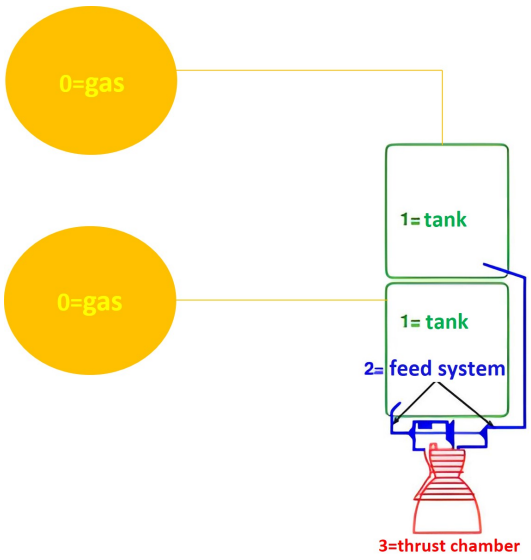

Figure 1.1. Structural scheme of a liquid propellant rocket engine.

As illustrated in Figure 1.1, the LRE has three main systems, each consisting of several subsystems:

1. main storage tanks for liquid propellants, such as oxidizer and fuel;
2. liquid propellant feed system, which in turn includes:
   - feeding mechanism (distinction between gas pressure feed systems and turbopump feed systems);
   - feeding lines (pipes);
   - valves.
3. thrust chamber, articulated in:
   - injectors;
   - combustion chamber;
   - nozzle;

- ignition system;
- refrigeration system.

Always in figure 1.1, upstream of the propellant tanks, it is also depicted the Zero system, denoted by 0, which is the Pressure Management system. It generally consists of gas tanks containing GHe/GN_2 used for the pressurization of the main propellant tanks. The number and arrangement of these tanks are chosen based on various factors such as optimization of dimensions, weight, and other relevant considerations. The function of the Zero system is to manage and maintain the pressure level required by the main tanks.

1.2 Introduction to cryogenic liquid propellants

Cryogenic fluids are a commonly used choice for liquid bi-propellant rocket engines when higher performance is necessary. This is due to their high energy content and resulting high specific impulse (I_{sp}).

Liquid propellants can be classified into two main categories: bi-propellants and mono-propellants.
Two-propellants are further classified as cryogenic or storable, depending on whether they are in a liquid state at extremely low temperatures or ambient temperatures, respectively. Two-propellant systems store the oxidizer and fuel separately, in distinct storage tanks, to prevent them from reacting upstream of the thrust chamber, and they are combined later in the combustion chamber. Furthermore bi-propellants that ignite and undergo combustion spontaneously when they come into contact, leading to a rapid and self-sustaining combustion process, without requiring an ignition system, are known as hypergolic propellants.
Mono-propellants, on the other hand, consist of a single substance that decomposes exothermically with the help of a catalyst, producing gas at a high temperature. They require simpler feed systems than bi-propellants but can provide less high performance.
Cryogenic liquids have the advantage of being more energetic and environmentally friendly than storable propellants, resulting in a higher specific impulse I_{sp}. However, a significant disadvantage of cryogenic liquids is that they remain in a liquid state only at extremely low temperatures, which limits their storage times and requires special handling and storage techniques.
The Vega E launcher, currently under development at AVIO SPA, will feature a new engine for its third stage, called the $M10$. This engine will use cryogenic liquid propellants, specifically liquid oxygen LO_X and liquid methane LCH_4. Oxygen exists in a liquid state at extremely low temperatures, around 90K, while methane is in a liquid state at slightly higher temperatures, around 110K. The use of these cryogenic propellants will provide high performance and reduced environmental impact compared to traditional propellants.

1.3 Functioning phases of a *LRE*

The functioning scheme of a liquid propellant rocket engine can typically be divided into several phases, as follows:

1. The first phase, called *feeding*, concerns the transfer, through suitable ducts and fluidic feed lines, of the liquid propellant, from the tanks in which it is stowed to the injectors upstream of the combustion chamber. Afterwards it is injected into the chamber, according to an appropriate mixture ratio and specific conditions, by means of the injectors.

2. The second phase, called *ignition*, is the engine firing phase, it consists in the ignition of the mixture present in the combustion chamber by means of the igniters.

3. The third phase follows, the actual *combustion*, in which we can distinguish two stages:

   - *steady state*, in which the stationary conditions of the propulsion system are reached;
   - *shut down*, final phase in which the engine is switched off.

During the feeding phase, the liquid propellants are usually pressurized by a pressurization system, which may consist of pressurization tanks, helium gas, or turbopumps. The pressurization system allows the propellants to flow from the tanks to the combustion chamber against the pressure drop that occurs along the flow path.

In the ignition phase, a spark or other energy source is used to ignite the propellant mixture in the combustion chamber. The igniter typically consists of a spark plug or a pyrotechnic device that produces a hot flame.

During the steady-state combustion phase, the propellant mixture burns continuously, generating a high-temperature, high-pressure exhaust gas that produces thrust. The combustion process is carefully controlled to maintain a stable, efficient burn, while also preventing excessive heat buildup that could damage the engine.

In the shutdown phase, the fuel and oxidizer flow is terminated, and the combustion process gradually comes to a stop. The engine is typically shut down by closing valves that regulate the flow of propellants into the combustion chamber. The shutdown phase is critical to prevent damage to the engine and to ensure that it can be restarted if needed.

1.3.1 Cryogenic propellants vs storable propellants: need to chill-down

The operating pattern of a liquid propellant rocket engine depends on whether it uses cryogenic or storable propellants. When using storable propellants at ambient temperature, the engine follows the feeding-ignition-combustion process described earlier. However, when using cryogenic fluids, an additional stage known as the "chill-down" is necessary before the feeding phase to the thrust chamber.
The chill-down stage involves cooling the transfer lines of the propellants to overcome

the high thermal difference of over 150 degrees between the components and the pipes downstream of the tanks which are in thermal equilibrium with the external environment, and the cryogenic fluids. This is crucial for ensuring that the cryogenic fluid remains in liquid phase in the combustion chamber, feed system, and bearing compartment, where it serves as a lubricant and coolant for bearings. Failure to achieve this could result in cavitation of the pumps and other complications, such as a poorly functioning engine.
The cooling process brings the components to a temperature close to that of the cryogenic liquid in the storage tank.

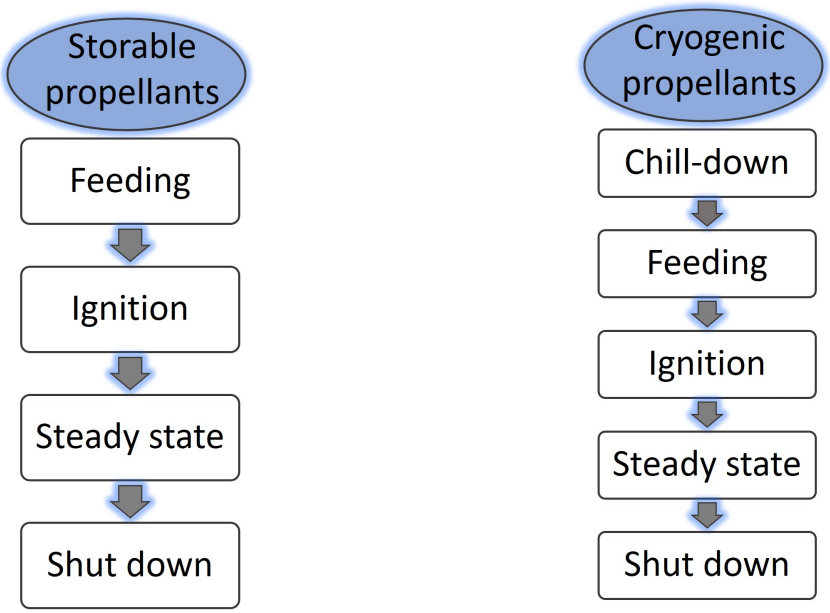

Figure 1.2. Functioning of a LRE for storable propellants vs cryogenic propellants.

Chapter 2

Chill-down: Generalities on the process

The thermal conditioning process of the cryogenic propellant transfer lines, also known as *chill-down*, is crucial in cooling the feed lines that connect the main propellant storage tanks to the thrust chamber and the thruster feed system. The process is necessary to overcome the significant temperature difference between the cryogenic liquid and the ducts at ambient temperature. To achieve a continuous cryogenic propellant flow between the various system components, an adequate amount of propellant must be estimated to cool the walls of the pipes, bringing them to the same temperature as the liquid fluid. The *chill-down time* is the duration required to establish a stationary monophasic liquid flow at the temperature of the cryogenic liquid in the tank and stable pressure levels in all the lines that carry the cryogenic propellant. Failure to achieve this can result in a disruption of the engine operation and potential damage to the components.

2.1 Behavior of cryogenic fluid in propellant transfer fluidic lines

The process of *chill-down* involves cooling the propulsion system components and transfer pipes to the temperature of the cryogenic liquid, in order to establish a stationary monophasic flow of the liquid propellant. This cooling process is a transient thermal transfer problem that involves rapid heat exchanges from a solid structure at a higher temperature T_{amb} to a liquid flux at the tank temperature $T_{fl_{tank}}$, which can result in monophasic and biphasic flows and phase changes. Due to the high thermal difference between the cryogenic fluid and the solid walls, the physical phenomena that occur during the process are complex and difficult to determine, such as heat transfers with changes of state, pressure and velocity instabilities of the fluid.

Studies on chill-down have been conducted since the 1960s, but the subject is still complex and ongoing research is focused on simulations and experimentation in order to optimize its characteristics.

During the cooling of the tubes, the wall temperature T_{wall} decreases over time, although not necessarily monotonically, passing through a series of regimes between the initial flow condition 0 and the final steady state.

The chill-down process begins when the inlet fluid is in subcooled conditions, meaning it is in a liquid state at a temperature lower than its saturation temperature at the given pressure. This means that there is some margin for the fluid to absorb heat and increase in temperature before reaching the saturation point and boiling. This reduces the chill-down time since the vapor phase of the fluid is reduced, increasing the liquid phase which is more efficient at convection.

In contrast, if the fluid is at its saturation point, then any decrease in pressure will cause it to boil, which means that the fluid will start to vaporize as soon as it enters the system, even before the cooling process starts. This can result in a less efficient cooling process and a longer chill-down time.

Therefore, subcooling of the inlet fluid is preferred for a more efficient chill-down process.

At the moment the fluid in the liquid state is injected into the ducts, due to the high $\Delta T = T_{wall} - T_{fl,0}$ between the fluid and wall, the fluid vaporizes almost instantly, creating a monophasic flow of pure steam. In this phase, the thermal exchanges between the fluid and solid are of the convective type, with heat exchanges occurring by forced convection, where the wall transfers heat to the fluid in the liquid state, which vaporizes due to the high ΔT.
Continuing to inject the propellant flow rate $\dot{m}_{propellant}$, not all the liquid introduced vaporizes, and a *dispersed flow* condition occurs, where the first liquid drops appear dispersed in a film of continuous steam. As time progresses, the volume fraction of the liquid increases, and the flow regime changes to become annular, known as *annular flow*, where a core of central liquid, the *liquid core*, denser, is surrounded by a layer of external vapor, the *outer vapor ring*, lighter, which is placed in contact with the walls of the pipes. This biphasic flow condition is called *film boiling*, where the thermal exchanges are established by convection, both natural and forced.
As the wall temperature T_{wall} decreases further ($T_{wall} - T_{fluid} \leq 30°C$), the liquid fraction increases, and the annular pattern is replaced by a biphasic non-homogeneous flow, with a continuous liquid phase and then a vapor phase dispersed in the form of bubbles. This fluid regime is called *nucleated boiling*, which is more efficient from the point of view of the convective heat transfers, which are increased since a continuous fluid in liquid state is in contact with the walls, creating greater friction with them. Since $h_{liquid} > h_{vapor}$ (because $h \propto \dot{m}$ and $\dot{m} \propto \rho$), there is a sudden increase in the *Heat Transfer Coefficient*. This phase is characterized by a more rapid and marked collapse of the $T_{wall} = f(t)$ curve. Downstream of the *nucleated boiling*, only a monophasic flux of liquid passes through the ducts, and the walls of the transfer lines have now reached the cryogenic liquid temperature $T_{fl_{tank}}$ required in the turbopumps, indicating that the chill-down process is complete.

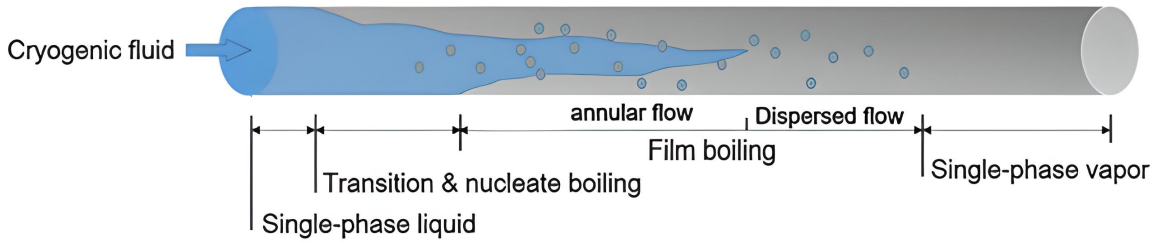

Figure 2.1. Typical thermal transfer and visualization of the flow regimes, long the pipe, during chill-down process of the cryogenic transfer lines. Jin et al., 2019, pag. 32.

2.1.1 Heat exchanges between the fluid and the solid walls of the pipes: T_{wall} as a function of time

Below, in figure 2.2 is proposed a qualitative graph of the typical T_{wall} and T_{fluid} trend during chill-down, with distinction between the various phases and the flow regimes characterizing the process, under *full flush flow* conditions. The two curves shown in fig. 2.2 are referred to the temperatures measured by the thermocouple located at the outlet of the pipe used for the chill-down test.

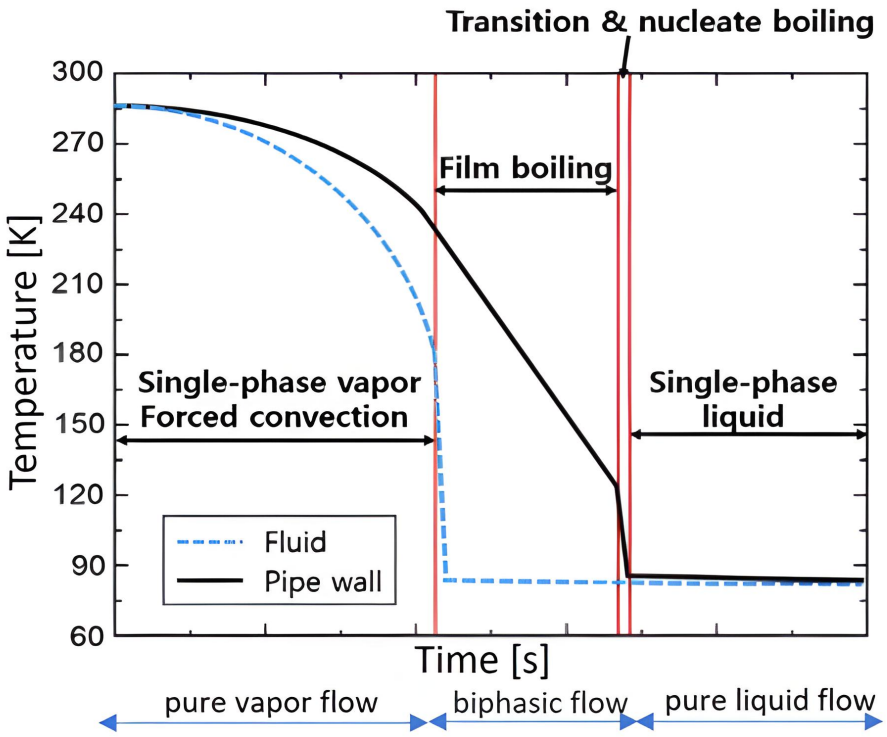

Figure 2.2. Typical phases of heat exchange between fluid and pipe wall during chill–down process. Jin et al., 2016, pag. 32.

When the propellant is injected into the pipe, due to the high temperature difference between the ambient temperature tube wall and the very low cryogenic temperature fluid, it tends to vaporize almost instantaneously. This vapor-only phase represents the first flow regime characterizing the process, which is visible in the $T_{wall} = f(t)$ curve in Figure 2.2. This phase is characterized by a weak decrease in wall temperature due to convective exchanges. Subsequently, as time progresses, the vapor-only phase is followed by the film boiling regime, which is characterized by a two-phase flow in which a thin layer of vapor is in contact with the walls, overlaid by the liquid phase. This vapor layer forms when the surface temperature is much higher than the boiling point of the liquid, and the liquid rapidly evaporates upon contact with the surface, forming a gaseous film. This vapor layer acts as a thermal insulator between the surface and the liquid, preventing the liquid from coming into direct contact with the surface and significantly slowing down the tube's cooling by convection ($h_{vapor} < h_{liquid}$). This physical phenomenon is known as the Leidenfrost effect. As the chill-down progresses and the wall temperature (T_{wall}) decreases over time, the film boiling regime is followed by the nucleate boiling regime, in which the liquid is in contact with the tube walls and therefore more efficient for convection. This results in a more marked drop in wall temperature. Downstream of this regime, the fluid inside the tubes and the tubes themselves have almost reached the cryogenic tank temperature, and the cooling process can be considered complete.

2.1.2 *Heat Transfer Coefficient* as a function of time

During the chill-down process, the primary mechanism of heat exchange between a fluid and a solid wall at different temperatures is convection, which can be categorized as either forced convection induced by external factors such as a pressure differential between the upstream tanks and downstream environment, or natural convection resulting from convective motion that arises spontaneously due to differences in density between the liquid and gaseous phases of the fluid.

The convective heat transfer coefficient, denoted as h, is a measure of the rate of heat flow exchanged between the fluid and the wall of the heat exchanger. It is defined as the ratio of the convective heat flow Q_{conv} to the product of the area of the heat exchange surface A and the temperature difference between the wall and the fluid $\Delta T = T_{wall} - T_{fluid}$, as shown in Equation 2.1.

$$h = \frac{Q_{conv}}{A \cdot \Delta T} \tag{2.1}$$

During the chill-down process, the heat transfer coefficient undergoes a characteristic trend as shown in Figure 2.3.

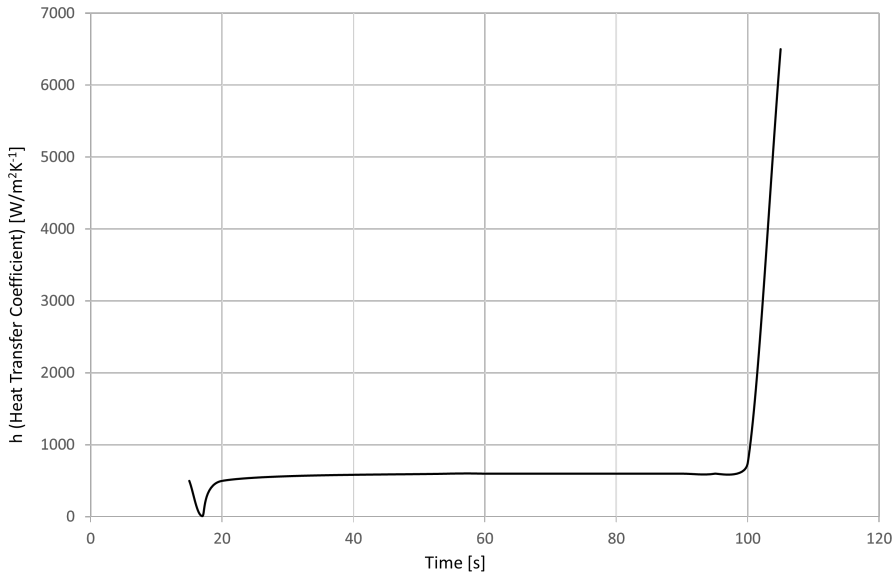

Figure 2.3. Qualitative trend of the *Heat Transfer Coefficient* over time, during chill-down process.

The convective heat transfer coefficient, h, which is proportional to the heat flow, Q_{conv}, exchanged between the fluid and the wall, can be observed to collapse in the initial phase of the cooling process. This is due to the fact that when the propellant flux, $\dot{m}_{propellant}$, is introduced into the tubes, the liquid vaporizes almost instantly, leading to a phase of vapor-only inside the pipes. As gases are less efficient at convection than liquids, the numerator in Equation 2.1, which characterizes h, decreases because the flow exchanged between the wall and the gaseous fluid is reduced, while the ΔT in the denominator increases with the greater thermal difference between the tubes at ambient temperature and the cryogenic liquid. This results in a valley in the trend of h, which reaches roughly zero.

Subsequently, the graph shows a constant trend where there is a balance between the convective heat exchanges and the temperature difference. This phase represents the biphasic flow region of Figure 2.2 where the film boiling stage occurs. Downstream of the film boiling comes the nucleate boiling phase, where the convective heat exchanges between the fluid and the wall are maximized. As a result, similar to Figure 2.2, it is possible to observe a rapid decrease in T_{wall}, leading to a sudden and almost vertical increase in the heat transfer coefficient, h, which indicates the end of the chill-down process. It should be noted that $h_{liquid} > h_{vapor}$, and therefore, during the nucleate boiling, h undergoes a rapid growth as the fraction of the liquid phase of the flow increases and comes into contact with the solid surface, intensifying the heat exchanges by convection.

Overall, the behavior of the heat transfer coefficient during the chill-down process can be explained by the changing phases of the fluid and the resulting changes in the efficiency of heat transfer by convective mechanisms.

2.2 Main characteristic parameters of chill-down process: *propellant consumption* and *chill-down time*

The chill-down process is a critical phase in the operation of a liquid rocket engine, as it significantly affects the correct operation of turbopumps, the proper combustion ignition process, and the performance of the engine during the mission.
The propellant consumption $m_{consumption}$ and chill-down time $\Delta t_{cooling}$ are two important parameters that characterize the cool-down process, and they need to be optimized in order to maximize the functioning of the overall propulsion system, which in turn improves the performance of the engine.

However, these two parameters have an antithetical behavior, which means that increasing one may negatively affect the other. For instance, increasing the mass flow rate injected into the transfer lines results in a shorter chill-down time as the cryogenic flow condition is achieved faster due to increased thermal exchanges by convection between the fluid and the wall. However, this also results in higher propellant consumption, which means that less propellant will be available for combustion in the thrust chamber for propulsive purposes, thereby reducing the efficiency of the propulsion system.
Conversely, reducing the mass flow rate injected into the feeding lines reduces the propellant consumption but increases the chill-down time as the thermal exchanges by convection decrease and those by evaporation increase. Therefore, the optimization process of the cool-down is a reasoned trade-off, which takes into account the application of the liquid rocket engine and the mission analysis.

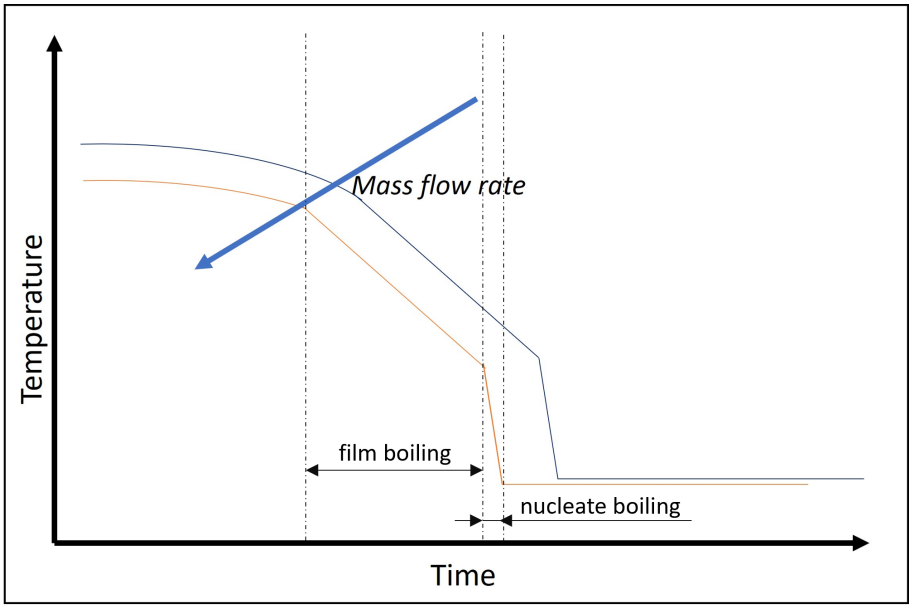

Figure 2.4. Qualitative visualization of the mass flow rate influence on the chill-down time.

Experimental studies have shown that the graph of $T_{wall} = f(t)$ reaches the nucleate boiling regime and cryogenic flow condition faster as the mass flow rate $\dot{m}$ injected into the chamber increases. This is due to increased thermal exchanges by convection between the fluid and the wall ($\dot{m} \propto h \propto Q_{conv}$), resulting in a higher efficiency of the process and a shorter chill-down time (Fig. 2.4).

The optimization of the chill-down process can have a significant impact on the safety and reliability of a liquid rocket engine. A well-designed chill-down process can help prevent thermal stresses and mechanical damage that can occur due to thermal gradients during engine operation. This, in turn, can reduce the likelihood of engine failure or malfunction during flight.

Moreover, optimizing the chill-down process can also improve the performance and efficiency of the engine, to be intended as the correct functioning of the engine components upstream of ignition, before the onset of thrust, which can have a positive impact on the mission outcome. This is because a faster and more efficient chill-down process can result in a more consistent and stable flow of propellant, which can help ensure proper operation of the propulsion system, reliable functioning of various engine parts, and successful engine ignition.

Overall, the optimization of the chill-down process is an important aspect of liquid rocket engine design and development, and can have a significant impact on the safety, reliability, and performance of the propulsion system.

2.2.1 Influence of the *inlet driving pressure* and *gravitational acceleration* g on cooling process

Experimental tests have shown that different gravity and pressure conditions at the inlet of the flow can affect the chill-down process. Increasing the inlet driving pressure, for instance, reduces the cooling time of the lines. This is due to the fact that the mass flow rate $\dot{m}$ is proportional to the flow velocity ($\dot{m} = \rho \cdot u \cdot A$) , which is in turn proportional to the pressure difference Δp between the inlet condition p_{inlet} and the ambient condition p_{amb} ($u \propto \sqrt{\Delta p}$, according to Equation 2.2). Therefore, as p_{inlet} increases, the $\dot{m}$ introduced also increases, resulting in a decrease in chill-down time (see Figure 2.5). However, if a gas pressure feed system is used, increasing the inlet driving pressure of the fluid means increasing the upstream pressure, i.e., the pressure of the tanks containing the propellant, which can increase their weight due to the need to withstand higher pressure levels and have greater thicknesses. But it is worth noting that when cryogenic liquids are used as propellants, the liquid propellant feed system used is typically a turbopump feeding system, as the goal of the LRE is to achieve high performance.

$$p_{tot} = p_{static} + \frac{1}{2} \cdot \rho \cdot u^2 \Rightarrow \Delta p = \frac{1}{2} \cdot \rho \cdot u^2 \Rightarrow u = \sqrt{\frac{2 \cdot \Delta p}{\rho}} \tag{2.2}$$

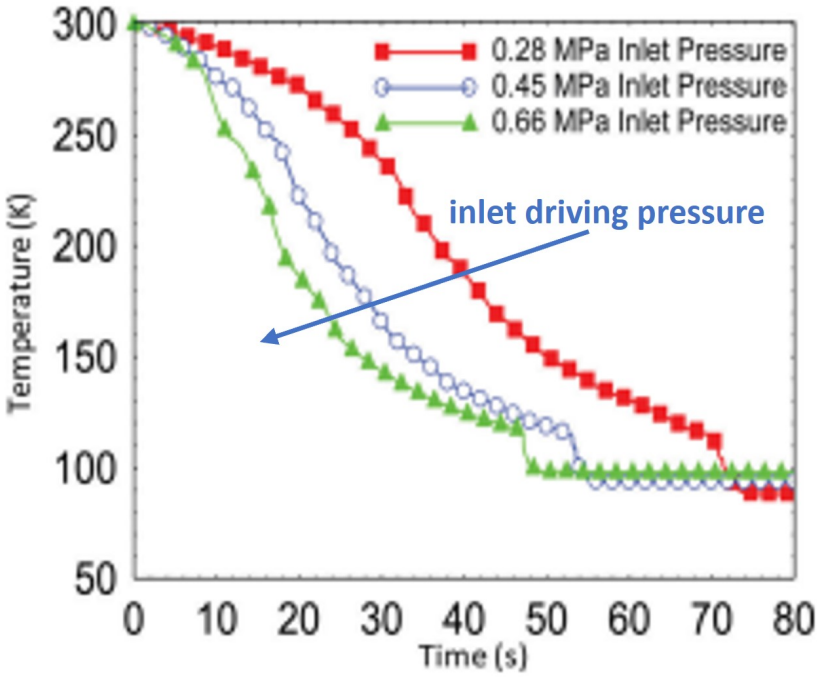

Figure 2.5. $T_{wall} = f(t)$ curve depending on the *inlet driving pressure* during chill-down. Agrawal et al., 2014, pag. 8.

In terms of gravity, experiments have shown that under conditions of microgravity $(0-g)$, compared to normal gravity $(1-g)$, the characteristic curve of chill-down shifts towards higher values of chill-down time (Figure 2.6). This is because film boiling and nucleate boiling regions increase in duration in microgravity conditions, as the heat transfer rate decreases with decreasing gravitational acceleration g (empirical models have been developed showing the influence of gravitational acceleration g on h).
Conversely, in normal gravity, the relationship between h and g causes an increase in the efficiency of convective heat exchange process and a decrease in cooling time. This is because an increase in g leads to an increase in convective motions, resulting in an increase in the heat exchange coefficient h and a reduction in the region of film boiling ($\uparrow g \Rightarrow \uparrow h$). Therefore, gravity has a beneficial effect on reducing chill-down time.

Additionally, for vertically positioned pipes under gravity conditions, g positively influences the pressure at the inlet of the flow, resulting in an increase in the inlet pressure level and a higher mass flow rate $\dot{m}$. This leads to an increase in convective heat transfer ($h \propto \dot{m}$) as mentioned before.

This can be described by the following equation:

$$p_{in} = p_{tot} = p_{static} + \frac{1}{2} \cdot \rho \cdot u^2 + \Delta p_{1-g} \tag{2.3}$$

where:

$$\Delta p_{1-g} = \rho \cdot g \cdot z \tag{2.4}$$

Therefore, in normal gravity, the gravitational force presses the fluid against the walls, intensifying its contact and resulting in greater pressure levels between the fluid and the walls of the duct. This leads to an increase in the propellant flow injected into the transfer line and consequently, an increase in the heat transfer coefficient.
For horizontally positioned pipes, gravity causes the liquid, which is denser, to be in contact with the walls while the vapor, which is lighter, is positioned above the liquid phase resulting in an *inverted annular flow* condition. This leads to an increase in convective heat exchanges and a reduction in the time required for cooling, as there is no gas phase film in contact with the wall and $h_{liquid} > h_{vapor}$. Moreover, in the initial phase of the cooling process when propellant is introduced into the line, the curves of the different conditions of g in Figure 2.6 are approximately coincident. This is because the greater friction between the wall and the fluid initially caused by the effect of gravity increases the temperature level, which works against the cooling process. However, as time progresses, the effects of attrition on convection in $1 - g$ gravity become preponderant, leading to a reduction in chill-down times.

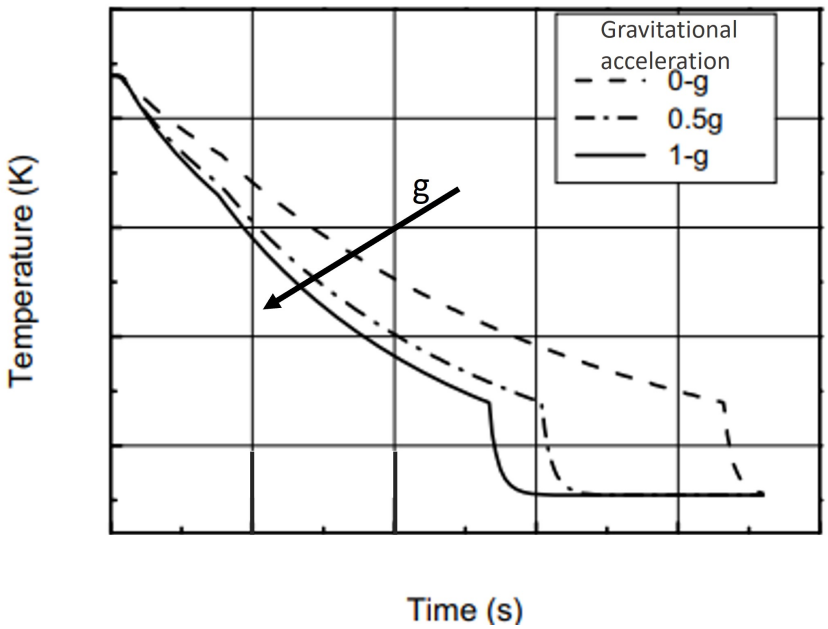

Figure 2.6. Influence of gravitational acceleration g on chill-down process. Yuan et al., 2008, pag. 52.

2.3 Chill-down techniques

The choice of methodology and system architecture for cryogenic chill-down process is not single, but rather the result of careful consideration of various constraints and requirements, particularly structural constraints of the launcher, mission target, and LRE application. This process is extremely complex, involving numerous boundary conditions that must be taken into account for the entire space mission.

Since the 1960s, several techniques have been developed to achieve cryogenic transfer line cooling, each with the aim of meeting mission requirements.

The main methodologies known to date are:

- *Full flush flow chill-down*
- *Trickle flow chill-down*
- *Pulsed flow chill-down*
- *CHV (Charge, Hold, and Vent) chill-down*
- *No bleed chill-down*
- *Two-phase thermosiphon method*
- *Recirculating pumps*

Figure 2.7 shows a simplified diagram of a typical chill-down architecture.

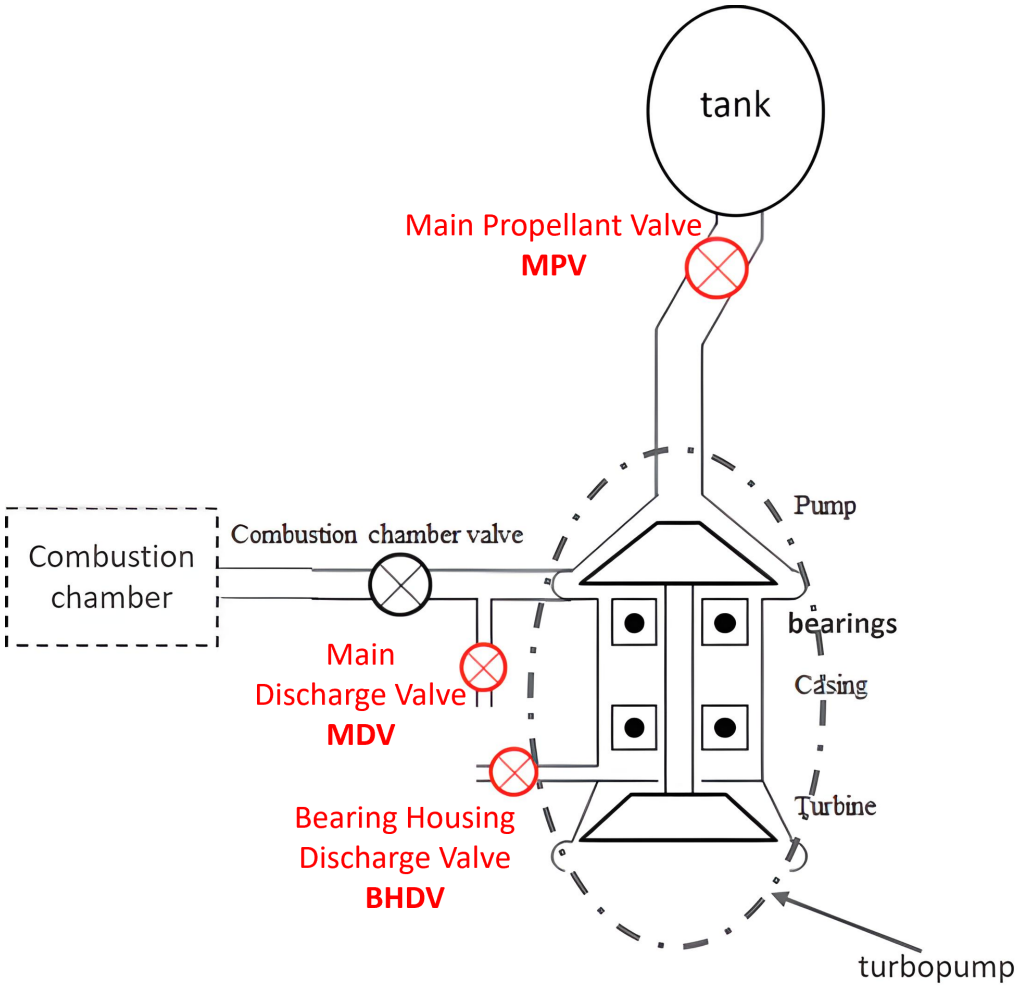

Figure 2.7. Classical chill-down architecture.

The process involves injecting propellant flow $\dot{m}_{prop}$ from the storage tank through the Main Propellant Valve (MPV) and transfer lines, passing through the turbopump assembly to cool the lines and continuously lubricate the bearings. It is important to note that the bearings must be continuously cooled and lubricated by the liquid propellant as they work in rotation, imparting torque to the fluid. If the liquid heats up and becomes vapor, it could lead to turbopump cavitation, which is to be avoided. Moreover, the lubrification is an important thing to avoid damages to bearings and increase their life and safety of operation. Moreover, lubrication is important to prevent damage to bearings and increase their lifespan, as well as ensure the safety of their operation.

The flux intended for chill-down and lubrication of the bearings compartment, which represents the "lost" propellant consumption, is continuously expelled through the Bearing Housing Discharge Valve (BHDV) downstream of the bearings. Furthermore, the mass flow rate employed for main feed line cooling is then ejected by the Main Discharge Valve (MDV) upstream of the combustion chamber (CC).

Regardless of the methodology used, the Combustion Chamber Valve (CCV) that connects the propellant to the injectors upstream of the combustion chamber is kept closed during cryogenic cooling of the lines. Once the chill-down process is completed, the MDV is closed while the BHDV is kept continuously open as the bearing housing must be constantly cooled and lubricated, to avoid damages and cavitation. Following this, the CCV is then opened to allow a steady cryogenic flow into the chamber for ignition and combustion. This means that the mass flow rate injected along the lines will no longer be considered a "propulsive loss", but rather a contribution to the system's propulsion.

2.3.1 Full flush flow chill-down

The full flush flow method is the first and most traditional technique used for chill-down. In this method, the entire propellant flow $\dot{m}_{prop}$ is taken from the tank and injected through the completely open MPV into the turbopump system circuit, and then expelled from the exhaust valves to cool the bearings and the main feed line. This method has the advantage of significantly reducing the chill-down time, which is necessary in mission phases where quick cooling is required. The full flow technique is typically used when the solid boosters of the first stage are ignited, and the LRE must quickly reach steady cryogenic flow conditions to avoid the expulsion of liquid propellants, which can cause a flame outside the engine and trigger an involuntary explosion. This technique is also required when there are strict constraints on the timing of engine ignition.

The reason for the reduced *chill-down time* is that, as the injected $\dot{m}$ increases, the liquid phase in the fluidic line grows, and the liquid fluid is more efficient at convection than gas alone, $h_{liquid} > h_{vapor}$, resulting in increased convective heat exchanges and faster cooling over time.

The full flow method has the advantage of reducing chill-down times, but its main drawback is the high propellant consumption. This is because the entire propellant flow

$\dot{m}_{prop}$ is used for the cooling process, which is not intended for the combustion chamber and is expelled from the exhaust valves. Therefore, this method requires a large quantity of propellant which will need to be minimized during the design phase.

2.3.2 Trickle flow chill-down

The trickle technique is typically used to thermally condition the upper stage transfer lines. In this method, a reduced mass flow rate $\dot{m}$ is continuously injected at the beginning of the process to maximize the residence time of the propellant in the feed lines, thus maximizing its capacity to absorb thermal energy from the walls through a phase change to vapor. By injecting a lower quantity of $\dot{m}$, the thermal exchanges through complete evaporation of the propellant are favored, which are added to the heat exchanges through natural and forced convection between the fluid and the wall. As a result, the propellant consumption is reduced, but the cooling times are longer, i.e. chill-down times are longer. Among the different ways in which the trickle technique can be performed, the trickle by-pass method uses an additional valve, parallel to the MPV, which regulates the mass flow rate $\dot{m}$. Initially, a lower flux of $\dot{m}$ is flowed through the valve for the reasons mentioned above, and then the regulating valve is closed, and the propellant flow is injected exclusively from the fully open MPV.

Both the full flow method and the trickle method involve the injection of a continuous mass flow rate.

2.3.3 Pulse flow chill-down

The pulsed method involves operating the main valve MPV in a pulsed manner. Specifically, one possible implementation of this technique involves cycling the MPV with the discharge valve DV, which is kept open, whereby the MPV provides pulsed $\dot{m}$ streams. Due to the ∇p between the tank and the external environment, the liquid fluid is forced into the lines at regular intervals.
By choosing an appropriate valve duty cycle, the propellant consumption fraction or the chill-down time can be optimized depending on the mission target. The advantage of pulsed operation is that injecting non-continuous $\dot{m}$ maximizes the heat exchanges by convection and/or evaporation with the wall. Depending on the valve cycle adopted, one of the process's characteristic parameters will be optimized, highlighting the critical role played by the mission phase in which cryogenic-LRE is employed.

2.3.4 CHV - Charge, Hold, and Vent chill-down

The CHV technique aims to minimize the propellant consumption, maximizing the heat transfer coefficient, by exploiting the latent heat of vaporization of the cryogenic propellant to completely vaporize small amounts of propellant $\dot{m}$ that are trapped within the fluidic feed lines. The method involves a sequence of phases, starting with the Charge phase, where small quantities of liquid propellant are injected into the feed lines by opening both the MPV and DV valves. This is followed by the Hold phase, where both valves are closed to lock the propellant inside the transfer lines until thermal equilibrium is reached (i.e.

the heat exchanges by convection and evaporation between fluid and wall are exhausted), or until the pressure level in the volume does not exceed a pre-established critical value (generally maximum pressure sustainable by tank). Finally, the Vent phase follows, in which the DV is opened to empty the cavities, and the cycle is repeated.
The CHV method is advantageous in terms of reduced propellant consumption, as the heat exchange power of the propellant is fully exploited, maximizing extraction of its cooling potential. However, it requires additional sensors for detecting/monitoring pressure and/or temperature levels and multiple opening/closing cycles of the valves, leading to synchronization problems and possible delays that can result in excessive pressurization not tolerated by the lines. Thus, this method is not suitable for "in-flight chill-down" and is only used for "ground chill-down" due to its complexity and the need for active control.

Both the pulsed functioning and CHV techniques involve the non-continuous injection of propellant, unlike the first two methods described that require a continuous mass flow rate.

2.3.5 No bleed chill-down

The no bleed technique operates without purge valves DV, and instead injects propellant and cools feed lines only through the main valve MPV, with exhaust gases being recirculated and reused downstream, for example, to pressurize the main propellant tank (figure 2.8). However, the gas pressure at the outlet of the line is lower than the propellant pressure in the tank, $p_{gas} < p_{tank}$, requiring an additional device, such as an electric pump, to repressurize the flow and separate the liquid from the gaseous phase of the fluid before returning it to the tanks. While the aim of utilizing otherwise "lost" propellant makes this technique appealing, the added complexity and drawbacks outweigh the advantages, rendering it an unused technology at present.

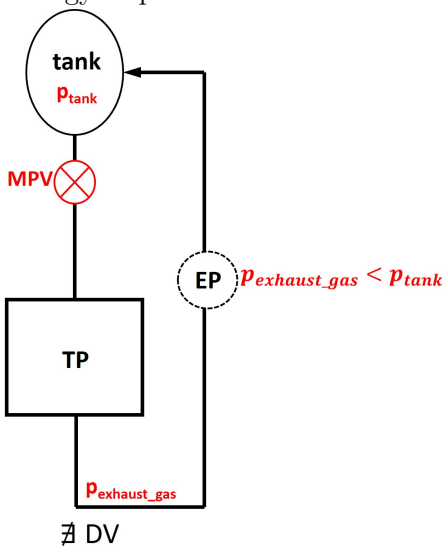

Figure 2.8. Simplified no bleed chill-down architecture.

2.3.6 Two-phase thermosiphon

The two-phase thermosiphon technique is an advancement of the previous no bleed method, which includes an additional non-isolated fluid circuit to provide a direct path for venting the vapor phase.
This technique involves a tank downstream of the transfer line, equipped with heaters to completely vaporize the exhaust flow and convert it into a pressurizing gas if necessary. To prevent back-flow of the fluid and increase the pressure in the tank, a non return valve must be installed upstream of the heaters.
However, due to its complex design and implementation, the benefits it offers are outweighed by the added complexity, and it is not currently used as a technology.

2.3.7 Recirculating pumps

The architecture of the latter chill-down process is characterized by the active use of electrically-driven pumps and valves dedicated to controlling the mass flow rate and the path of the propellant for optimal cooling. The pumps used are generally centrifugal, and can either be of the submerged type, where the motor coupled to the pump body is immersed in the fluid, or boxed, where the pump, motor, and liquid to be handled are integrated into a single block that is leak-free.
A typical chill-down operation using recirculating pumps involves two different electrically-actuated centrifugal pumps that allow for the recirculation of liquid propellants (such as LO_X and LH_2) from storage tanks to turbopumps via feed lines and back to the main tanks. This closed loop circuit aims to save propellant consumption, but it also increases the complexity of the system. During the initial cooling stage, the vapor phase of the propellant and the saturated liquid phase mix with the subcooled liquid, which can potentially increase thermal residues. It is also important to consider the destratification of the propellant levels.

2.3.8 Summary on chill-down techniques

To select the appropriate chill-down technique, the mission phase in which it will be employed must be considered. There are two types of chill-down: ground chill-down, which occurs on the ground, and in-flight chill-down, which occurs during flight, typically for an upper stage.
Performing ground chill-down is a crucial need when the first stage of a launcher is fueled with cryogenic liquid. However, this process requires the integration of additional valves and lines with an already complex and highly integrated engine system. Ground chill-down can also be considered when there is a need to save first boost propellant, although this increases the complexity of the process and reduce its feasibility.

Chapter 3

Preliminary trade-off of the different chill-down techniques

The purpose of this thesis, as indicated by its title, is to conduct an analysis and optimization of various chill-down techniques for a cryogenic liquid propellant rocket engine (Cryo-LRE), specifically the M10 engine of AVIO's upcoming Vega-E product.

In order to achieve this objective, it is essential to first select and narrow down the various chill-down methods before conducting a detailed analysis using the EcosimPro software. Chapter 3 focuses on this initial sorting process, as analyzing all methods would require excessive computational costs and time.
The approach taken in this phase involves conducting a preliminary trade-off by solving an optimization problem.

3.1 Background

To start, it is crucial to understand the context of this study. The focus is on the Cryo-LRE, specifically the $M10$ engine of VEGA-E, which is an upper stage engine that uses LO_X as oxidizer and LCH_4 as fuel. The engine operates with a turbopump feeding system using an *expander cycle* [1]. The engine operates in flight, in micro-gravity conditions ($\cong 0 - g$), and in a vacuum ($p_{atm} \cong 0$) [2].

It is important to mention that due to the micro-gravity conditions and the limited pressure difference between upstream and downstream of the line (p_{tank} is typically in the

[1] It is a closed cycle in which: IN-turbine: refrigerant fluid, that has become supercritical, coming from the refrigeration system of the thrust chamber; OUT-turbine: the exhaust gas goes into the combustion chamber and then expelled from the main nozzle.

[2] Starting from the second ignition of the engine, which has to do six ignitions; the first boost has not yet reached vacuum conditions.

low pressure range for turbopumps powered main tanks, $\cong 2-5$ bar; p_{atm} is approximately equal to 0 bar $\rightarrow$ consequently p_{inlet} is restrained), the convective heat exchange mechanisms are not favored, resulting in increased chill-down times.
The decision to use liquid methane instead of liquid hydrogen is due to cost-effectiveness and efficiency reasons. Liquid methane has greater absorbency characteristics than liquid hydrogen, allowing for heat to be removed from the walls of the thrust chamber and transfer lines more efficiently, ultimately leading to a reduction in chill-down times. Overall, this study will analyze and optimize different chill-down techniques for the Cryo-LRE in the context of the $M10$ engine of VEGA-E.

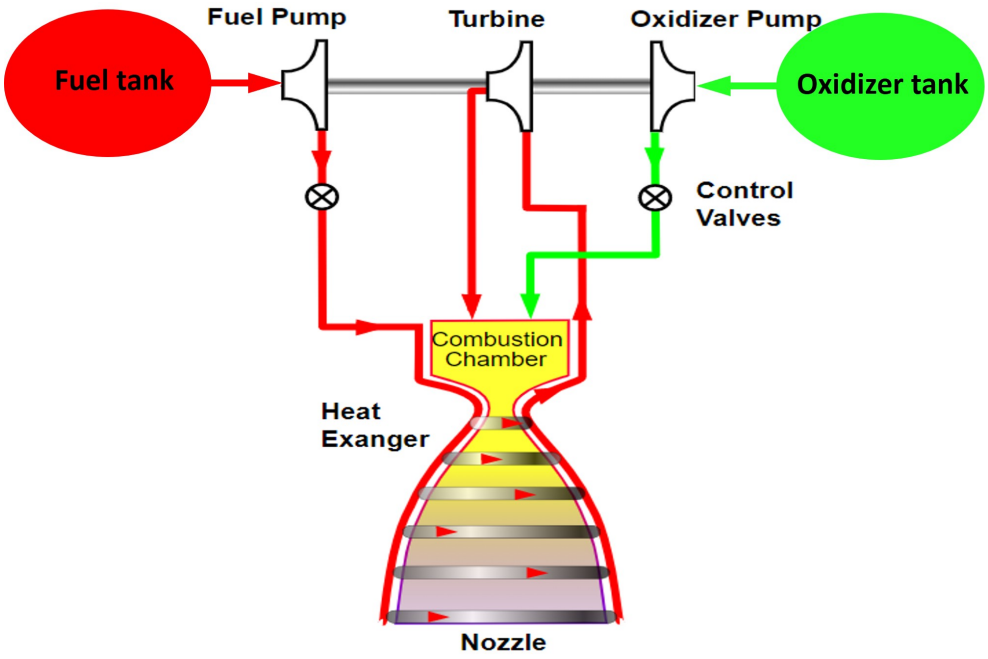

Figure 3.1. Schematic view of the turbopump feeding system - expander cycle.

3.2 Preliminary trade-off: optimization strategy

To perform a preliminary trade-off analysis of different chill-down techniques, the strategy adopted is to choose:

- Design Drivers $\Rightarrow$ guide parameters for the selection process [3], which are the principles, values, rules, variables and conditions that an organization or team uses to select an option or make a choice. They can help in creating a decision matrix.

[3]Such as propellant consumption, chill-down time, complexity, pressure drop etc...

- Compliance Criteria ⇒ decision parameters that are completely satisfied by the considered chill-down method (the value 1 is assigned).
- Not-compliance Criteria ⇒ decision parameters that are completely not satisfied by the considered chill-down method (the value 0 is assigned).
- Constraints ⇒ design parameters whose values are to be determined as the objective of the current design process, such as propellant consumption and chill-down time.
- Performance Parameters ⇒ parameters whose values depend on the constraints and provide indications of performance (ΔV - Thrust).

Since it must be kept in mind that:

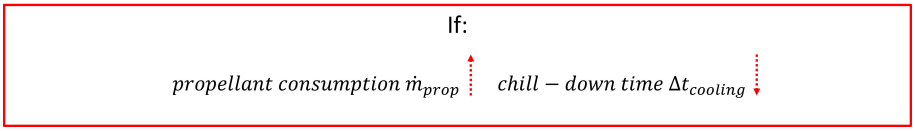

Figure 3.2. Need for trade-off.

A reasoned compromise is necessary → there is a need for trade off.
The best compromise is one that minimizes the drawbacks of the process, which always involves a waste (of both propellant and time, in this case).

The decision matrix will assist in making the best possible trade-off between the different chill-down techniques based on the chosen design drivers, compliance criteria, not-compliance criteria, constraints, and performance parameters.

3.2.1 Design Drivers

The guide parameters that were chosen for the preliminary trade-off of the chill-down techniques are:

1. *Propellant Consumption* $\dot{m}_{prop}$, which refers to the mass flow rate involved in the chill-down process;
2. *Chill-down time* $\Delta T_{cooling}$, which refers to the time required to achieve the thermal conditioning of the cryogenic transfer lines;
3. *Process feasibility*, which refers to the level of complexity involved in executing the process, also known as executive complexity;
4. *Constructive feasibility*, which refers to the level of complexity involved in the method architecture, also known as architecture simplicity/structural complexity;

5. *Pressure drop* [4], which refers to the pressure losses of the fluid in the pipes, due to viscous effects, boundary layer separation, contraction of the fluid vein, and so on;
6. *Complexity*, which is understood in the broad sense, and is strictly connected to 3 fundamental aspects:
    - 6.1 *Safety* of the engine and consequently the success of the mission;
    - 6.2 *Reliability* of the cooling process, so the good success of the chill-down process;
    - 6.3 *Costs* linked to the chill-down process, which are mainly due to the structural and executive complexity of the process, as well as to the propellant consumption $\dot{m}_{prop}$.
7. *Component stress*, which refers to the level of mechanical stress on the propulsive system components, mainly due to a non-continuous mass flow rate $\dot{m}$;
8. *Bearing housing lubrication*, which refers to the level of lubrication/refrigeration efficiency of the bearings. A good efficiency is achieved when a continuous and constant mass flow rate flows in the bearing compartment, which reduces the cooling time of the bearing housing;
9. *Upper stage thermal conditioning*, which refers to the capability of the technique to do chill-down in flight.

3.2.2 Optimization strategy adopted

In an initial phase of trade-off, during the preliminary selection of the chill-down methods, only two values/scores will be taken into account:

- A value of 1, with positive attribution, will be assigned if the design criterion is completely fulfilled;
- A value of 0, with negative attribution, will be assigned if the design criterion is not fulfilled at all;
- A value of 0.5 will be assigned if the design criterion is partially fulfilled or depends on specific conditions of the method.

Subsequently, the scores obtained for each technique will be summed up. The methods that will have a total score lower than or equal to 4 out of 11 will be discarded.

[4] The higher the pressure drop in the line, the greater the amount of energy consumed to maintain the desired process flow, requiring a higher power level. The pressure drop is mainly influenced by the complexity of the system geometry, the length of the pipes, the number of curves in the system and the number of components (the pressure drop increases with the increasing of the number of component in series, if in parallel it decreases, with decreasing of mass flow rate), such as valves, flow meters, adapters, couplings...

The decision matrix presented in Table 3.1 was used to assign scores and select the chill-down methods.

Methods ⇒ **Design Driver ⇓**	Full flush flow	Trickle by-pass	Pulse flow	CHV	No bleed	Two-phase thermosiphon	Recirculating pumps	Ground
Propellant consumption	0	0.5	0.5	0.5	1	1	1	0
Chill-down time	1	0	0	0	0.5	0.5	0.5	1
Process feasibility	1	1	0.5	0	0	0	0	0
Constructive feasibility	1	0.5	1	0	0	0	0	0
Pressure drop	1	1	1	0	0	0	0	0
Safety	1	1	0.5	0	0	0	0	1
Reliability	1	0.5	0.5	0	0	0	0	0.5
Costs	0	1	1	0	0	0	0	0
Component stress	1	1	0	0	0	0	0	0.5
Bearing compartment lubrication	1	0.5	0	0	1	0.5	1	1
In flight chill-down	1	1	0.5	0	0.5	0.5	0.5	0

Table 3.1. Decision Matrix

Score Table	
Method	**Total Score**
Full flush flow	9
Trickle by-pass	8
Pulse flow	5.5
CHV	0.5
No bleed	3
Two-phase thermosiphon	2.5
Recirculating pumps	3
Ground chill-down	4

Table 3.2. Score summary table

As indicated by the scoring table 3.2, the only chill-down techniques that will be further analyzed using EcosimPro software are Full flush flow, Trickle by-pass, and Pulse flow. A separate discussion applies to the ground chill-down (yellow line in Table 3.2).

3.2.3 Ground chill-down

Ground chill-down is not a cooling technique itself, but rather a method used to implement one of the previously discussed techniques. It is typically used when the first stage of the launcher uses cryogenic liquid or when there are strict constraints on the time available during the ascent phase, or when in-flight propellant consumption needs to be minimized in order to reduce mass budget and increase payload.

As such, ground chill-down is not part of this trade-off analysis for different chill-down techniques discussed earlier, since it is not a competing method, but rather a complementary one that can be used in addition to others to minimize propellant loss during the cooling process of the transfer lines.

However, for informational purposes only, the assigned values are justified below, even though this method will not be considered in the optimization.
The performance of ground chill-down has been assessed based on the following criteria:

- The propellant consumption is high ($\dot{m}_{prop}$ from the main tanks or external tanks), but the chill-down time is relatively short and independent of the mission.
- The executive complexity is high, and the process procedure is complex.
- The structural complexity is high, and a large number of components are required.
- The fluid path and system geometry are complex, leading to a high pressure drop.

- The safety requirement, understood as the safety of the mission, is satisfied, and the reliability requirement is almost satisfied since the process procedure is independent of the mission, even if it is complex. However, the costs of the process are high due to the complexity and high propellant consumption.
- The level of stress suffered by the components depends on the process procedure.
- The efficiency of lubrication/refrigeration of the method is good, as there is a continuous mass flow rate after the end of chill-down, when the pumps are running.
- This technique cannot be used for in-flight cooling, as it requires being on the ground to execute.

3.3 Rationale for the Selected Values

3.3.1 Full flush flow method

The following justifications were taken into account while selecting the values for the Full Flush Flow method:

- *Propellant consumption*: The high propellant consumption results in a lower chill-down time.
- *Process feasibility*: The executive complexity is low, making the process procedure simple and easy to execute.
- *Constructive feasibility*: The structural complexity is low, and the number of components required is also low.
- *Pressure drop*: The fluid path is simple, resulting in low pressure losses.
- *Complexity*: Due to the executive and constructive simplicity, the level of safety is high. Also, the method meets the reliability requirement. However, the costs of the process are high since the propellant consumption of the method is high.
- *Component stress*: The level of stress suffered by the components is low since there is a continuous mass flow rate.
- *Bearing compartment lubrication*: The efficiency of lubrication/refrigeration of the method is high since there is a continuous mass flow rate.
- *Upper stage thermal conditioning*: This technique is especially useful for in-flight cooling as the demand for short times is met[5].

[5]This procedure is essential when there are, for example, close engine reignitions.

3.3.2 Trickle by-pass method

- The chill-down time for the trickle by-pass method will be higher compared to the full flush flow method due to the reduced propellant consumption (0.5 $\rightarrow$ reduced $\dot{m}_{prop}$).
- The trickle by-pass method has a simple process procedure and a low executive complexity.
- The structural complexity is quite low, but the number of components required is slightly higher than the full flush flow method.
- The fluid path is simple and includes an additional parallel valve to regulate the flow, resulting in low pressure losses ($p_{loss} \propto \dot{m}$).
- Despite the slight increase in component requirements, the trickle by-pass method still has a high level of safety [6] due to the simplicity of its design, and the reliability requirement is almost met with the control of the by-pass valve. Additionally, the method is cost-effective as its main objective is to reduce propellant consumption.
- The trickle by-pass method has a low level of stress on its components due to the continuous mass flow rate.
- The efficiency of lubrication/refrigeration of the method is quite high with a continuous mass flow rate that starts reduced and then becomes full.
- This technique is particularly useful for in-flight cooling, as it meets the demand for low propellant consumption.

3.3.3 Pulse flow method

- The propellant consumption is lower (0.5 $\rightarrow$ reduced $\dot{m}_{prop}$ compared to full flow method), consequently the chill-down time will be higher.
- The executive complexity is quite low, and the process procedure is quite simple because there is the need to cycle the MPV appropriately.
- The structural complexity is low, requiring a small number of components.
- The fluid path is simple, with a low-pressure drop due to the simple geometry of the system.
- The simplicity of the executive and constructive aspects of this method results in a high level of safety, though the reliability requirement is only partially satisfied due to the delicate problem of MPV duty cycle. However, the low propellant consumption and number of components make the costs of the process low.

[6] Any delay in valve control does not compromise the safety of the engine and the mission.

- The level of stress suffered by the components is not negligible, as there is not a continuous mass flow rate and load cycles occur.
- The efficiency of lubrication/refrigeration of the method is not high due to the lack of a continuous mass flow rate.
- This technique can be used for in-flight cooling, meeting the demand for low propellant consumption. However, the reduced reliability can put the mission at risk.

3.3.4 CHV method

- The propellant consumption is lower ($0.5 \rightarrow$ reduced $\dot{m}_{prop}$), resulting in a longer chill-down time.
- The executive complexity is high, making the process procedure complex.
- The structural complexity is high, requiring a large number of components.
- The fluid path is not simple, with a complex geometry resulting in high pressure drop.
- Due to the high executive and constructive complexity, the level of safety is low; the reliability requirement is not satisfied, as the complex process procedure leads to increased likelihood of failure; the costs of the process are high due to the large number of components and high complexity.
- The level of stress suffered by the components is significant, as there is not a continuous mass flow rate (load cycles).
- The efficiency of lubrication/refrigeration of the method is not high, as there is not a continuous mass flow rate.
- This technique cannot be used for in-flight cooling, as it is too complex and unreliable, which could jeopardize the mission.

3.3.5 No bleed method

- The propellant consumption is eliminated ($1 \rightarrow$ zero $\dot{m}_{prop}$), and the chill-down time depends on the circuit and the amount of mass flow rate injected.
- The executive complexity is high, and the process procedure is complex.
- The structural complexity is high, and the number of components required is also high.
- The fluid path is not simple, and the system geometry is complex, resulting in a high pressure drop.

- Due to the high executive and constructive complexity, the level of safety is low, and the reliability requirement is not satisfied because of the complex process procedure. Despite the primary goal of eliminating propellant consumption, the method has high costs due to the large number of components.

- The level of stress suffered by the components is not negligible, as there is a two-phase flow downstream of the line that goes towards the electric pump, which poses a risk of cavitation.

- The efficiency of lubrication/refrigeration of the method is good, as there is a continuous mass flow rate.

- The technique could be used for in-flight cooling, although it should be avoided due to its high complexity.

3.3.6 Two-phase thermosiphon method

- The propellant consumption is eliminated ($1 \rightarrow$ zero $\dot{m}_{prop}$), and the chill-down time depends on the circuit and the quantity of mass flow rate.

- The executive complexity is high, and the process procedure is complex.

- The structural complexity is high, and the number of components required is high, including heaters and non-return valves.

- The fluid path is also complex, and the system geometry as well, resulting in a high pressure drop.

- Due to the high executive and constructive complexity, the level of safety is low, and the reliability requirement is not satisfied because of the complex process procedure. Despite the objective of eliminating propellant consumption, the high number of components and complexity results in high costs.

- The level of stress suffered by the components is not negligible, as there is a biphasic flow downstream of the line which goes towards the eventual tank equipped with heaters, increasing the risk of cavitation.

- The efficiency of lubrication/refrigeration is quite good since there is a continuous mass flow rate, but the flux downstream of the heaters is all in vapor phase, which can be a limitation.

- This technique could be used for in-flight cooling, but the high complexity makes it less desirable, especially given the high reliability requirements for successful missions.

3.3.7 Recirculating pumps method

- The propellant consumption is eliminated ($1 \rightarrow$ zero $\dot{m}_{prop}$), and the chill-down time depends on the circuit and the quantity of mass flow rate.
- The executive complexity is high, and the process procedure is complex.
- The structural complexity is high, and a large number of components are required (centrifugal pumps and control valves).
- The fluid path is not simple, and the geometry of the system is complex, resulting in a high pressure drop.
- Due to the high executive and constructive complexity, the level of safety is low, and the reliability requirement is not satisfied because the process procedure is complex. The costs of the process are high, despite the main objective being to eliminate the propellant consumption.
- The level of stress suffered by the components is not negligible.
- The efficiency of lubrication/refrigeration of the method is good, since there is a continuous mass flow rate.
- This technique could be used for in-flight cooling, but it should be avoided due to the high complexity, high costs, and low reliability. The success of the mission is a very strict requirement.

Chapter 4

Simulation and Analysis of Experimental Reports on Chill-Down of Cryogenic Transfer Lines

The goal of this section is to simulate and analyze various chill-down experimental tests available from literature in order to validate or not the *EcosimPro* software regarding the cooling of cryogenic transfer lines.
The results show that the software is not able to correctly simulate the chill-down process, so a new pipe custom component shall be developed.
Six chill-down test cases were considered, and they all highlighted the inadequacy of the program. In particular, three main limitations of the software were identified:

1. Firstly, EcosimPro is not able to correctly simulate the subcooled condition of the cryogenic fluid. There are excessive numerical oscillations before reaching the steady flow condition, making it impossible to obtain accurate predictions. This limitation is particularly visible on the mass flow rate $\dot{m}$ and the quality factor, $.x = \frac{mass_{gas}}{mass_{liquid}}$, of the cryogenic fluid.

2. Secondly, in subcooled cryogenic liquid conditions, the temperature curves of the fluid and the wall are not coincident at the end of the chill-down process. The temperature of the fluid is different from that of the wall ($T_{wall} \neq T_{fluid}$), leading to non-physical solutions and preventing the steady state from reaching equilibrium. This limitation becomes more pronounced as the length of the pipe increases. This limitation is visible from the graphs obtained with the software, such as those shown in the figures 4.1, 4.2, and 4.3.

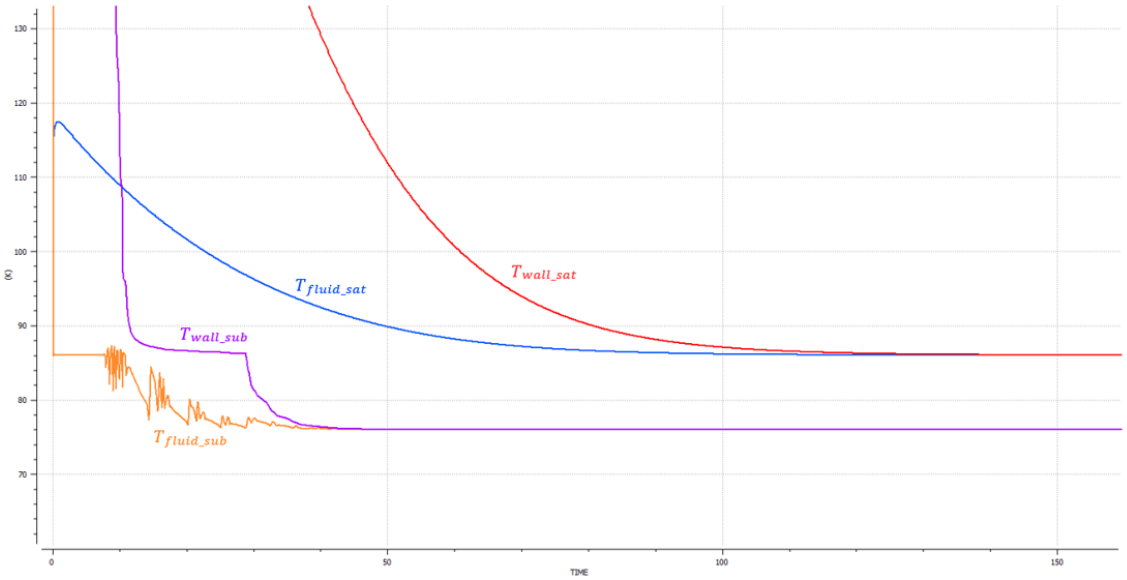

Figure 4.1. T_{fluid} and T_{wall} in subcooled and saturated conditions, during a classic chill-down simulation in EcosimPro.

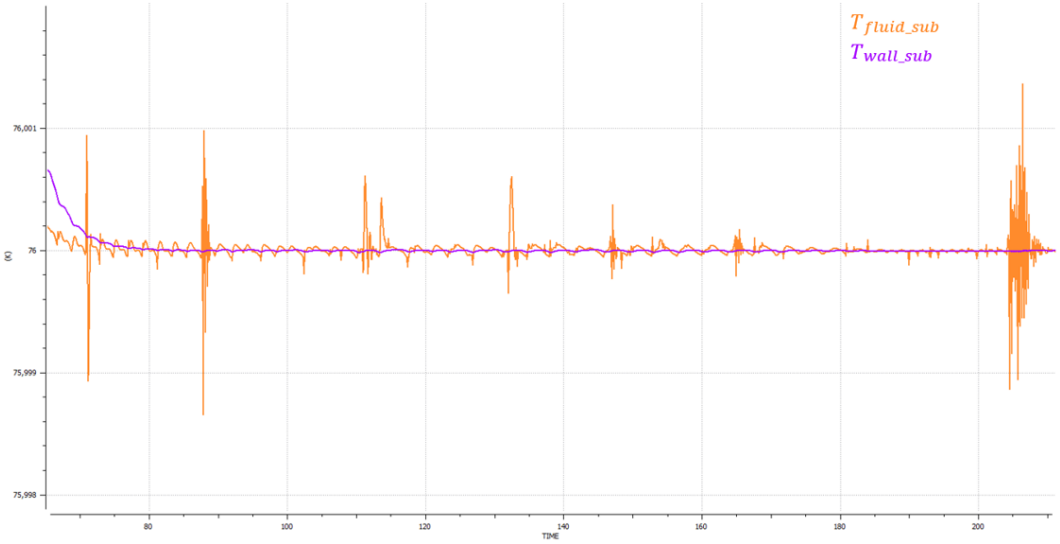

Figure 4.2. Detail on the numerical oscillations of fluid and wall temperature, in subcooling conditions, during a classic chill-down simulation in EcosimPro.

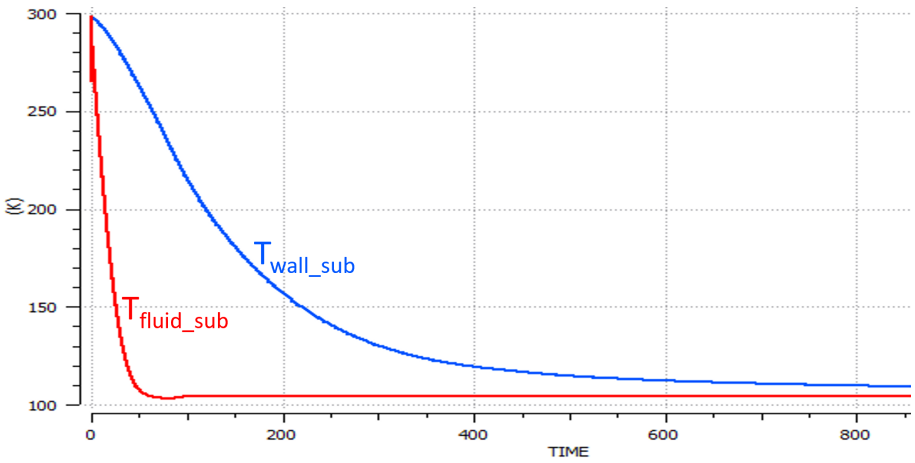

Figure 4.3. Detail on fluid and wall temperature, in subcooling conditions, which do not coincide in EcosimPro at the end of chill-down process.

3. Thirdly, the software does not consider the effects of gravity on the chill-down process. In particular, the inlet driving pressure increases due to the presence of gravity $\Delta P = \rho \cdot g \cdot z$, resulting in an increase in the mass flow rate and a reduction in the chill-down time. This effect becomes more pronounced as the length of the transfer lines increases. However, EcosimPro shows that the solution in microgravity conditions coincides with the solution obtained considering the presence of gravity, indicating that the software does not consider the effects of gravitational acceleration g in the heat exchanges and the heat transfer coefficient h.

The first two limitations are typical of the subcooled condition, while the third one is always present, both in the subcooled and saturated fluid state.

The various experimental test cases have been analyzed in detail, and the several limitations of the software have been highlighted and are presented below.

4.1 Experimental Setup used in the Simulation Environment

The basic pipe model built and used in EcosimPro to simulate various experimental tests is shown in Figure 4.4.

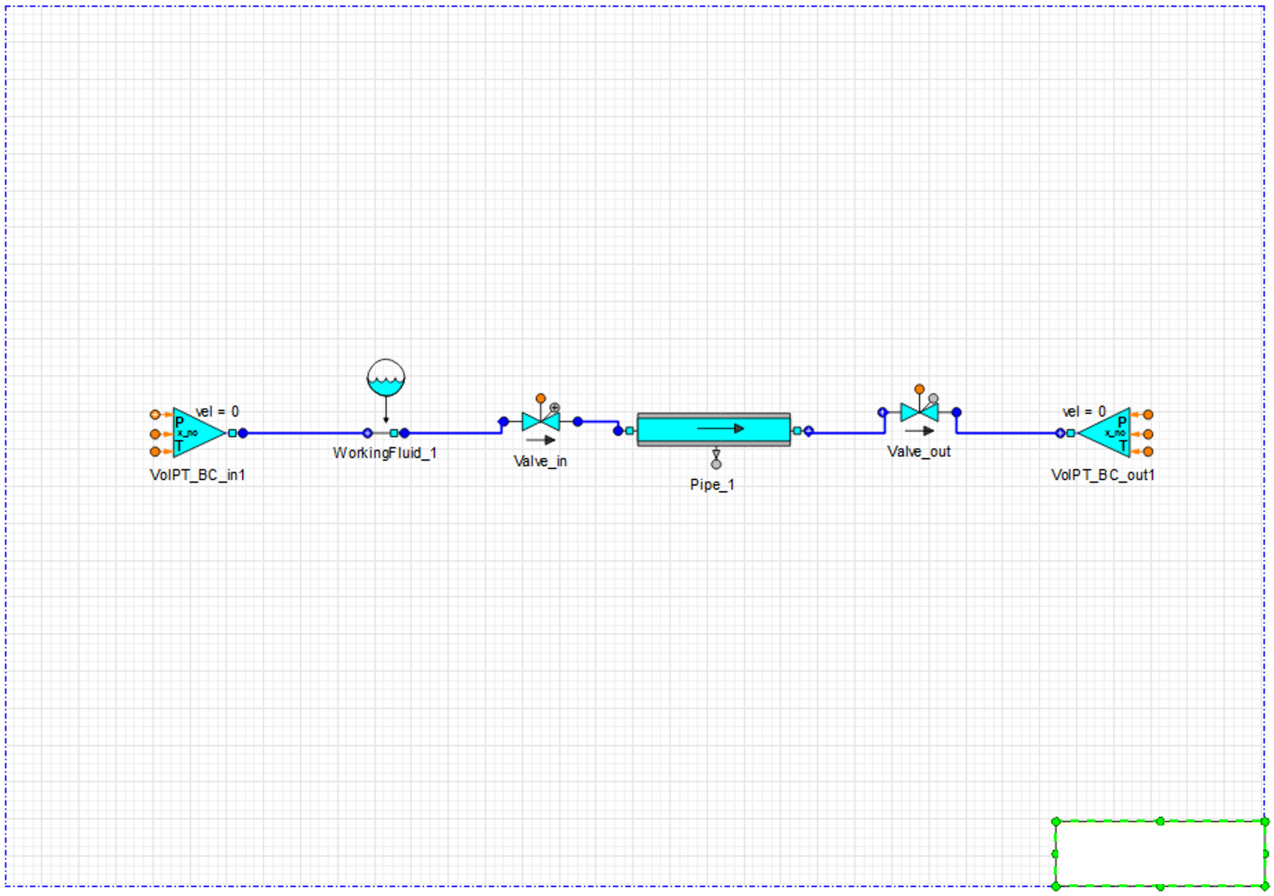

Figure 4.4. Experimental setup in EcosimPro.

The simple system comprises a horizontal pipe through which the cryogenic working fluid flows, two valves at the inlet and outlet of the duct, which can be fully or partially opened or closed by adjusting the stroke value, and two boundary conditions upstream and downstream of the pipe that can be set for pressure and temperature.
The program requires other values to be set, such as the geometry of the components (such as valves area, length L, inner diameter ID, outer diameter OD, number of nodes of the pipe in which to evaluate the different quantities, wall thickness t, material), the type of fluid and the heat transfer coefficient model, and so on.

The apparatus shown in Figure 4.4 was used to simulate the Full Flush Flow and Trickle with Bypass chill-down techniques. For the Pulse method, a control on the inlet valve was introduced, which we will analyze in detail later.

4.2 Test case 1

The first test case concerns the replication of the experimental setup described in the report by Brennan et al. [1966] in EcosimPro.
The following figure displays the schematic of the experimental equipment used in the report to conduct various chill-down tests.

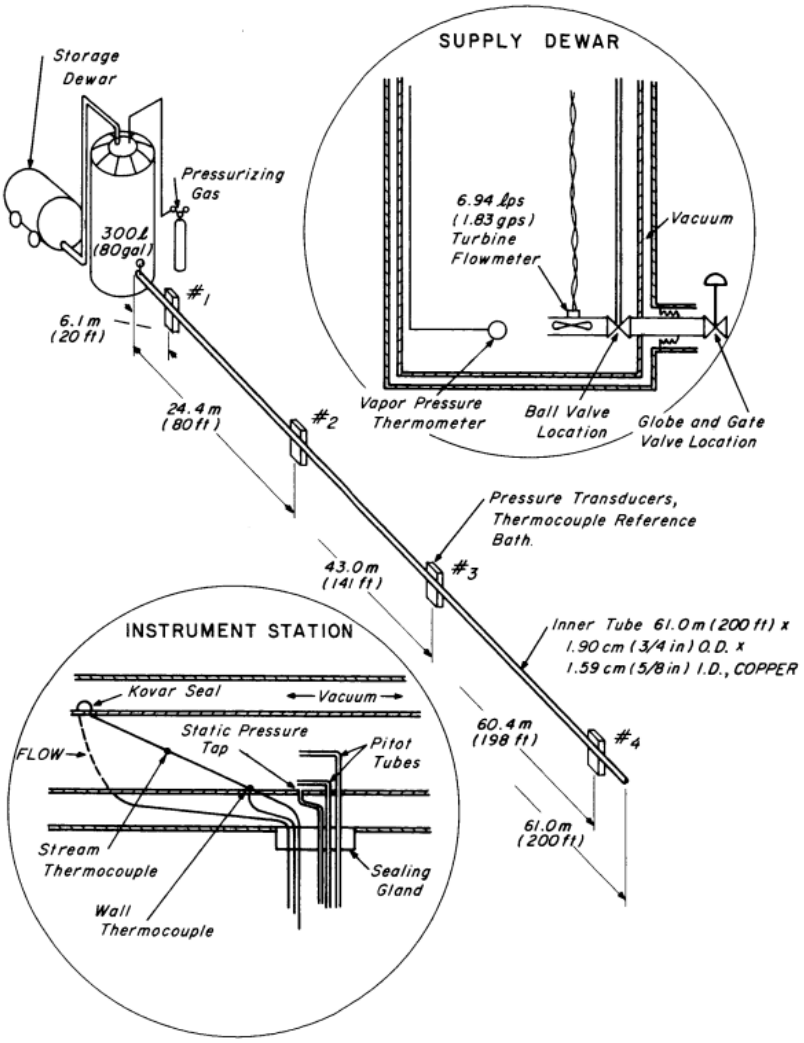

Figure 4.5. Schematic of test apparatus.

The experimental conditions obtained from the article are presented in the following table:

L_{pipe} $[m]$	ID $[cm]$	OD $[cm]$	t_{wall} $[mm]$	material $[-]$	$port_{inlet_{valve}}$ $[cm]$	working fluid $[-]$	p_{out} $[atm]$
61	1.90	1.59	1.55	copper	1.9 or 2.54	LH_2 or LN_2	0.1

Table 4.1. Case 1 experimental conditions

At four points along the line, labeled as 1 through 4 in figure 4.5, instrumentation stations were placed to measure pressures and temperatures. These stations correspond to cells 13, 77, 135, and 190 in EcosimPro, where a total of 192 nodes were defined. The chill-down technique that was simulated is full flush flow method.

4.2.1 Liquid hydrogen LH_2, $A_{0_{valve,1}}$

For the experimental tests conducted with liquid hydrogen, both subcooled and saturated conditions were considered. The inlet valve area for these tests was $A_{0_{valve,1}} = 2.83529 \cdot 10^{-4} m^2$ ($D = 1.9$cm).

When the test is run with LH_2 in saturated condition, the inlet liquid temperature T_{in} is set to the saturation temperature T_{sat} of the liquid at the selected driving pressure p_{in}, which is derived from Antoine's equation. On the other hand, when the test is performed with subcooled LH_2, T_{in} is set to the subcooling temperature $T_{sub} = 19.5$K.

Saturated LH_2, $p_{in} = 5.1$ atm

- Inlet driving pressure $p_{in} = 5.1$ atm $= 516757.5$ Pa $\rightarrow T_{in,sat} = 27.4$K
- Ambient temperature $T_{out} = T_{amb} = 280$K

The experimental paper by Brennan et al. [1966] does not provide information on the stroke of the valve used in the tests ($Valve_{in}$ in fig. 4.4). To replicate the experimental results, the valve stroke has been set to be equal to the valve area, which is $A_{0_{valve,1}} = 2.83529 \cdot 10^{-4} m^2$ (D=1.9cm). This choice was made to ensure that the simulated chill-down times match the experimental ones.
As a result, the stroke value will be fixed for all the subsequent tests:

$$Stroke_{valve} = 1 \rightarrow \text{valve fully open}$$

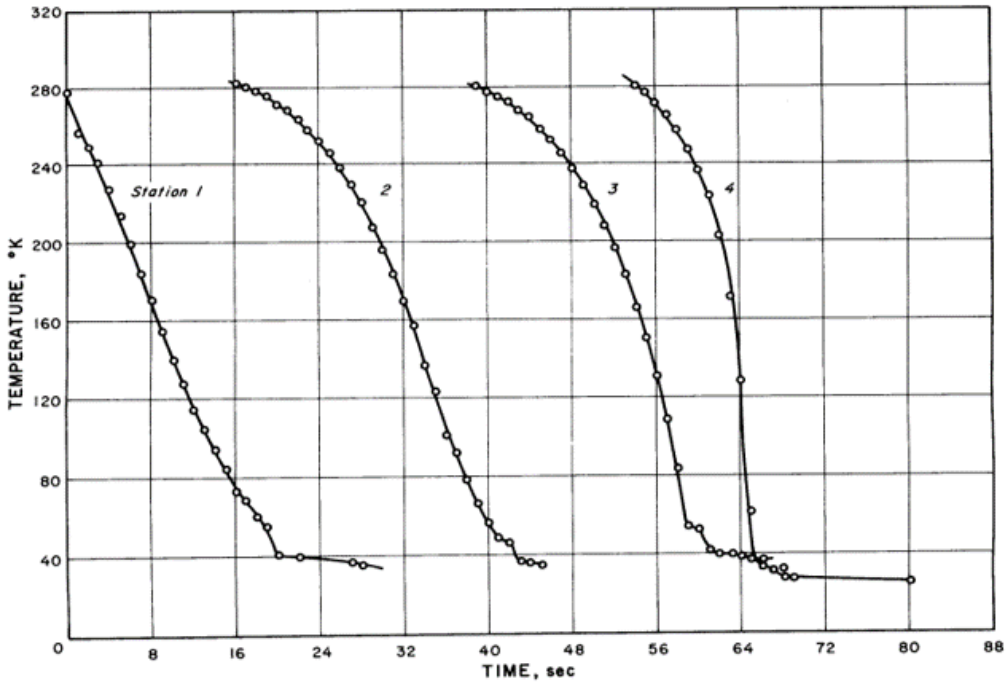

Figure 4.6. T_{wall} history with saturated LH_2 at $p_{in} = 5.1atm$, experimental case.

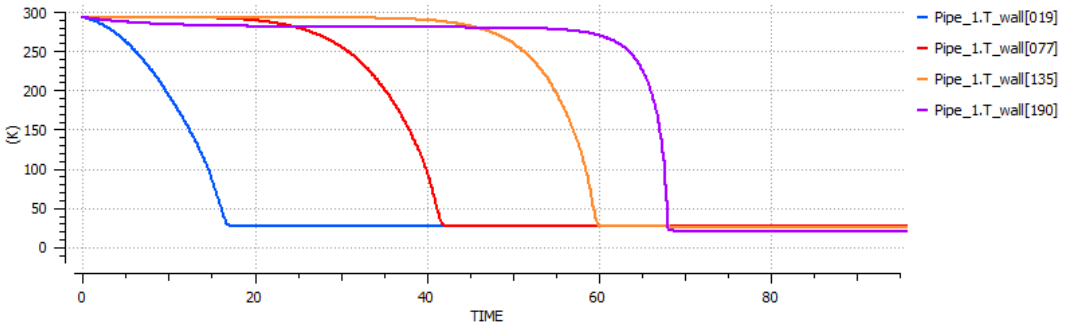

Figure 4.7. $T_{wall} = f(t)$ with saturated LH_2 at $p_{in} = 5.1atm$, EcosimPro.

Comparison of the experimental results (Figure 4.6) with those obtained from EcosimPro (Figure 4.7) shows that the software performs well under conditions of saturated liquid, with chill-down times that are almost in agreement with the experimental results. However, the propellant consumption from the simulation is underestimated as the fluid downstream of the chill-down process is partially in the vapor phase, whereas in reality, it is in monophasic liquid conditions, leading to a decrease in the mass flow rate (since $\rho_{vapor} < \rho_{liquid} \rightarrow \dot{m} \downarrow$). Additionally, the simulated curves appear to be excessively smooth, similar to each other, and regular and do not match the concavities seen in the

experimental data. As a result, EcosimPro does not reproduce the physical flow behavior accurately, and the heat transfer coefficient model used does not reflect the complexity of the actual heat exchanges between the fluid and the wall.

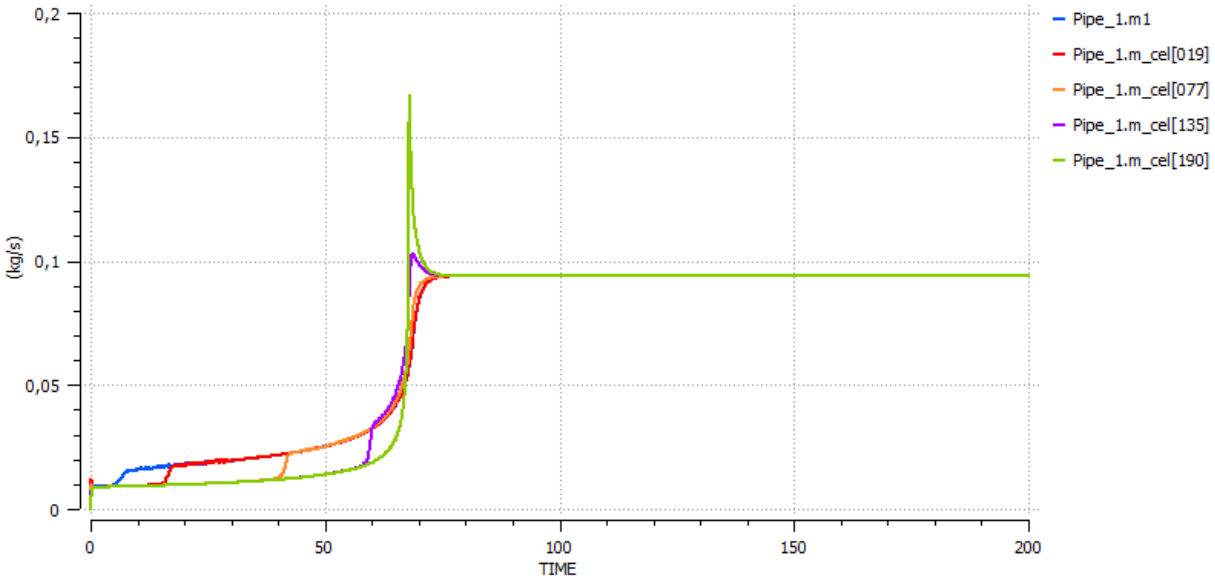

Figure 4.8. Mass flow rate $\dot{m}$ history during chill-down, in EcosimPro.

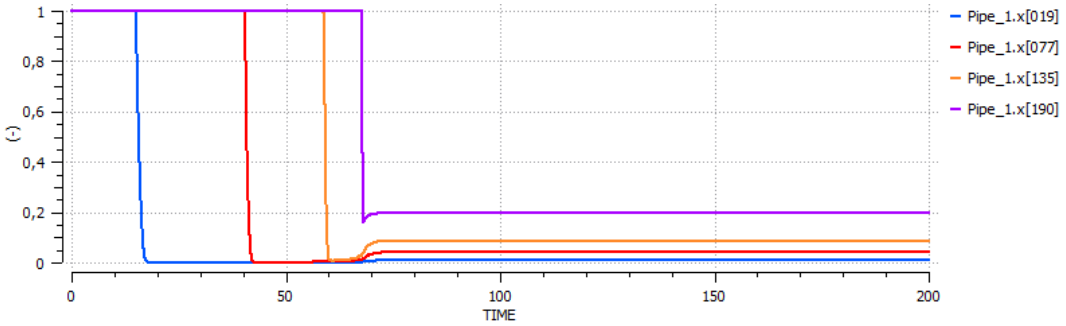

Figure 4.9. Quality factor $.x$ history, in EcosimPro.

Figure 4.8 shows the mass flow rate $\dot{m}$ history in EcosimPro during the chill-down process, and the area under the curve represents the fraction of propellant consumption during the process until the steady-state is reached. The quality factor [1] $.x$ (vapor fraction

[1]The quality factor, also known as the vapor fraction or vapor quality, is a dimensionless quantity that represents the ratio of the mass of vapor in a two-phase mixture to the total mass of the mixture. It is often denoted by the symbol $.x$ and can range from 0 to 1, where 0 represents a completely liquid

in the liquid) history in EcosimPro is shown in Figure 4.9.

At the outlet of the pipe, i.e., in cell 190, the density of the fluid is $\rho_{out} = 3.8552 \frac{kg}{m^3}$, which is lower than the saturation density at the selected driving pressure, $\rho_{sat} = 60.3938 \frac{kg}{m^3}$. This confirms that the fluid exiting the pipe is not in the liquid phase, but in the vapor phase.

For the test case with saturated liquid at $T_{in,sat} = 27.4K$, the propellant consumption was $2.19155kg$, and the chill-down time was approximately $\Delta t_{cooling} \cong 70s$.

$$T_{in,sat} = 27.4\text{K} \rightarrow m_{consumption} = 2.19155 \text{ kg}, \Delta t_{cooling} \cong 70\text{s}$$

The same conditions were tested for the subcooled liquid at $T_{in} = T_{sub} = 19.5$K, and the results are presented in the following graphs.

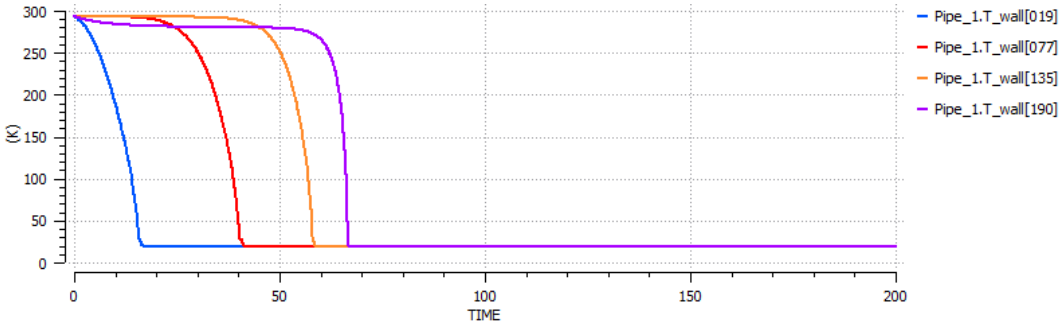

Figure 4.10. $T_{wall} = f(t)$ with subcooled LH_2 at $p_{in} = 5.1atm$, EcosimPro.

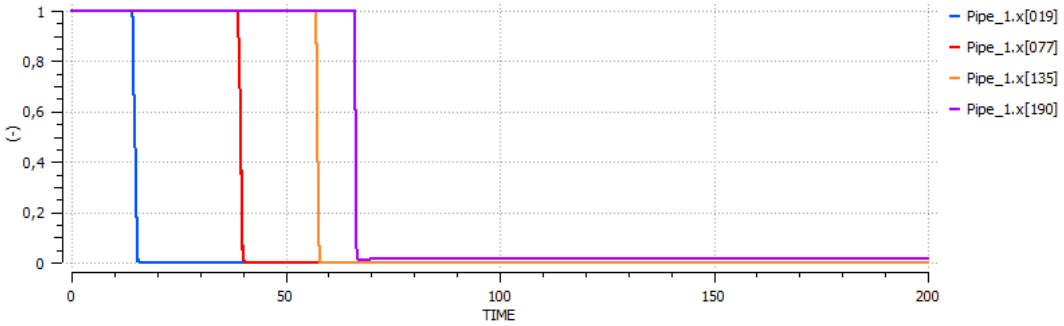

Figure 4.11. Quality factor $.x$ history with subcooled LH_2.

mixture and 1 represents a completely vapor mixture.

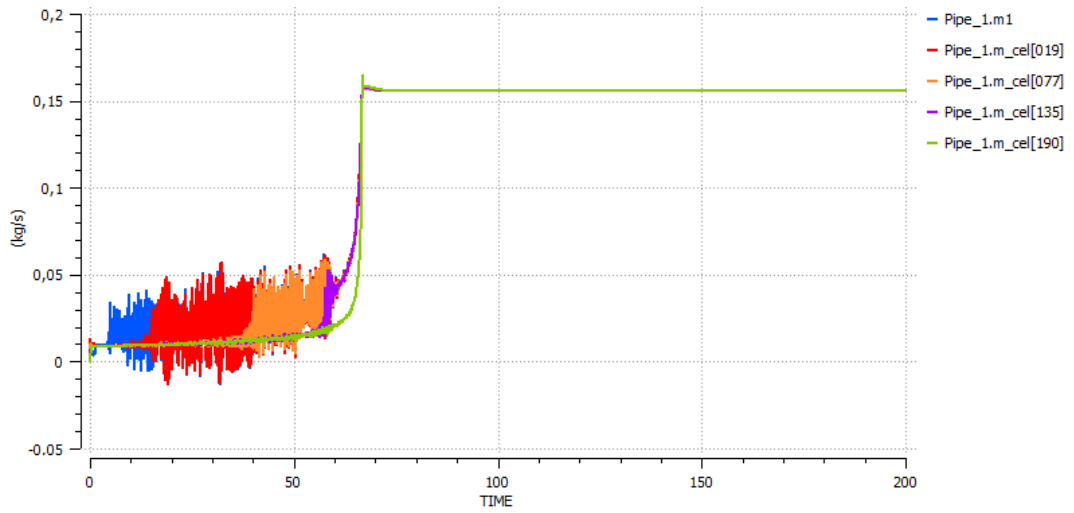

Figure 4.12. Mass flow rate $\dot{m}$ history with subcooled LH_2.

The results obtained from the simulations show that in subcooled flow conditions, the fluid leaving the pipe is almost in the liquid phase (fig. 4.11) and the chill-down times are consistent with those obtained from the simulation (4.10). However, in subcooled flow conditions, the mass flow rate history does not match the real physical trend, exhibiting excessive numerical oscillations before reaching the steady state (4.12). As a result, the propellant consumption during the chill-down process is not correctly estimated, leading to fictitious values. These findings confirm the previous statement that EcosimPro does not perform well in subcooled flow conditions.

By comparing the mass flow rate graphs in both saturation (fig. 4.8) and subcooled conditions (fig. 4.12), it can be observed that in saturation conditions, the curve is unstationary but not oscillatory, which is in agreement with the real physical trend, but it underestimates the propellant consumption, since the fluid leaving the pipe is not completely in the liquid state. Overall, these results suggest that while EcosimPro may have limitations in accurately modeling the real physical behavior and heat transfer coefficient in subcooled flow conditions, it can still be a useful tool for simulating chill-down processes in conditions of saturated liquid.

Subcooled LH_2, $p_{in} = 2.5$ atm

- Inlet driving pressure $p_{in} = 2.5\text{atm} = 253312.5\text{Pa}$
- Inlet liquid temperature $T_{in,sub} = 19.5\text{K}$
- Ambient temperature $T_{out} = T_{amb} = 273\text{K}$

The limitations of EcosimPro are once again highlighted in the various cases analyzed and reported here. The graphs clearly demonstrate the software's poor performance in

subcooled conditions, as seen in the mass flow rate history (4.15), where it underestimates the chill-down times and consequently the propellant consumption. The curves of $T_{wall} = f(t)$ (4.14) at different nodes also appear to be excessively regular and similar to each other, failing to accurately represent the fluid's actual physical behavior.

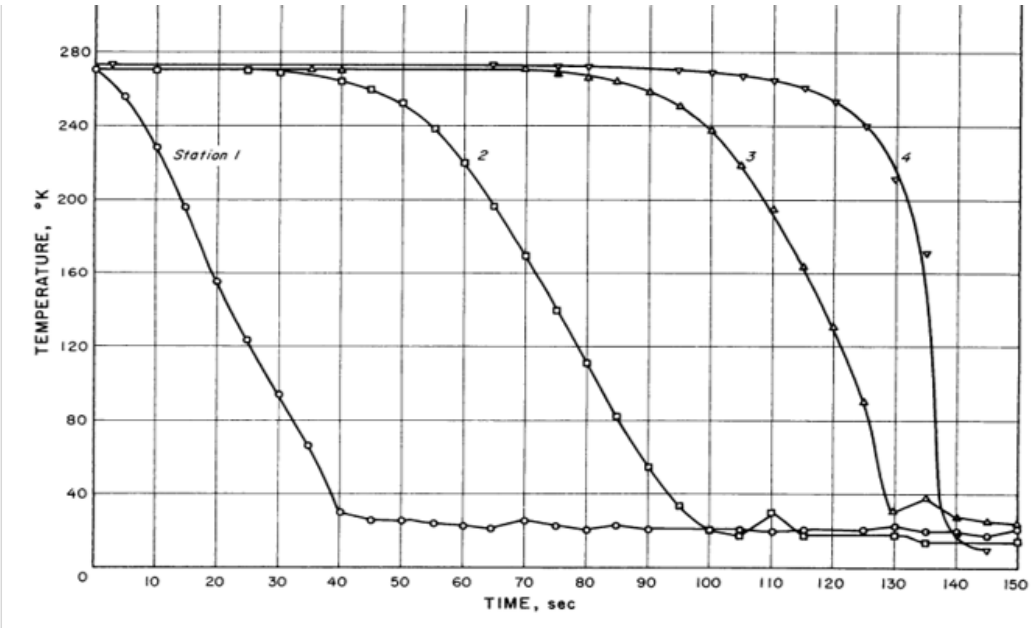

Figure 4.13. T_{wall} history with subcooled LH_2 at $p_{in} = 2.5atm$, experimental case.

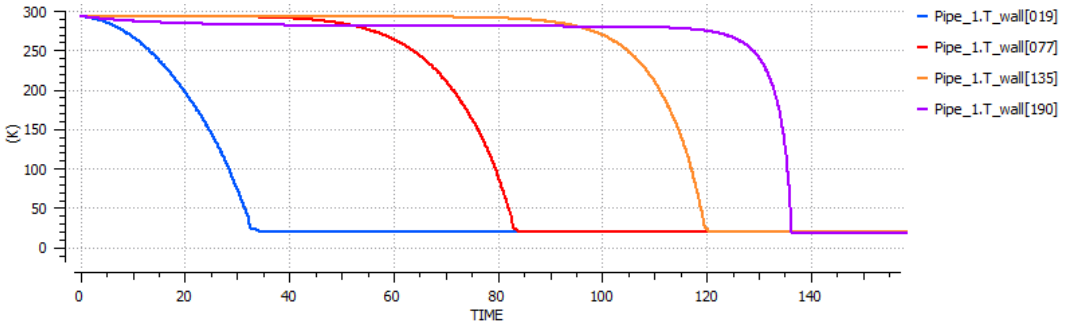

Figure 4.14. $T_{wall} = f(t)$ with subcooled LH_2 at $p_{in} = 2.5atm$, EcosimPro.

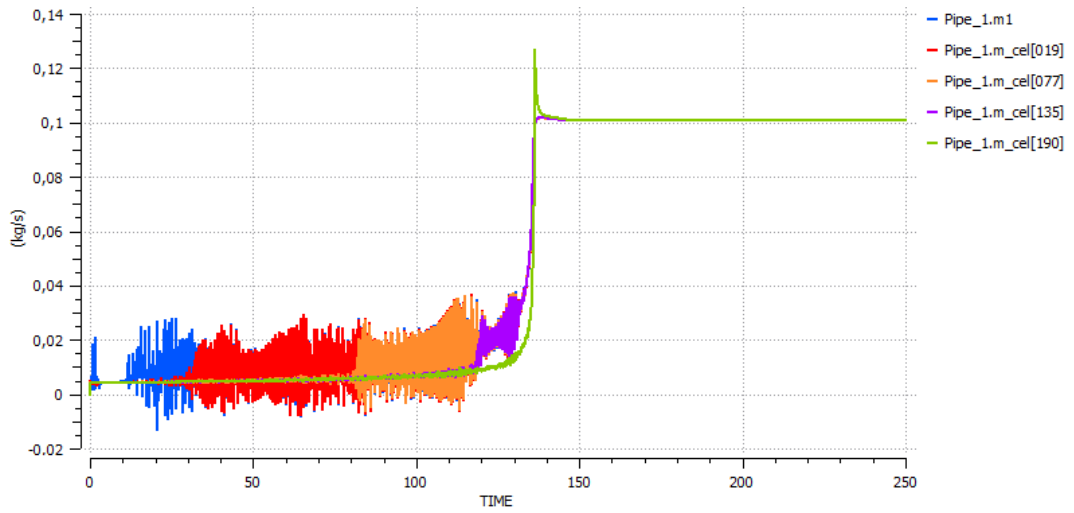

Figure 4.15. Mass flow rate $\dot{m}$ history with subcooled LH_2 at $p_{in} = 2.5atm$, EcosimPro.

At the subcooled state with $T_{in} = T_{sub} = 19.5K$, the propellant consumption during the chill-down process is estimated to be 1.91418kg, and the corresponding chill-down time is approximately $\cong$ 146s.

$$T_{in,sub} = 19.5K \rightarrow m_{consumption} = 1.91418\text{kg},\ \Delta t_{cooling} \cong 146\text{s}$$

Subcooled LH_2, $p_{in} = 4.2$ atm

- Inlet driving pressure $p_{in} = 4.2\text{atm} = 425565\text{Pa}$
- Inlet liquid temperature $T_{in,sub} = 19.5\text{K}$
- Ambient temperature $T_{out} = T_{amb} = 280\text{K}$

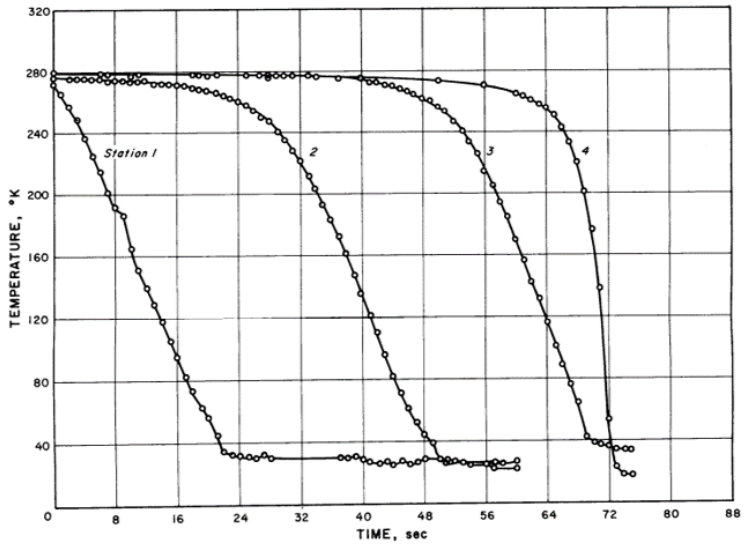

Figure 4.16. T_{wall} history with subcooled LH_2 at $p_{in} = 4.2atm$, experimental case.

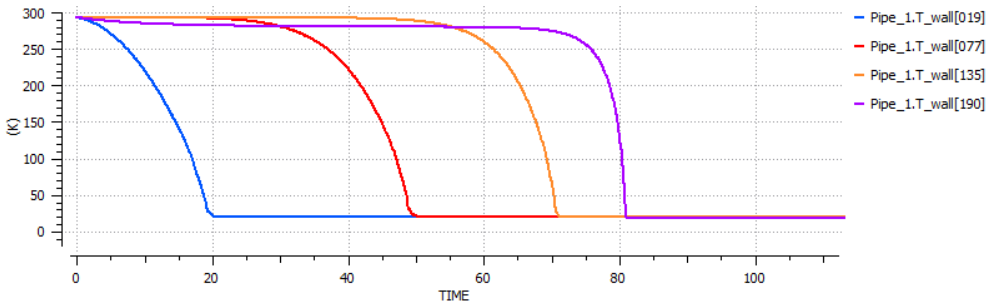

Figure 4.17. $T_{wall} = f(t)$ with subcooled LH_2 at $p_{in} = 4.2atm$, EcosimPro.

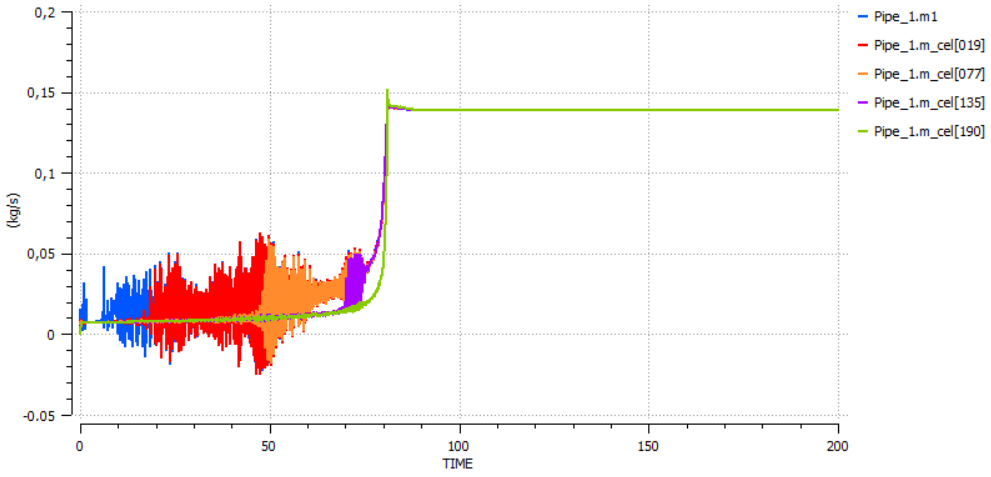

Figure 4.18. Mass flow rate $\dot{m}$ history with subcooled LH_2 at $p_{in} = 4.2atm$, EcosimPro.

$$T_{in,sub} = 19.5K \rightarrow m_{consumption} = 1.88054\text{kg},\ \Delta t_{cooling} \cong 83\text{s}$$

Subcooled LH_2, $p_{in} = 5.9$ atm

- Inlet driving pressure $p_{in} = 5.9\text{atm} = 597817.5\text{Pa}$
- Inlet liquid temperature $T_{in,sub} = 19.5\text{K}$
- Ambient temperature $T_{out} = T_{amb} = 293\text{K}$

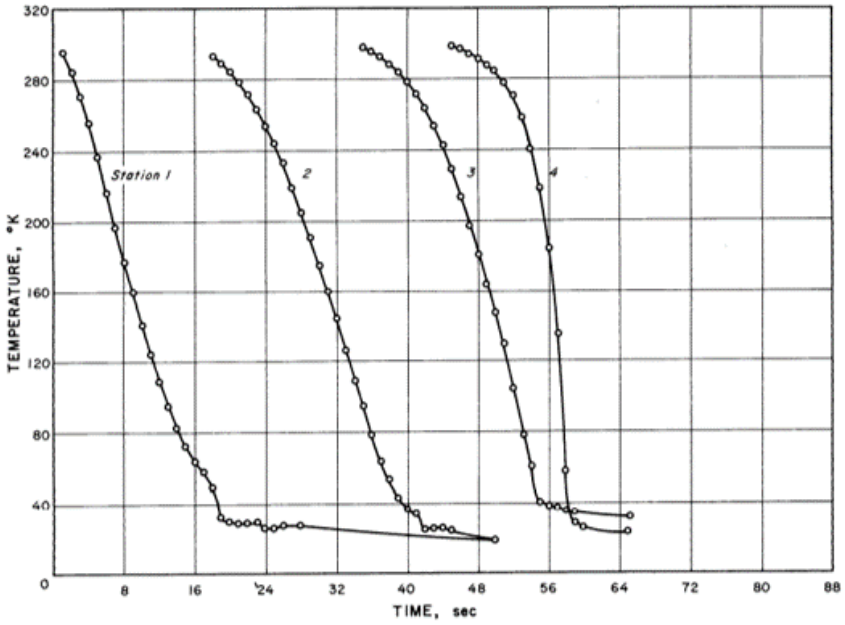

Figure 4.19. T_{wall} history with subcooled LH_2 at $p_{in} = 5.9atm$, experimental case.

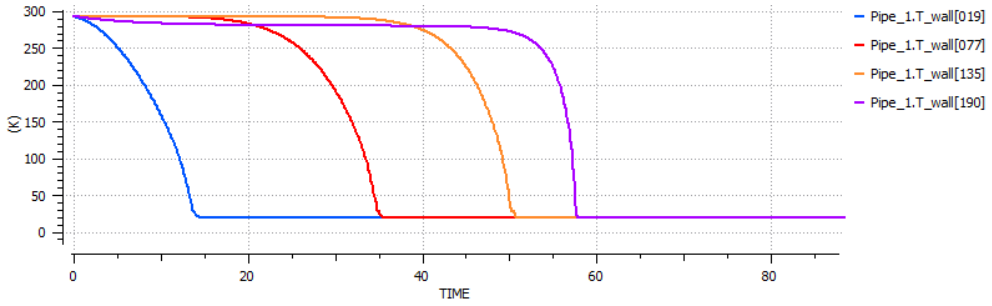

Figure 4.20. $T_{wall} = f(t)$ with subcooled LH_2 at $p_{in} = 5.9atm$, EcosimPro.

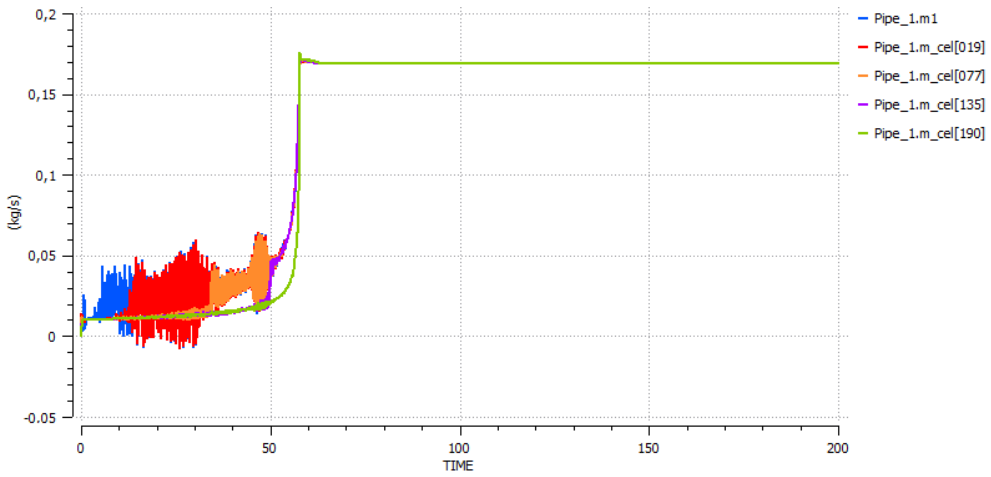

Figure 4.21. Mass flow rate $\dot{m}$ history with subcooled LH_2 at $p_{in} = 5.9atm$, EcosimPro.

$$T_{in,sub} = 19.5K \rightarrow m_{consumption} = 1.83829\text{kg},\ \Delta t_{cooling} \cong 58\text{s}$$

Subcooled LH_2, $p_{in} = 7.6$ atm

- Inlet driving pressure $p_{in} = 7.6\text{atm} = 770070\text{Pa}$
- Inlet liquid temperature $T_{in,sub} = 19.5\text{K}$
- Ambient temperature $T_{out} = T_{amb} = 293\text{K}$

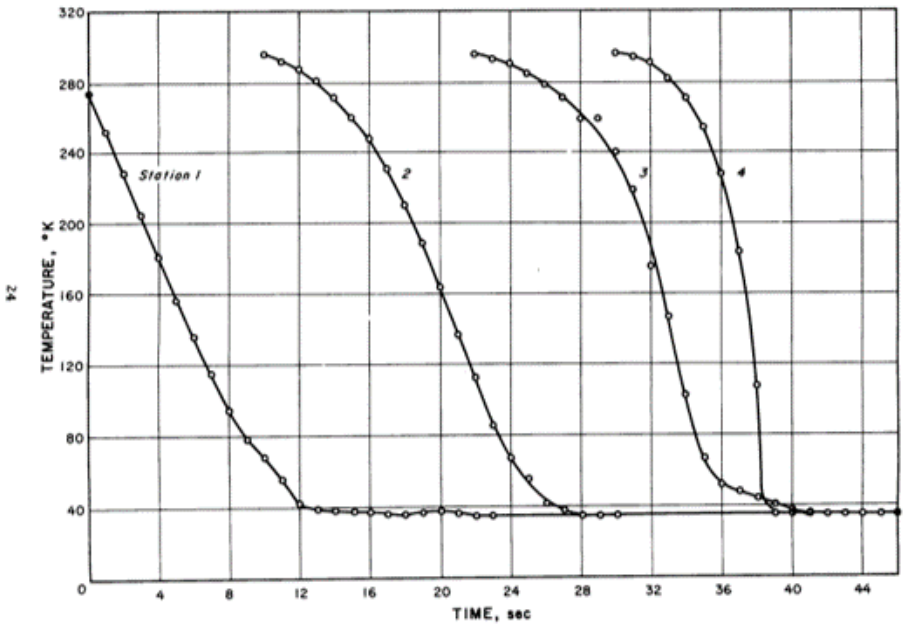

Figure 4.22. T_{wall} history with subcooled LH_2 at $p_{in} = 7.6atm$, experimental case.

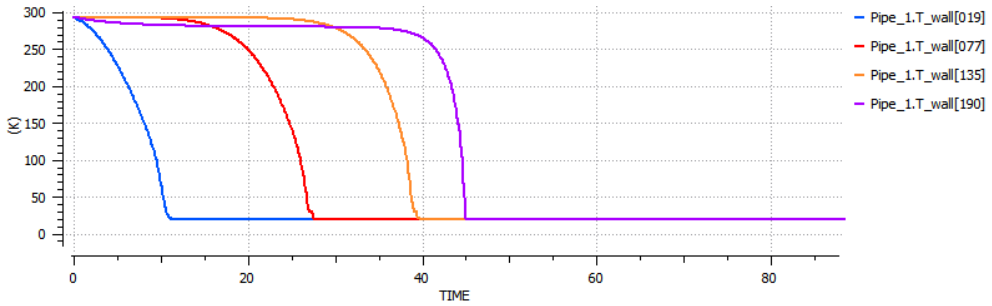

Figure 4.23. $T_{wall} = f(t)$ with subcooled LH_2 at $p_{in} = 7.6atm$, EcosimPro.

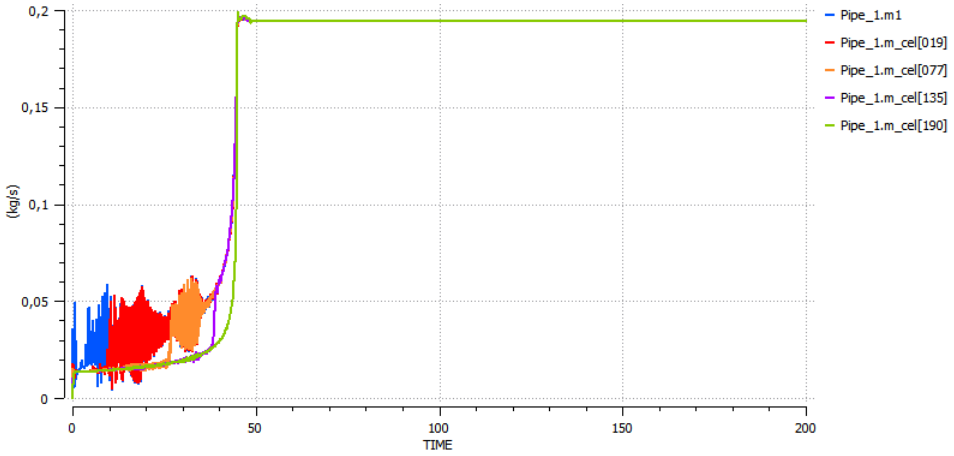

Figure 4.24. Mass flow rate $\dot{m}$ history with subcooled LH_2 at $p_{in} = 7.6atm$, EcosimPro.

$$T_{in,sub} = 19.5K \rightarrow m_{consumption} = 1.88479\text{kg},\ \Delta t_{cooling} \cong 46\text{s}$$

Subcooled LH_2, $p_{in} = 11$ atm

- Inlet driving pressure $p_{in} = 11\text{atm} = 1114575\text{Pa}$
- Inlet liquid temperature $T_{in,sub} = 19.5\text{K}$
- Ambient temperature $T_{out} = T_{amb} = 280\text{K}$

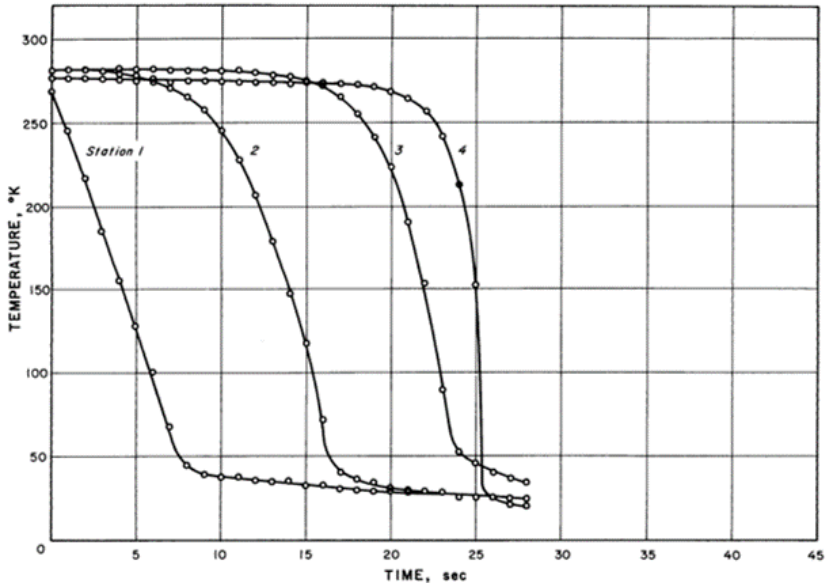

Figure 4.25. T_{wall} history with subcooled LH_2 at $p_{in} = 11atm$, experimental case.

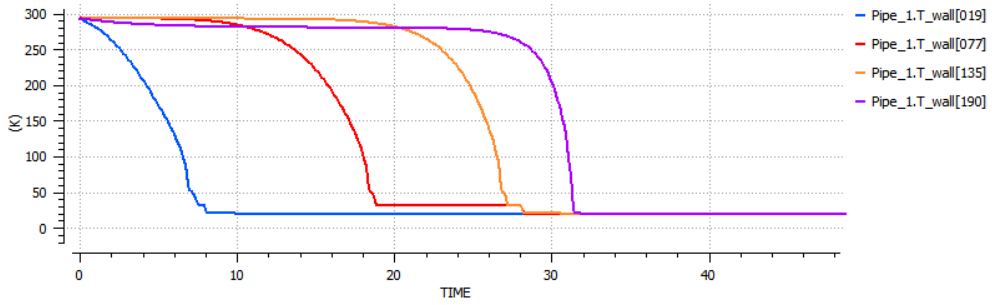

Figure 4.26. $T_{wall} = f(t)$ with subcooled LH_2 at $p_{in} = 11atm$, EcosimPro.

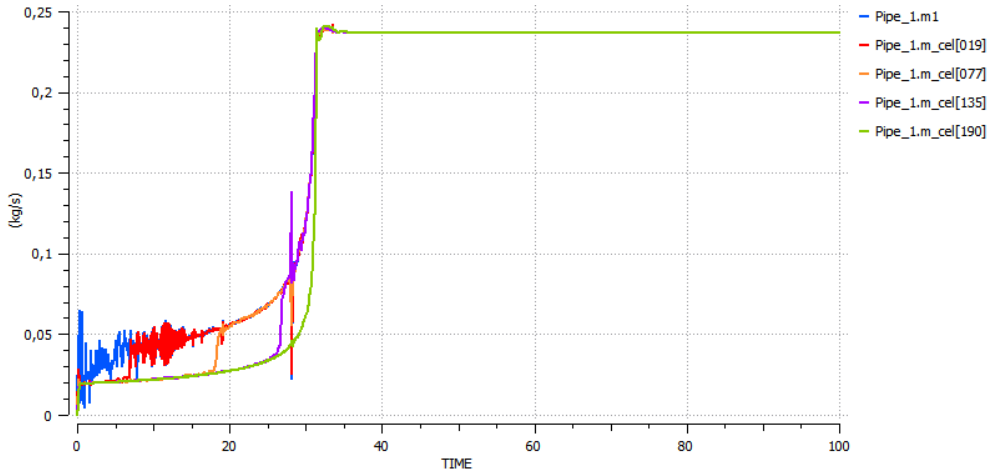

Figure 4.27. Mass flow rate $\dot{m}$ history with subcooled LH_2 at $p_{in} = 11atm$, EcosimPro.

$$T_{in,sub} = 19.5K \rightarrow m_{consumption} = 1.9231\text{kg},\ \Delta t_{cooling} \cong 32\text{s}$$

4.2.2 Liquid nitrogen LN_2, $A_{0_{valve,1}}$

The experimental tests conducted with liquid nitrogen under both subcooled and saturated conditions will now be considered.
The tests were performed with an inlet valve area of $A_{0_{valve,1}} = 2.83529 \cdot 10^{-4} m^2$ (D=1.9cm). In the case where the test was conducted with LN_2 in saturated condition, the inlet liquid temperature T_{in} was equal to the saturation temperature T_{sat} of the liquid at the chosen driving pressure p_{in}, which was obtained from Antoine's equation. On the other hand, if the test was conducted with subcooled LN_2, the inlet liquid temperature was set to $T_{in} = T_{sub} = 76$K.

Saturated LN_2, $p_{in} = 2.5$ atm

- Inlet driving pressure $p_{in} = 2.5$atm = 253312.5 Pa $\rightarrow T_{in,sat} = 86.066$K
- Ambient temperature $T_{out} = T_{amb} = 280$K

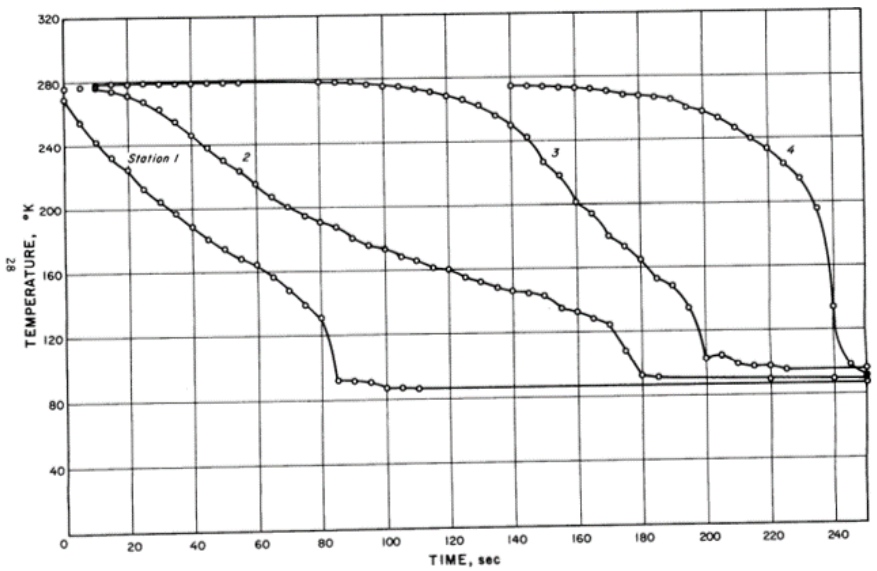

Figure 4.28. T_{wall} history with saturated LN_2 at $p_{in} = 2.5atm$, experimental case.

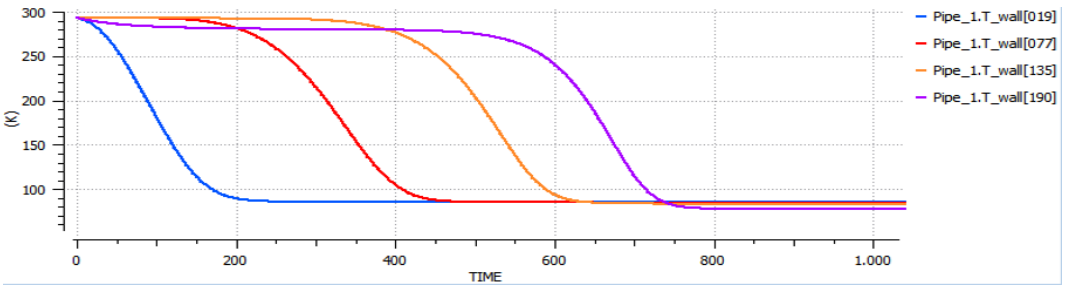

Figure 4.29. $T_{wall} = f(t)$ with saturated LN_2 at $p_{in} = 2.5atm$, EcosimPro.

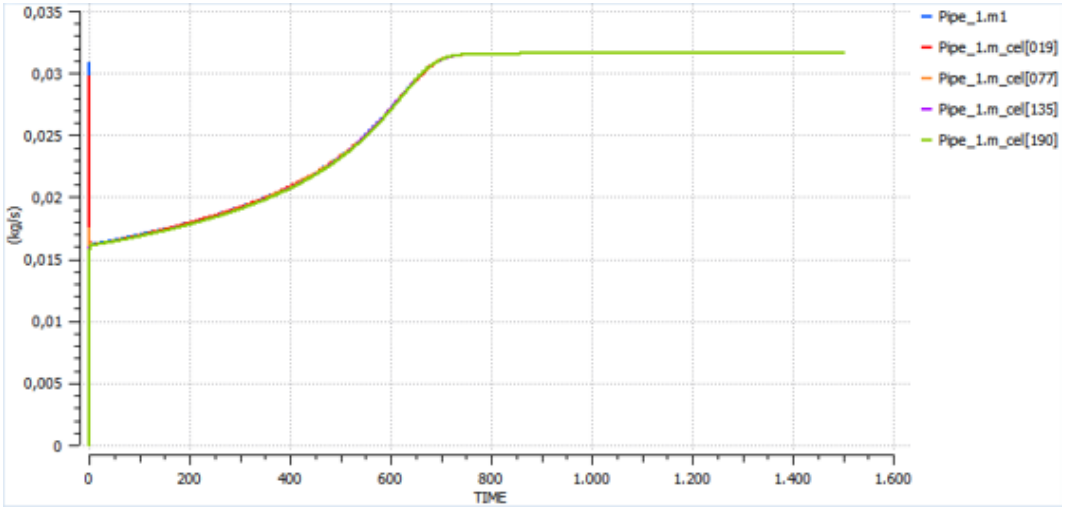

Figure 4.30. Mass flow rate $\dot{m}$ history with saturated LN_2 at $p_{in} = 2.5atm$, EcosimPro.

The limitations of EcosimPro, as discussed earlier, are also evident in the experimental tests conducted with liquid nitrogen. Furthermore, the software performs poorly not only in subcooled conditions but also in saturation conditions for nitrogen.
The chill-down times obtained from the simulation, previously close to the experimental values, are now significantly different, as seen in Figures 4.28 and 4.29.

It is worth noting that for $T_{in,sat} = 86.066$K, the simulated propellant consumption is 23.6925kg, and the chill-down time is approximately 750s.

$$T_{in,sat} = 86.066\text{K} \rightarrow m_{consumption} = 23.6925\text{kg},\ \Delta t_{cooling} \cong 750\text{s}$$

With the same boundary conditions, subcooled flow with $T_{in,sub} = 76$K was considered, which resulted in the correct cooling times (fig. 4.31). However, the mass flow rate history and propellant consumption were not consistent due to the presence of excessive numerical oscillations (fig. 4.32).

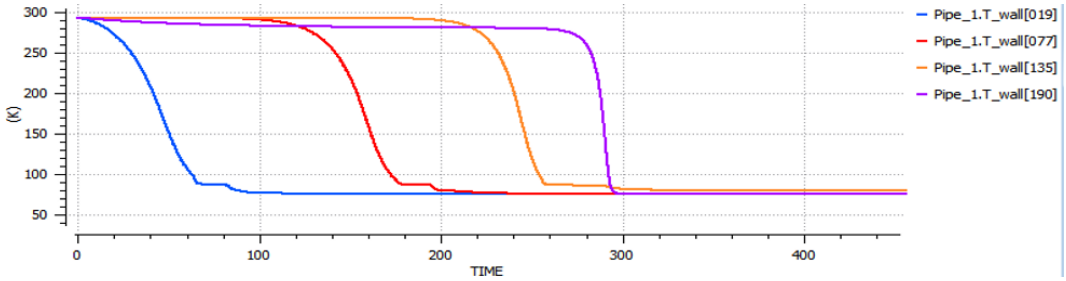

Figure 4.31. $T_{wall} = f(t)$ with subcooled LN_2 at $p_{in} = 2.5atm$, EcosimPro.

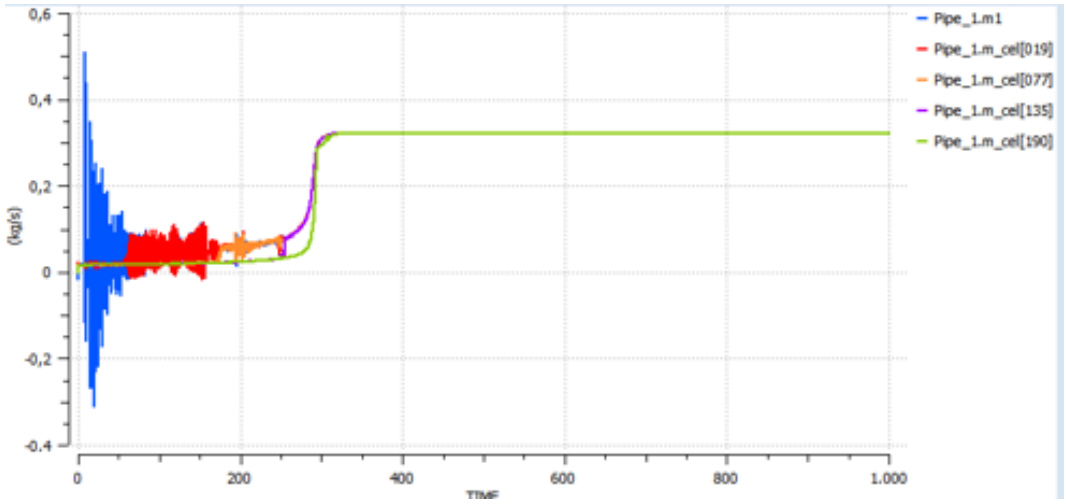

Figure 4.32. Mass flow rate $\dot{m}$ history with subcooled LN_2 at $p_{in} = 2.5atm$, EcosimPro.

Saturated LN_2, $p_{in} = 3.4$ atm

- Inlet driving pressure $p_{in} = 3.4\text{atm} = 344505\text{Pa} \rightarrow T_{in,sat} = 89.475\text{K}$
- Ambient temperature $T_{out} = T_{amb} = 293\text{K}$

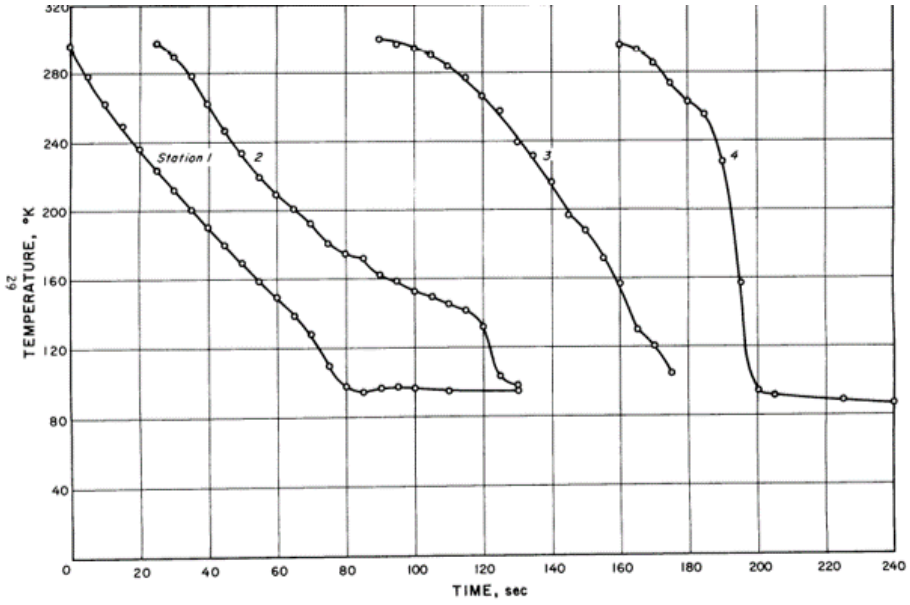

Figure 4.33. T_{wall} history with saturated LN_2 at $p_{in} = 3.4atm$, experimental case.

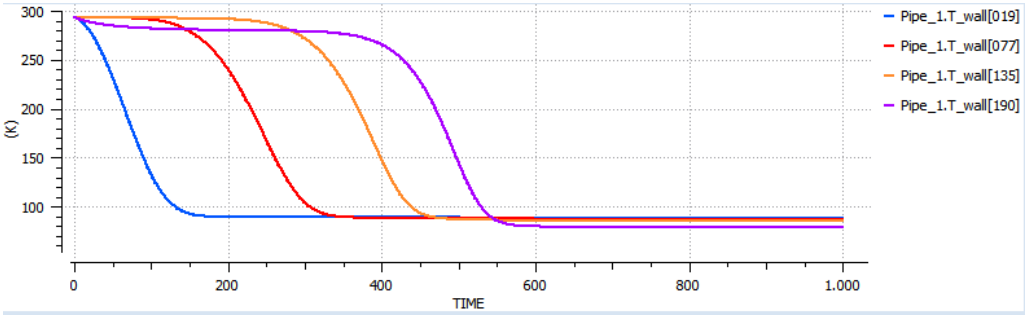

Figure 4.34. $T_{wall} = f(t)$ with saturated LN_2 at $p_{in} = 3.4atm$, EcosimPro.

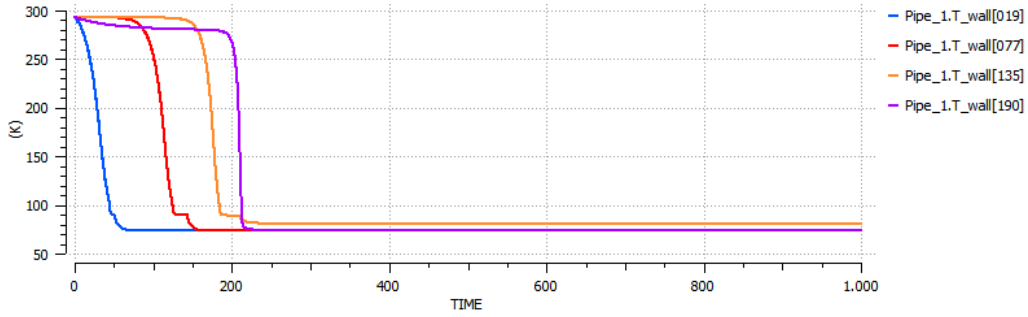

Figure 4.35. $T_{wall} = f(t)$ with subcooled LN_2 at $p_{in} = 3.4atm$, EcosimPro.

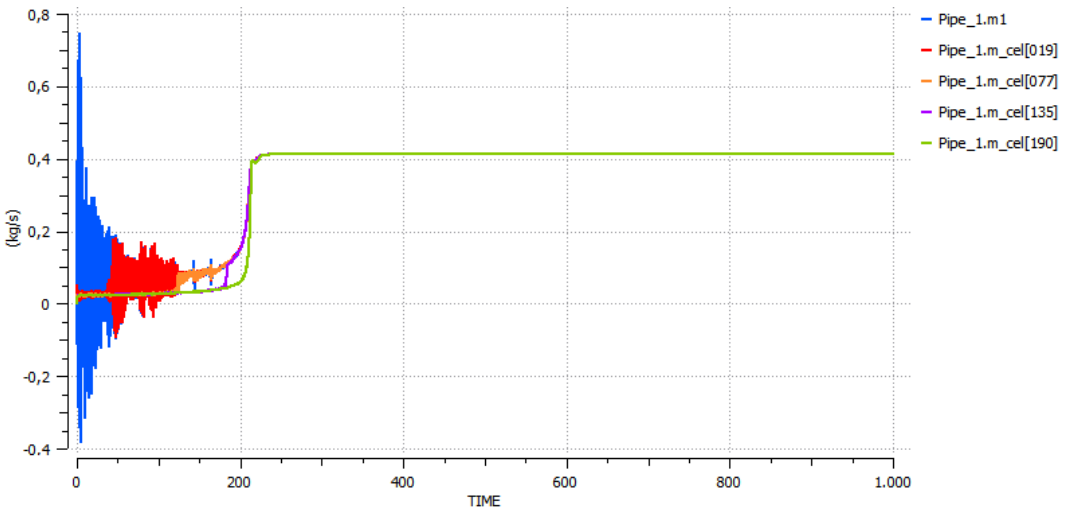

Figure 4.36. Mass flow rate $\dot{m}$ history with subcooled LN_2 at $p_{in} = 3.4atm$, EcosimPro.

$$T_{in,sub} = 76\text{K} \rightarrow m_{consumption} = 25.2802\text{Kg},\ \Delta t_{cooling} \cong 220\text{s}$$

Saturated LN_2, $p_{in} = 5.9$ atm

- Inlet driving pressure $p_{in} = 5.9\text{atm} = 597817.5\text{Pa} \rightarrow T_{in,sat} = 96.332\text{K}$
- Ambient temperature $T_{out} = T_{amb} = 293\text{K}$

In the interest of brevity, only the graphs corresponding to the subcooled condition have been presented, as they align with the experimental chill-down times.

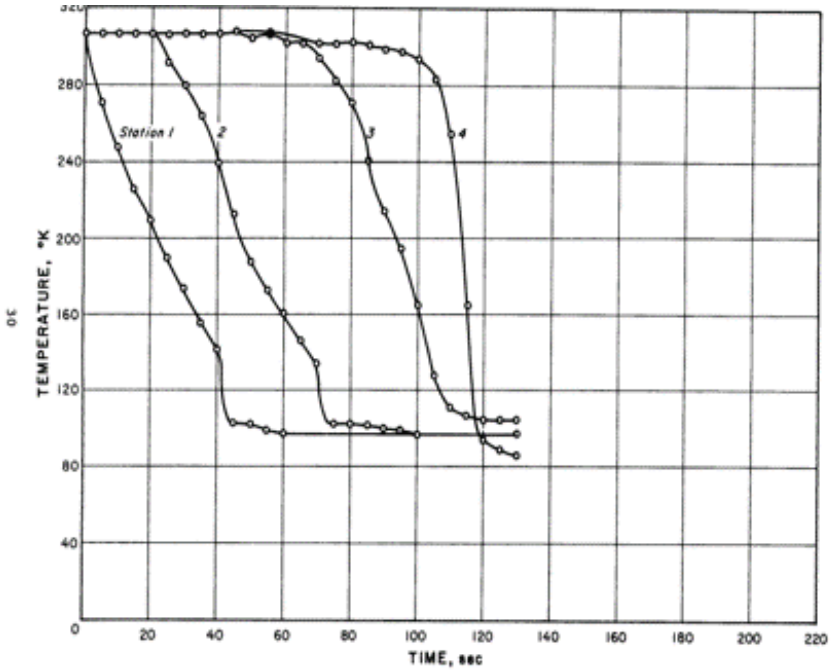

Figure 4.37. T_{wall} history with saturated LN_2 at $p_{in} = 5.9atm$, experimental case.

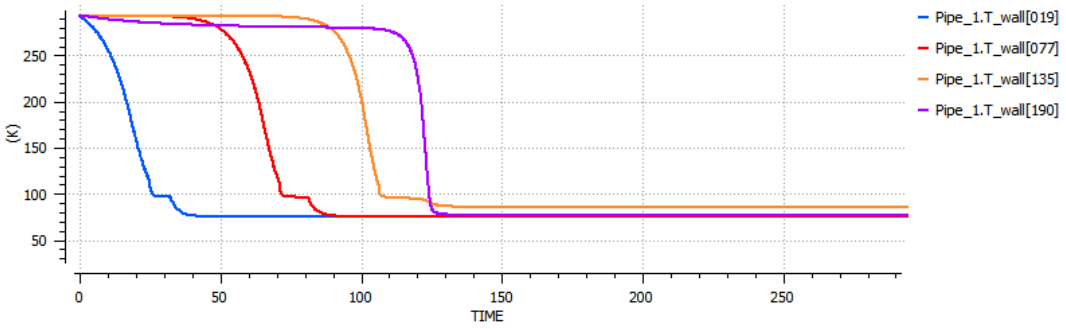

Figure 4.38. $T_{wall} = f(t)$ with subcooled LN_2 at $p_{in} = 5.9atm$, EcosimPro.

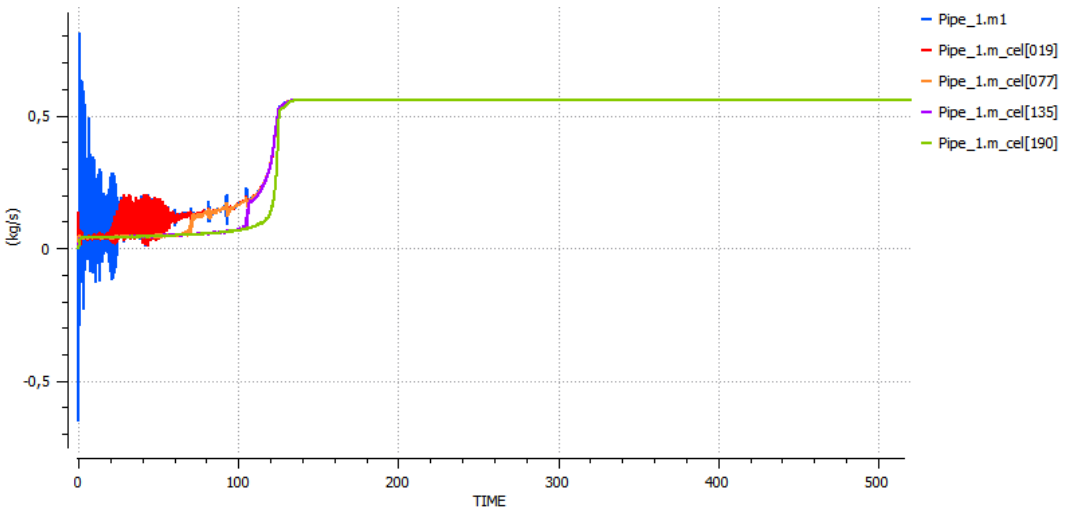

Figure 4.39. Mass flow rate $\dot{m}$ history with subcooled LN_2 at $p_{in} = 5.9atm$, EcosimPro.

$$T_{in,sub} = 76\text{K} \rightarrow m_{consumption} = 16.00367\text{Kg},\ \Delta t_{cooling} \cong 136\text{s}$$

Subcooled LN_2, $p_{in} = 4.2$ atm

- Inlet driving pressure $p_{in} = 4.2\text{atm} = 425565\text{Pa}$
- Inlet liquid temperature $T_{in,sub} = 76\text{K}$
- Ambient temperature $T_{out} = T_{amb} = 293\text{K}$

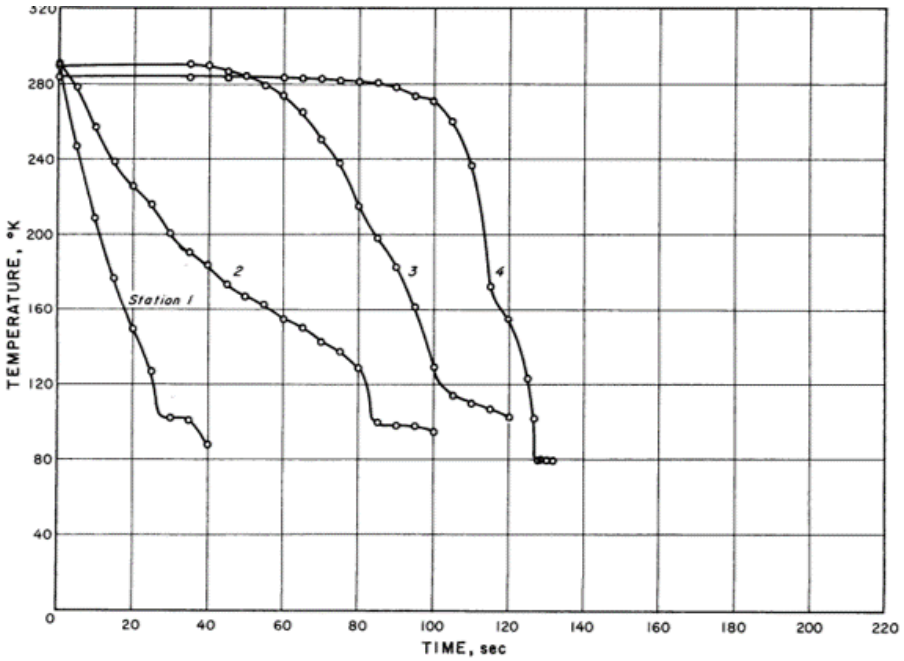

Figure 4.40. T_{wall} history with subcooled LN_2 at $p_{in} = 4.2atm$, experimental case.

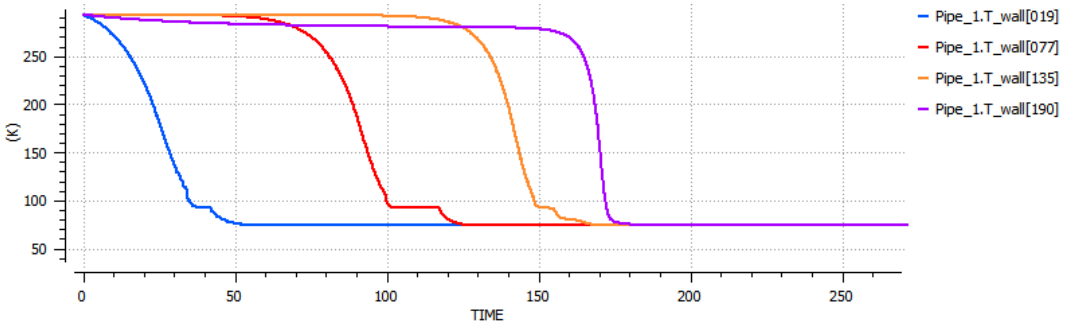

Figure 4.41. $T_{wall} = f(t)$ with subcooled LN_2 at $p_{in} = 4.2atm$, EcosimPro.

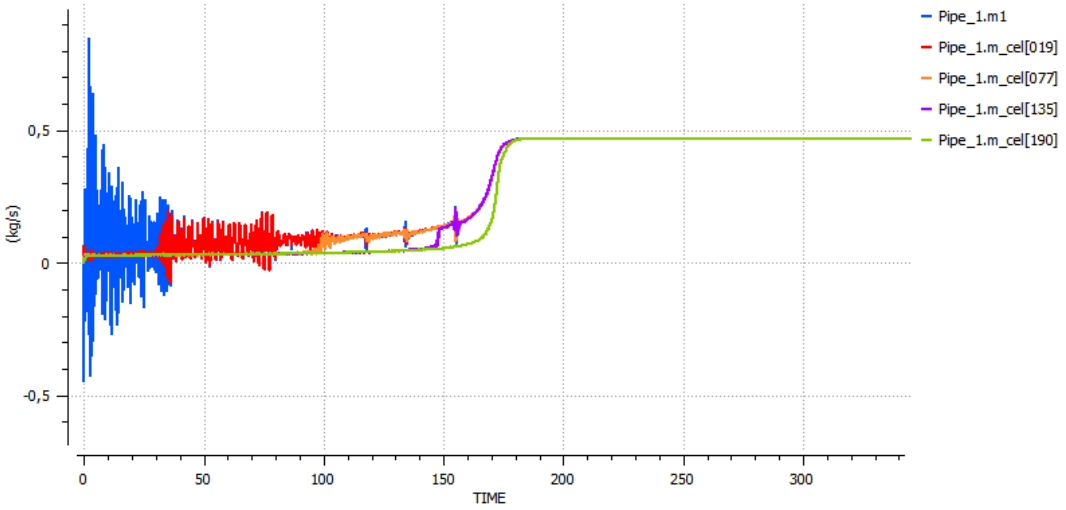

Figure 4.42. Mass flow rate $\dot{m}$ history with subcooled LN_2 at $p_{in} = 4.2atm$, EcosimPro

$$T_{in,sub} = 76\text{K} \rightarrow m_{consumption} = 14.26432\text{Kg},\ \Delta t_{cooling} \cong 179\text{s}$$

Subcooled LN_2, $p_{in} = 5.9$ atm

- Inlet driving pressure $p_{in} = 5.9\text{atm} = 597817.5\text{Pa}$
- Inlet liquid temperature $T_{in,sub} = 76\text{K}$
- Ambient temperature $T_{out} = T_{amb} = 293\text{K}$

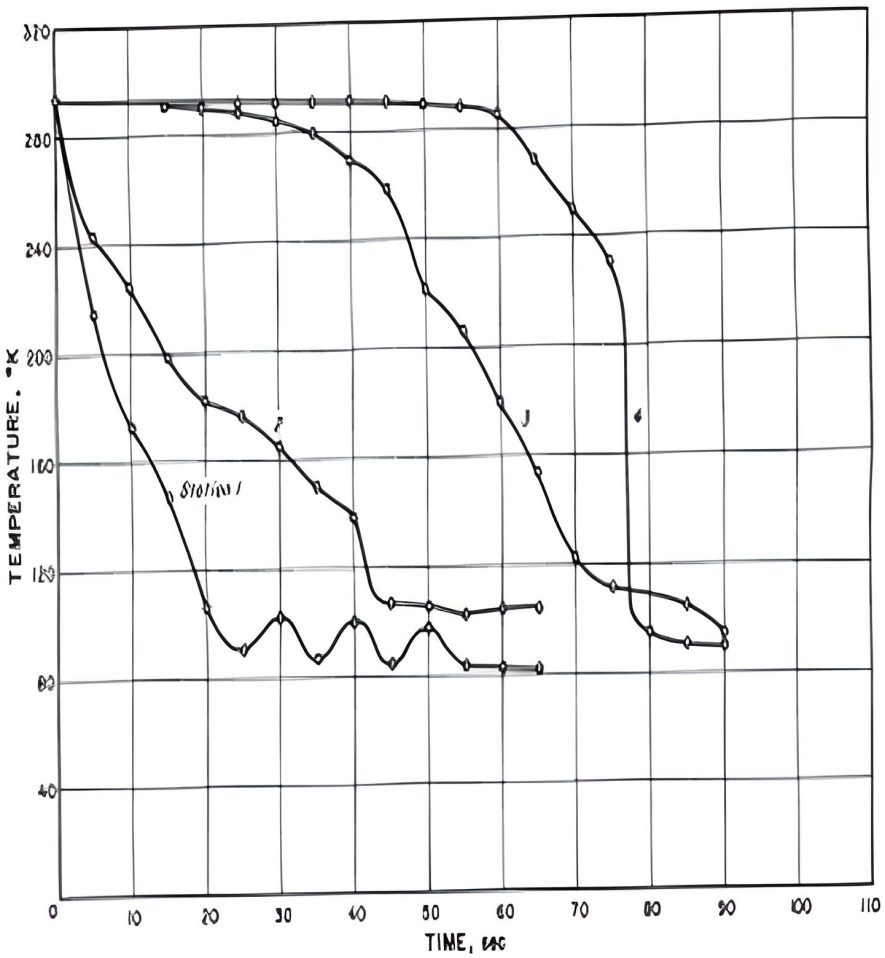

Figure 4.43. T_{wall} history with subcooled LN_2 at $p_{in} = 5.9atm$, experimental case.

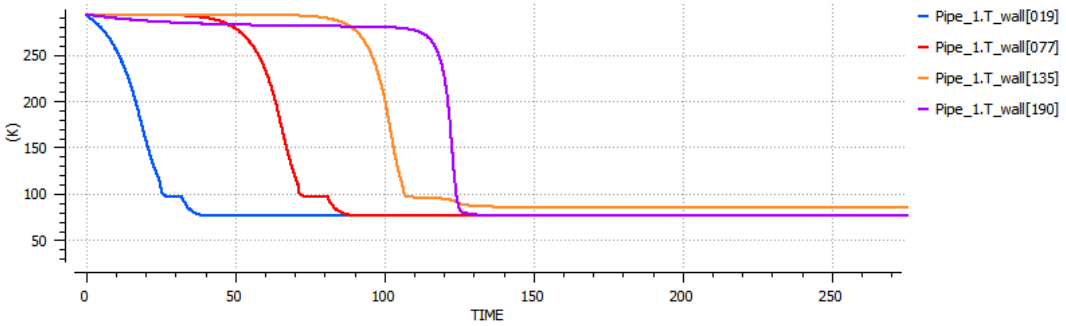

Figure 4.44. $T_{wall} = f(t)$ with subcooled LN_2 at $p_{in} = 5.9atm$, EcosimPro.

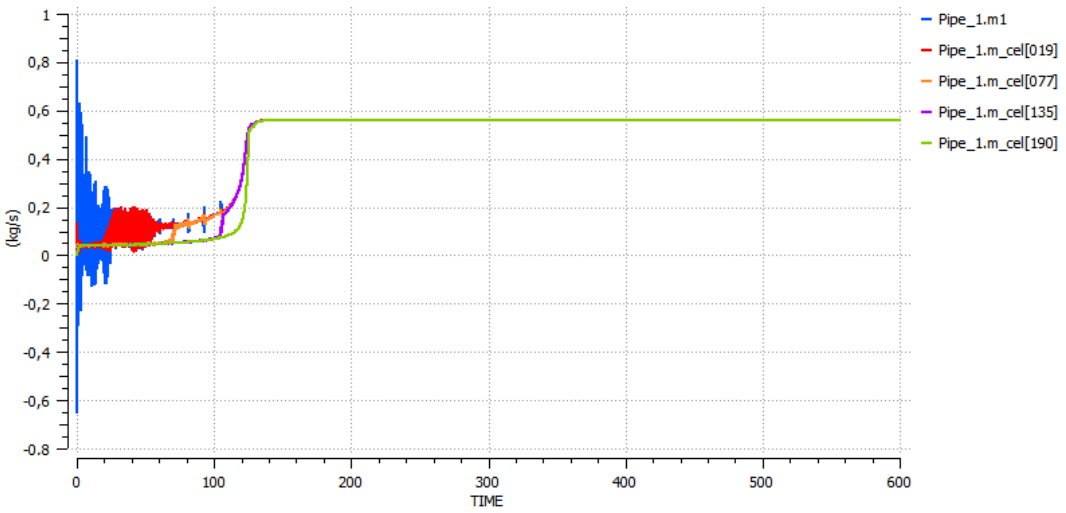

Figure 4.45. Mass flow rate $\dot{m}$ history with subcooled LN_2 at $p_{in} = 5.9atm$, EcosimPro.

$$T_{in,sub} = 76\text{K} \rightarrow m_{consumption} = 16.00367\text{Kg},\ \Delta t_{cooling} \cong 135\text{s}$$

4.2.3 Conclusions about test case 1

Conclusions drawn from the simulation of test case 1 are as follows:

- EcosimPro does not simulate the subcooling state well. The numerical oscillations of mass flow rate are too large and the transient behavior is excessively unstable. On the other hand, it simulates the saturation state well, which is much smoother and numerically cleaner.
- EcosimPro does not work well with liquid nitrogen. The chill-down times do not coincide with the experimental ones. The problem with the subcooling state is further aggravated with LN_2.
- EcosimPro does not take into account the right concavity changes of the $T_{wall} = f(t)$ curves, which are too linear and similar to the different nodes. These concavity changes are related to the phase changes of the flow, and thus the software does not simulate the real flow behavior, which is the same for several cells along the pipe.

Physical observations include:

- The chill-down times are much greater for LN_2 than LH_2, even though liquid nitrogen has greater absorbency characteristics, because ΔT between fluid and wall is greater.
- The propellant consumption is higher for nitrogen than for hydrogen ($\cong$ 20kg vs 2kg), both because ΔT is higher (consequently $\Delta t_{cooling}$ higher) and because LN_2 is denser.

- The mass flow rate curve related to the last tube detection station (e.g. green curve in 4.45), in the subcooled condition, does not present excessive oscillations. This is because the fluid does not reach subcooled but saturated at the last cell, hence the curve relative to the last cell is appreciable even if in subcooling conditions.

Similar analysis was also carried out with the inlet valve area $A_{0_{valve,2}} = 5.0671 \cdot 10^{-4} m^2$ (D=2.54cm), and the results were consistent with the previously reported conclusions. However, for the sake of brevity, these results have not been included in this report.

4.3 Test case 2

The second experimental test case, described in A.K.Shukla et al. [2017], was also simulated using EcosimPro. The schematic of the experimental setup is shown in figure 4.46, and consists of a liquid nitrogen (LN_2) Dewar pressurized with high pressure gaseous nitrogen (GN_2) cylinder. Two test sections, denoted as S_1 and S_2, are made of seamless stainless steel 304 tubes, with inner diameters ID of 13.5 mm and 21 mm and wall thicknesses t_{wall} of 1.2 mm and 2 mm, respectively. The experiments were carried out for different mass flow rates of $10\frac{g}{s}$ and $66\frac{g}{s}$ and inlet pressure values, all using liquid nitrogen LN_2 as the working fluid.

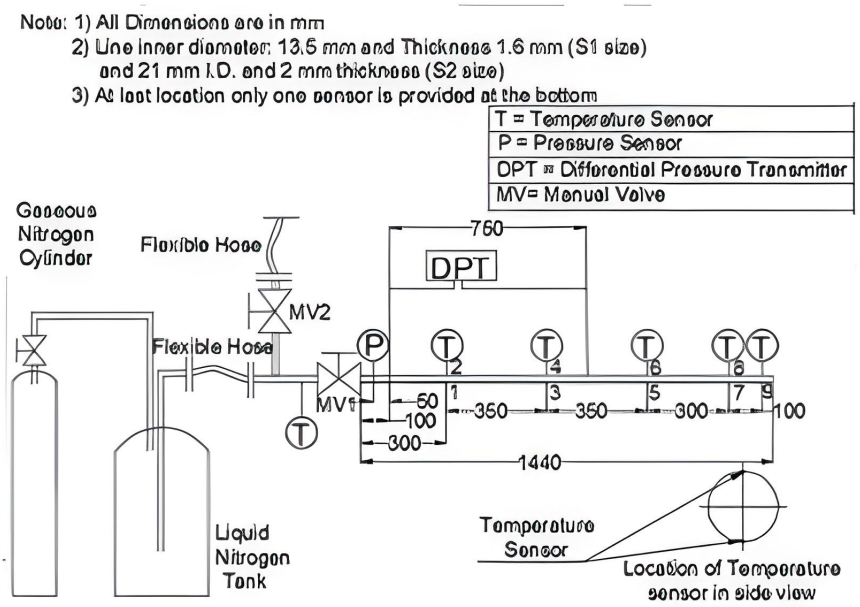

Figure 4.46. Schematic of the test setup with instrumentation details of the test section.

Three temperature sensors were placed at three different axial locations along the test sections, namely 300mm, 650mm, and 1300mm from the inlet for both line sizes S_1 and S_2. In the case of test section S_1, these detection stations correspond to nodes 2-3, 5,

and 10 in EcosimPro, where 11 nodes were set. For test section S_2, the detection stations correspond to nodes 1-2, 3, and 6, and the number of nodes set in EcosimPro is 7.

The chill-down technique simulated in this test case is the Full Flush Flow method.

The following table presents the experimental conditions extracted from the paper:

S $[-]$	L $[mm]$	ID $[mm]$	t_{wall} $[mm]$	material $[-]$	$A_{inlet_{valve}}$ $[mm^2]$	working fluid $[-]$	$\dot{m}$ $[\frac{g}{s}]$	p_{out} $[atm]$
S_1	1440	13.5	1.2	stainless steel 304	$1.431 \cdot 10^{-4}$	LN_2	10 or 66	0.1
S_2	1440	21	2	stainless steel 304	$3.4636 \cdot 10^{-4}$	LN_2	10 or 66	0.1

Table 4.2. Case 2 experimental conditions

The boundary conditions for both test sections S_1 and S_2 are as follows:

- The inlet LN_2 temperature is set to $T_{in} = 76$K.
- The ambient temperature, which is the initial wall temperature, is set to $T_{out} = T_{amb} = 293.15$K.

4.3.1 Test Section S_1, mass flow rate $\dot{m}_1 = 10\frac{g}{s}$

Two pieces of information missing from the paper have been determined for the simulations. The first one is the valve stroke, which has been set to 0.22, resulting in a valve stroke area of $A_0 = 0.22 \cdot A_{in} = 0.22 \cdot (1.431 \cdot 10^{-4} m^2) = 3.1482 \cdot 10^{-5} m^2$. This choice was made to ensure that the simulated mass flow rate value at steady state matches the experimental one, which is constrained to $\dot{m} = 10$ or $66\frac{g}{s}$.
The stroke value will remain constant for all tests.

The second missing information is the inlet driving pressure, which has been set to the saturation pressure of the fluid at $T_{in} = 76K$. This is because EcosimPro has been found to perform well in saturation condition.

The inlet driving pressure is $p_{in} = p_{sat} = 86101.932$Pa.

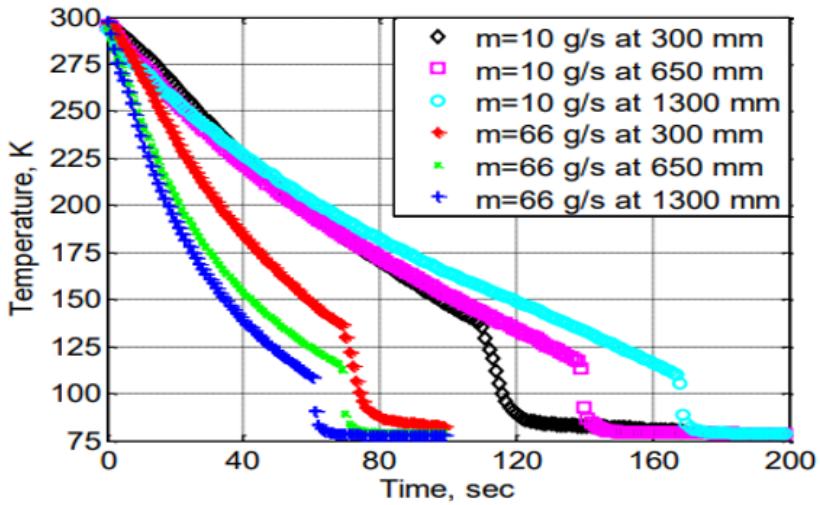

Figure 4.47. $T_{wall} = f(t)$ history for LN_2, test section S_1, experimental case.

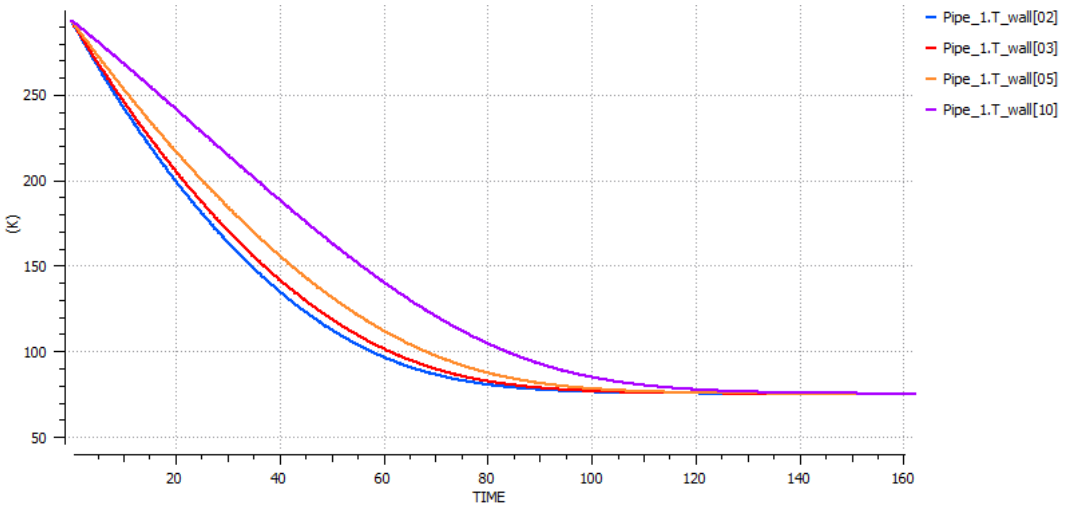

Figure 4.48. $T_{wall} = f(t)$ history for LN_2, test section S_1, $\dot{m}_1 = 10\frac{g}{s}$, EcosimPro.

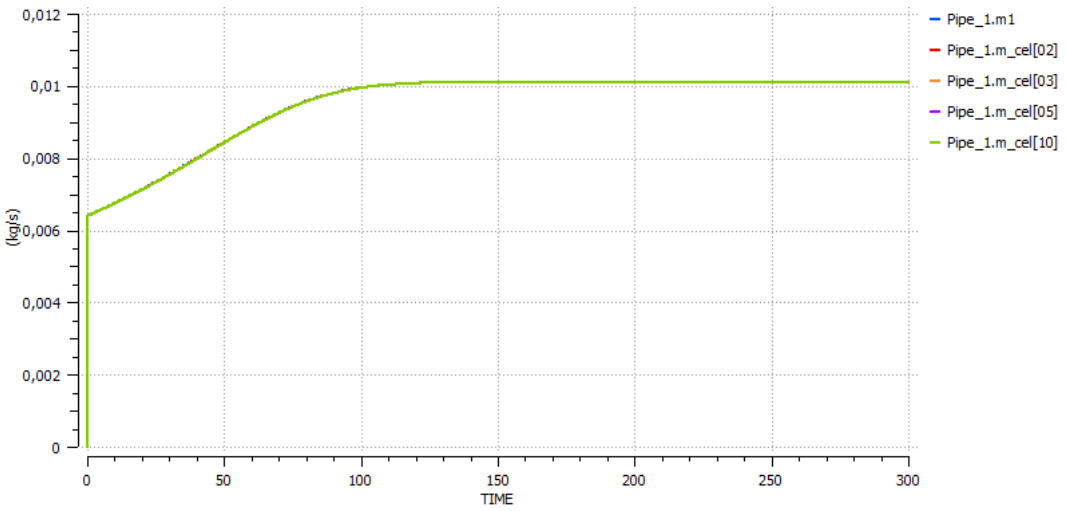

Figure 4.49. Mass flow rate $\dot{m}$ history for LN_2, test section S_1, $\dot{m}_1 = 10\frac{g}{s}$, EcosimPro.

4.3.2 Test Section S_1, mass flow rate $\dot{m}_2 = 66\frac{g}{s}$

To achieve a mass flow rate of $66\frac{g}{s}$ in test section S_1 with an inlet fluid temperature of $T_{in} = 76K$, the inlet pressure p_{in} was increased to 0.85atm. This was necessary to ensure that the simulated mass flow rate value at steady state matched the experimental value, as the constraint was on $66\frac{g}{s}$.

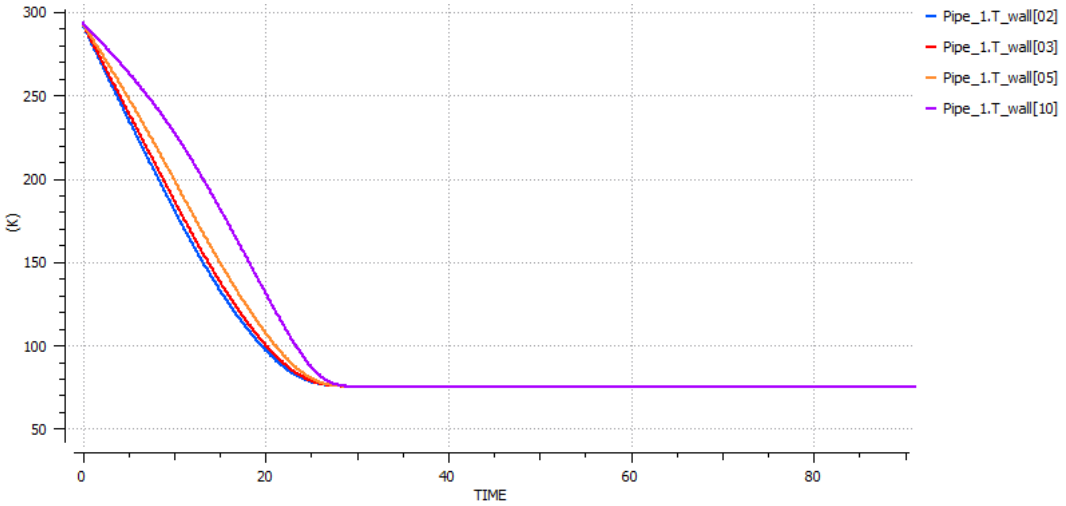

Figure 4.50. $T_{wall} = f(t)$ history for LN_2, test section S_1, $\dot{m}_2 = 66\frac{g}{s}$, EcosimPro.

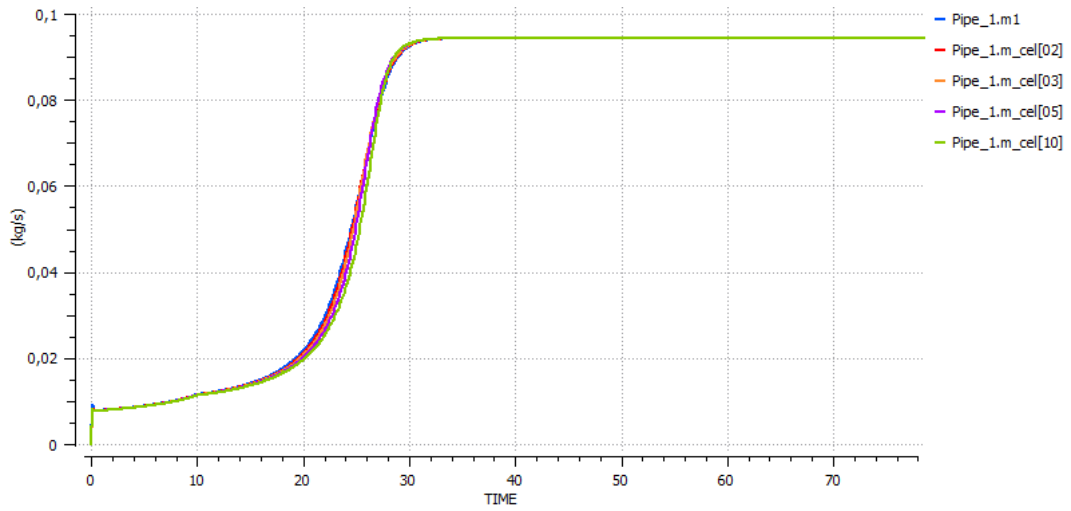

Figure 4.51. Mass flow rate $\dot{m}$ history for LN_2, test section S_1, $\dot{m}_2 = 66\frac{g}{s}$, EcosimPro.

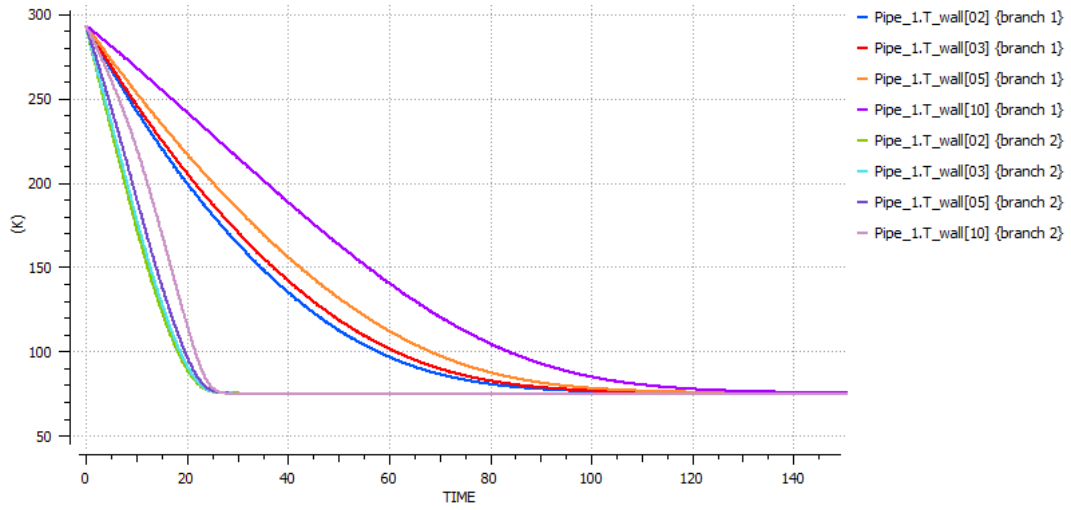

Figure 4.52. $T_{wall} = f(t)$ history for LN_2, test section S_1, $\dot{m}_1$ (branch 1) and $\dot{m}_2$ (branch 2), EcosimPro.

When comparing the experimental graph shown in Figure 4.47 with the simulation graph shown in Figure 4.52, the following observations can be made:

- $\Delta t_{cooling} \cong 130$s ($T_{in} = 76$K, $p_{in} = p_{sat}$, $\dot{m}_1$), in EcosimPro.
- $\Delta t_{cooling} \cong 200$s ($\dot{m}_1$), in experimental case.
- $\Delta t_{cooling} \cong 35$s ($T_{in} = 76K, p_{in} = 0.85$atm, $\dot{m}_2$), in EcosimPro.
- $\Delta t_{cooling} \cong 100$s ($\dot{m}_2$), in experimental case.

Relative errors on chill-down time, in EcosimPro:

$$\dot{m}_1, S_1 \rightarrow Err = 26.9\%$$
$$\dot{m}_2, S_1 \rightarrow Err = 75\%$$

4.3.3 Test Section S_2, mass flow rate $\dot{m}_1 = 10\frac{g}{s}$

For this test case, the reference is to the second row of Table 4.2.

The stroke of the valve is missing from the paper, but it is known that the simulated mass flow rate value at steady state must coincide with the experimental one, which is constrained to be $\dot{m} = 10$ (or 66)$\frac{g}{s}$. In order to achieve this, the stroke of the valve is set to 0.1, so that the valve stroke area is $A_0 = 0.1 \cdot A_{in} = 0.1 \cdot (3.4636 \cdot 10^{-4} m^2) = 3.4636 \cdot 10^{-5} m^2$. The valve stroke area is kept fixed for all tests.

The inlet driving pressure is also missing from the paper, but it is set to the saturation pressure of the fluid at $T_{in} = 76K$, since EcosimPro works well in saturation condition. Therefore, $p_{in} = p_{sat} = 86101.932$Pa.

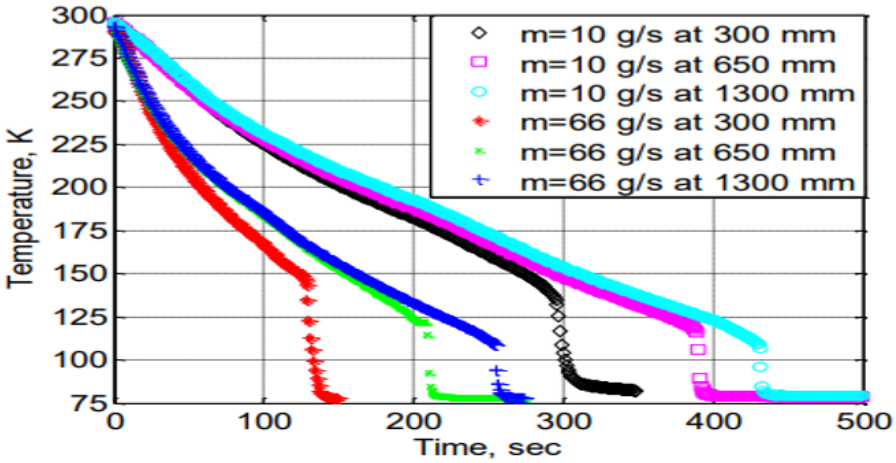

Figure 4.53. $T_{wall} = f(t)$ history for LN_2, test section S_2, experimental case.

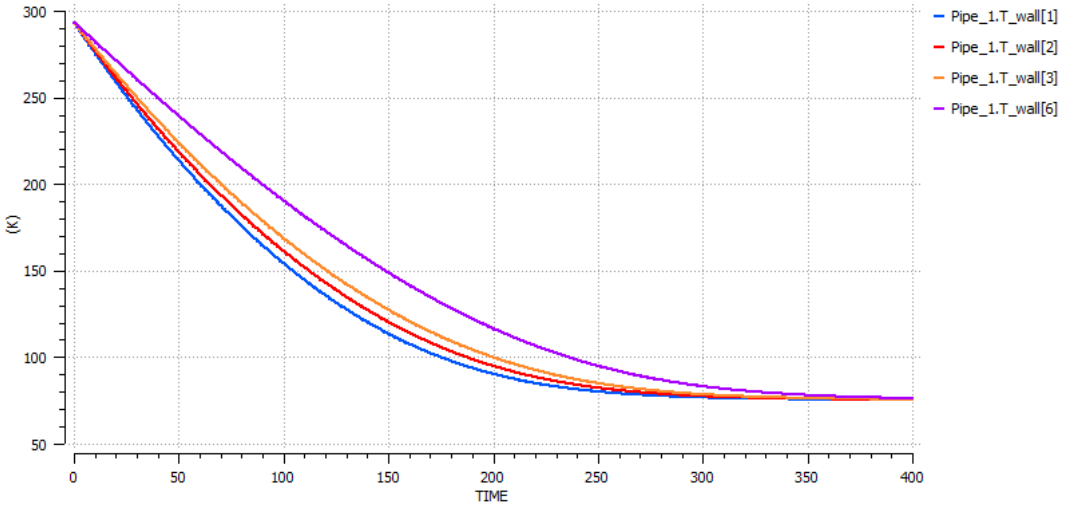

Figure 4.54. $T_{wall} = f(t)$ history for LN_2, test section S_2, $\dot{m}_1 = 10\frac{g}{s}$, EcosimPro.

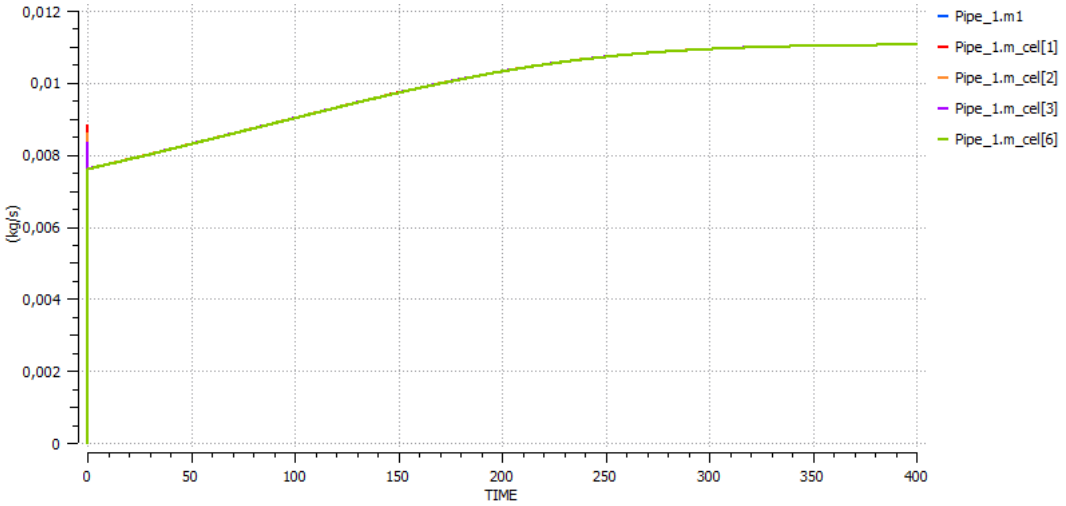

Figure 4.55. Mass flow rate $\dot{m}$ history for LN_2, test section S_2, $\dot{m}_1 = 10\frac{g}{s}$, EcosimPro.

4.3.4 Test Section S_2, mass flow rate $\dot{m}_2 = 66\frac{g}{s}$

To meet the constraint of $66\frac{g}{s}$ while maintaining the same test section S_2 and inlet fluid temperature $T_{in} = 76$K, the inlet pressure p_{in} was increased to 0.85atm.

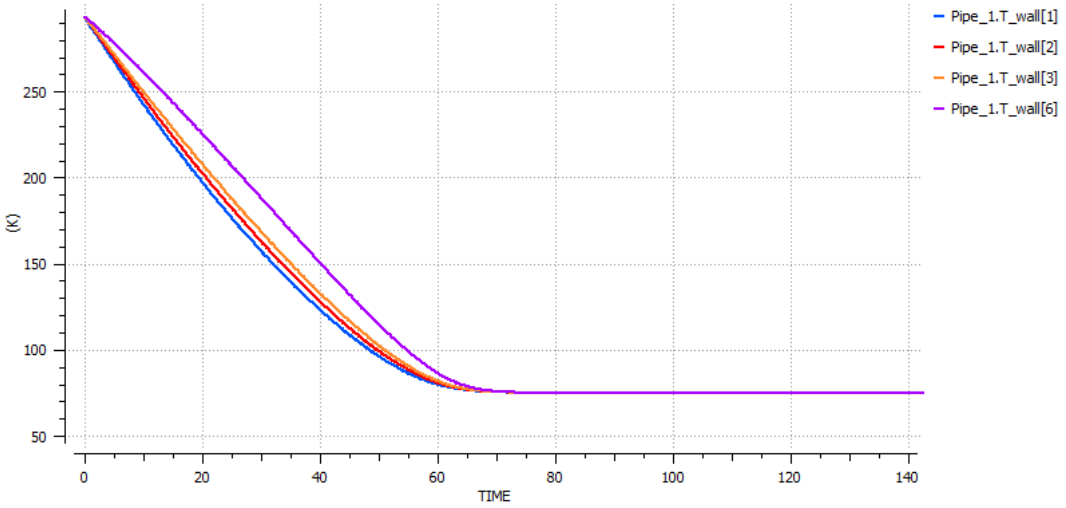

Figure 4.56. $T_{wall} = f(t)$ history for LN_2, test section S_2, $\dot{m}_2 = 66\frac{g}{s}$, EcosimPro.

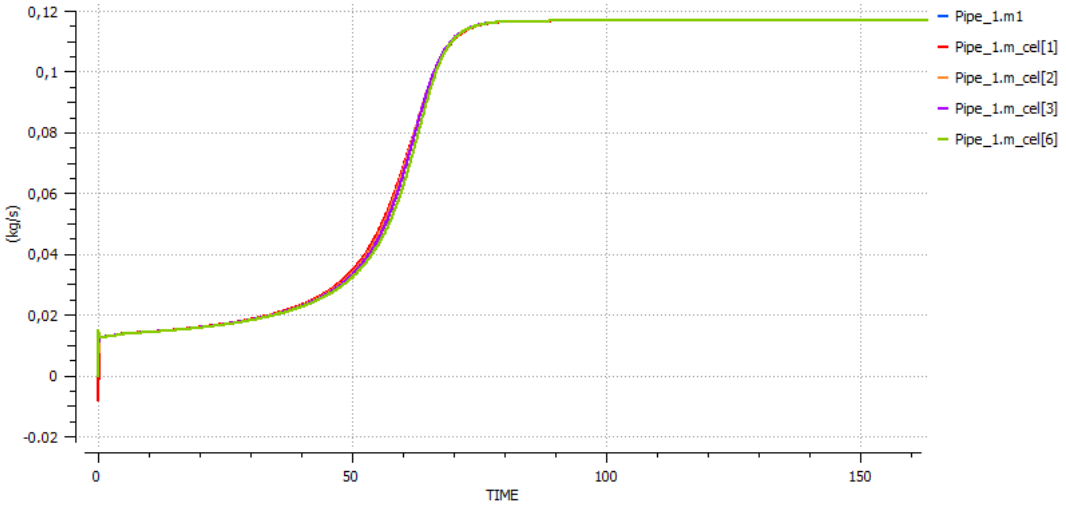

Figure 4.57. Mass flow rate $\dot{m}$ history for LN_2, test section S_2, $\dot{m}_2 = 66\frac{g}{s}$, EcosimPro.

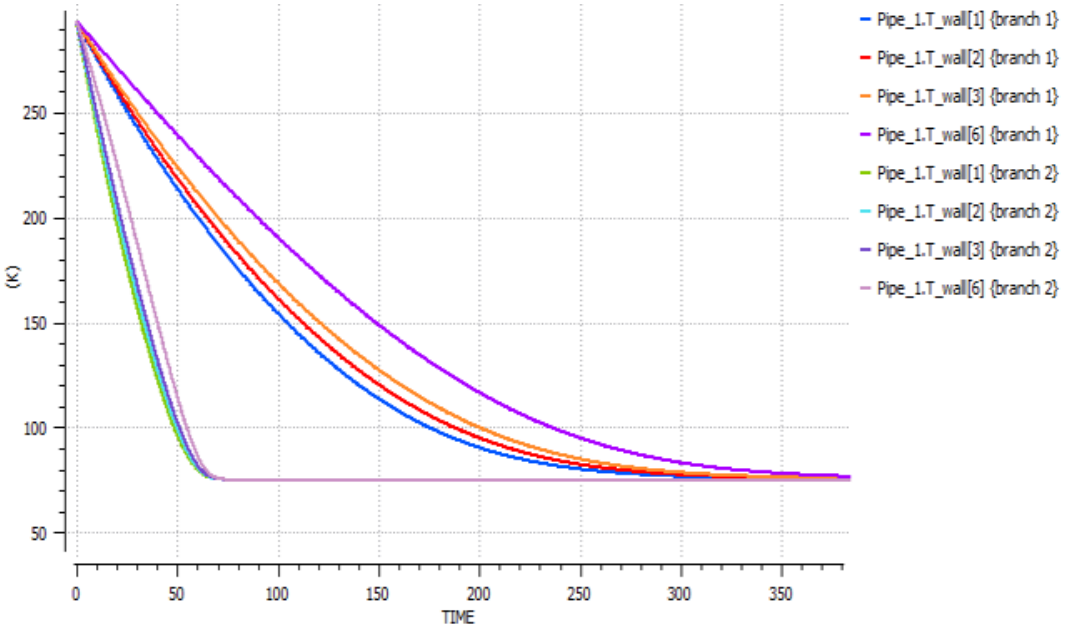

Figure 4.58. $T_{wall} = f(t)$ history for LN_2, test section S_2, $\dot{m}_1$ (branch 1) and $\dot{m}_2$ (branch 2), EcosimPro.

When comparing the experimental graph shown in Figure 4.53 with the simulation graph shown in Figure 4.57, the following observations result:

- $\Delta t_{cooling} \cong 400$s ($T_{in} = 76$K, $p_{in} = p_{sat}$, $\dot{m}_1$), in EcosimPro.
- $\Delta t_{cooling} \cong 500$s ($\dot{m}_1$), in experimental case.
- $\Delta t_{cooling} \cong 90$s ($T_{in} = 76$K, $p_{in} = 0.85$atm, $\dot{m}_2$), in EcosimPro.
- $\Delta t_{cooling} \cong 250$s ($\dot{m}_2$), in experimental case.

Relative errors on chill-down time, in EcosimPro:

$$\dot{m}_1, S_2 \rightarrow Err = 12.5\%$$
$$\dot{m}_2, S_2 \rightarrow Err = 88\%$$

4.3.5 Conclusions about test case 2

In test case 2, it is evident from the comparison between the simulation results obtained using EcosimPro and the experimental data (particularly, see figures 4.52 and 4.58) that EcosimPro underestimates the chill-down times. This leads to an underestimation of the propellant consumption required for cooling the transfer lines.
These discrepancies become more pronounced as the length of the pipes increases and under microgravity conditions ($\approx 0 - g$).

4.4 Test case 3

The third test case simulated in EcosimPro corresponds to an experimental analysis conducted by Yuan et al. [2008]. This experiment was chosen to demonstrate the limitations of EcosimPro in accurately evaluating the effects of gravity on the chill-down process. The following table presents the information available from the paper related to the test section employed.

L $[cm]$	ID $[cm]$	OD $[cm]$	t_{wall} $[mm]$	material $[-]$	working fluid $[-]$	$\dot{m}$ $[\frac{g}{s}]$	gravity conditions $[-]$	$Stroke_{Valve}$ $[-]$
70	0.432	0.635	1.015	stainless steel	LN_2	$40\frac{g}{s}$	$0-g$ or $1-g$	1

Table 4.3. Case 3 experimental conditions

The test section was mounted vertically inside a vacuum jacket, and saturated liquid nitrogen was injected from the beginning of the test section while the end of the test section was opened to the atmosphere.
In EcosimPro, the stroke of the valve has been set equal to 1 since the experimental setup does not have any valves, and therefore the flow passage area is equal to the area of the tube.
Two thermocouples were positioned respectively at 20cm and 30cm from the pipe inlet, which correspond to nodes 3 and 4 in EcosimPro, where 8 cells have been established.

The boundary conditions for the experiment include:

- Inlet fluid temperature at the saturation temperature of LN_2 at atmospheric pressure $p_{in} = 1$atm, resulting in $T_{in} = T_{sat} = 77.355$K.
- The ambient or room temperature is $T_{out} = T_{amb} = 293$K, which is the initial wall temperature.
- The inlet driving pressure is $p_{in} = 1$atm.
- The outlet pressure is $p_{out} = 0.1$atm.

4.4.1 Saturated LN_2, gravity condition $1-g$

The experimental conditions from the paper, p_{in} and T_{sat}, were applied to the simulation. However, the simulation results did not match the mass flow rate constraint of $40\frac{g}{s}$, yielding a mass flow rate of $\dot{m} = 3.3\frac{g}{s}$ and a chill-down time of $\Delta t_{cooling} \cong 40$s.
To satisfy the mass flow rate constraint, the inlet driving pressure was increased to $p_{in} = 1.3$atm.

The following figures show the simulation results for a mass flow rate of $40\frac{g}{s}$ under $1-g$ conditions:

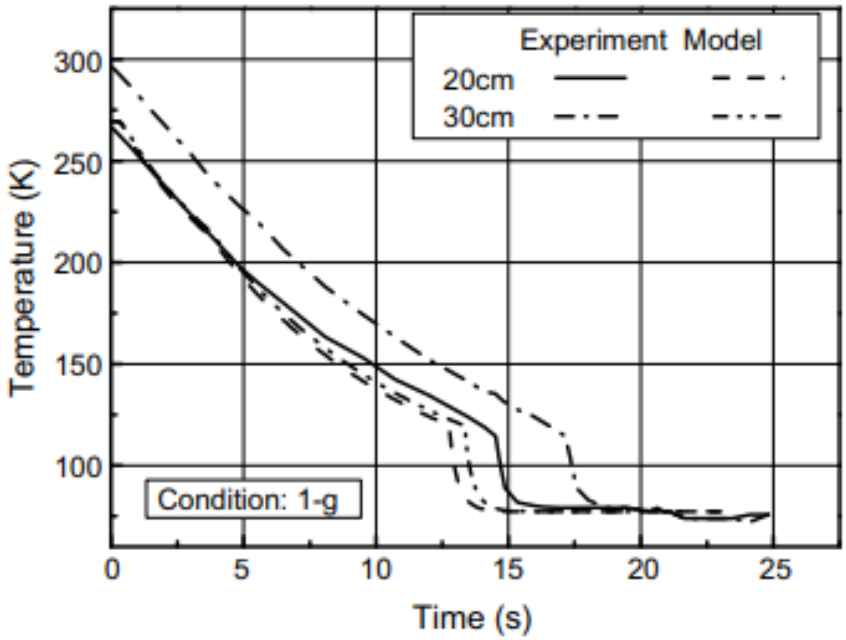

Figure 4.59. $T_{wall} = f(t)$ history under $1-g$ condition, flow rate of $40\frac{g}{s}$, experimental case.

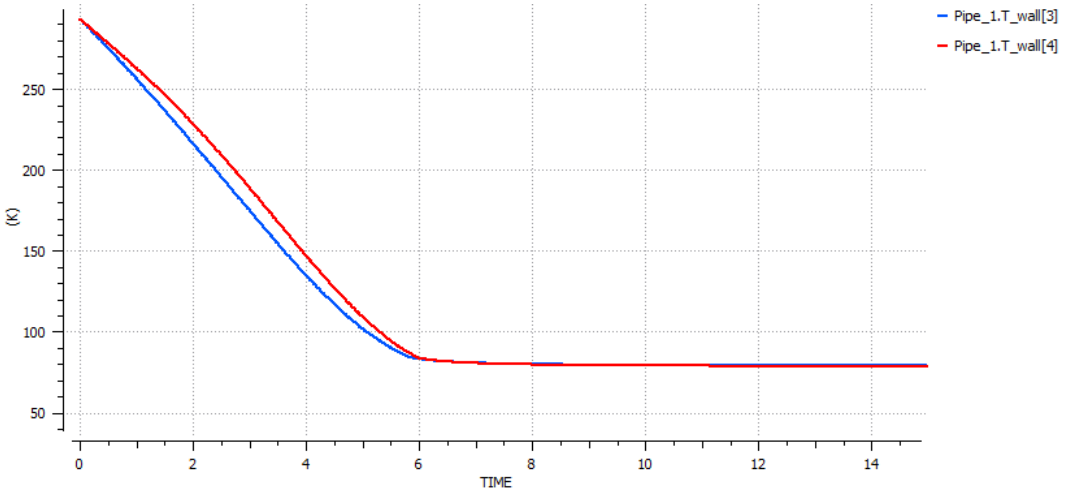

Figure 4.60. $T_{wall} = f(t)$ history under $1-g$ condition, flow rate of $40\frac{g}{s}$, EcosimPro.

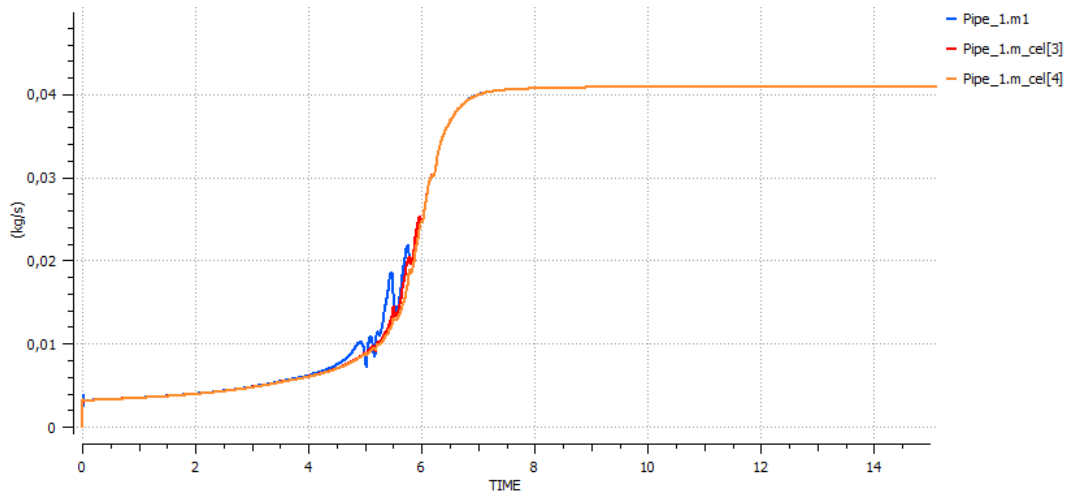

Figure 4.61. Mass flow rate $\dot{m}$ history under $1-g$ condition, flow rate of $40\frac{g}{s}$, EcosimPro.

It has been found again that EcosimPro underestimates the chill-down times, which leads to underestimation of propellant consumption as compared to the experimental results:

- $\Delta t_{cooling} = 17s$, experimental case;
- $\Delta t_{cooling} = 7s$, EcosimPro.

The relative error on the chill-down time is of the order of 70 % (71%).

4.4.2 Saturated LN_2, microgravity condition $0-g$

Under the experimental conditions outlined in the paper, with T_{sat} and $p_{in} = 1.3$atm to match the mass flow rate constraint of $40\frac{g}{s}$ and microgravity conditions ($\cong 0-g$), the simulation results are presented below.

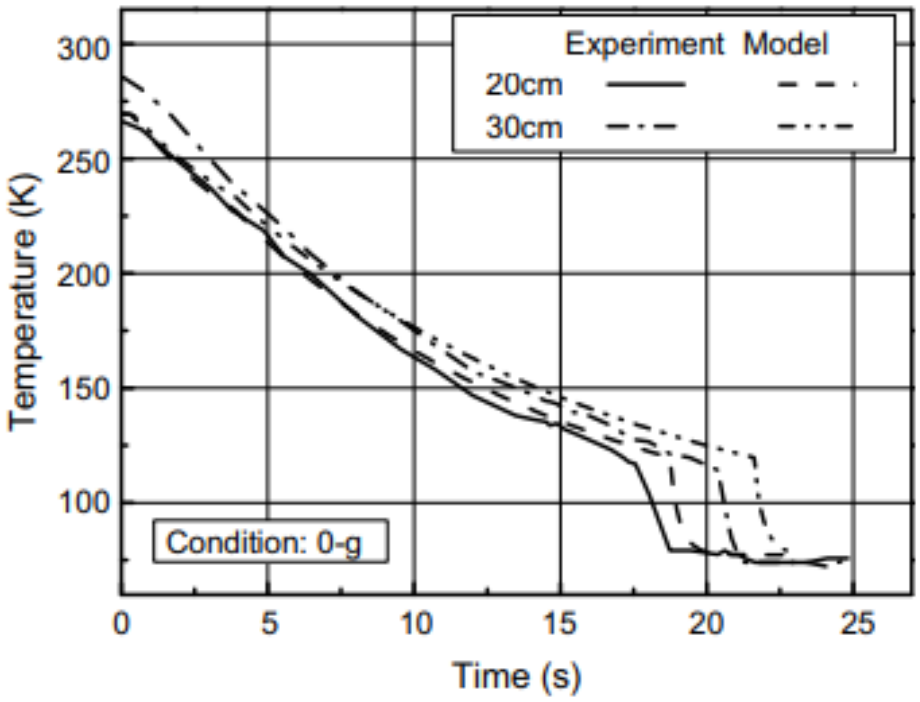

Figure 4.62. $T_{wall} = f(t)$ history under $0 - g$ condition, flow rate of $40\frac{g}{s}$, experimental case.

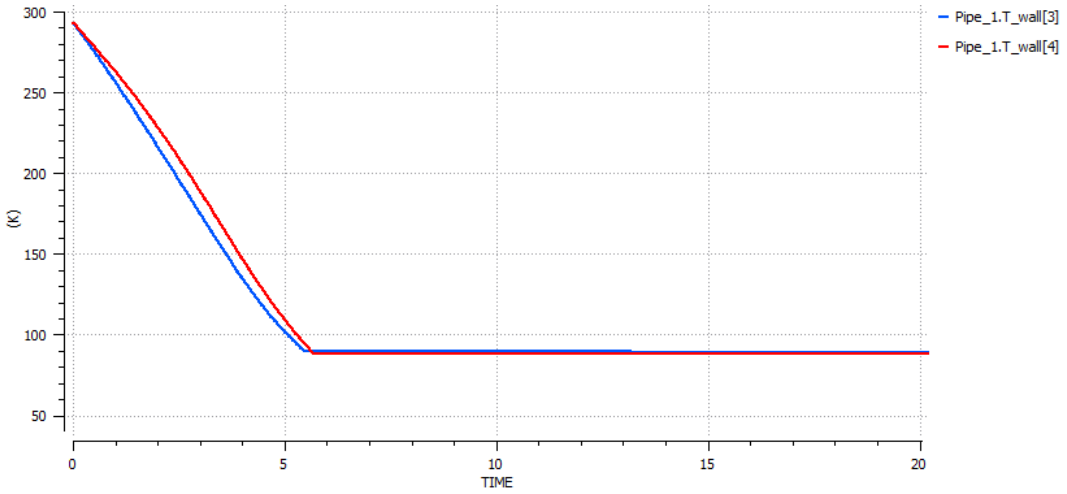

Figure 4.63. $T_{wall} = f(t)$ history under $0 - g$ condition, flow rate of $40\frac{g}{s}$, EcosimPro.

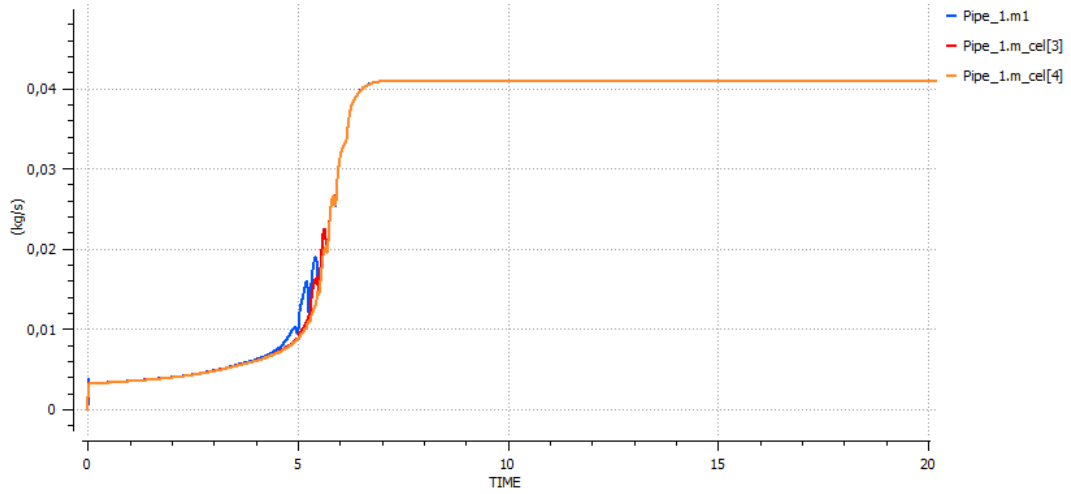

Figure 4.64. Mass flow rate $\dot{m}$ history under $0-g$ condition, flow rate of $40\frac{g}{s}$, EcosimPro.

The graphs show that EcosimPro does not account for the effects of gravity on the chill-down process. Experimentally (figures 4.59 and 4.62), passing from the $1-g$ to the $0-g$ condition shows an increase in cooling time from about $17s$ to $22s$ due to the increase in inlet pressure p_{in} under gravitational acceleration g ($p_{in} = p_{static} + \frac{1}{2}\rho \cdot v^2 + \Delta p_{1-g}$, where $\Delta p_{1-g} = \rho \cdot g \cdot z$). In other words, gravity aids the decrease in chill-down time. However, EcosimPro does not consider the effect of g on the driving pressure, and consequently, it underestimates the chill-down times. Furthermore, the software generally underestimates the chill-down times in gravity conditions, and this underestimation is further exacerbated in microgravity conditions.

Chill-down times in $0-g$:

- $\Delta t_{cooling} = 22s$, experimental case;
- $\Delta t_{cooling} = 7s$, EcosimPro.

This results in a relative error on chill-down time of 107%.

Furthermore, setting the chill-down time (rather than the flow rate) as the constraint to be respected, by lowering the inlet driving pressure, a reduction of the mass flow rate and consequently the propellant consumption can be obtained: $\dot{m} = 20\frac{g}{s}$ (fig. 4.65).

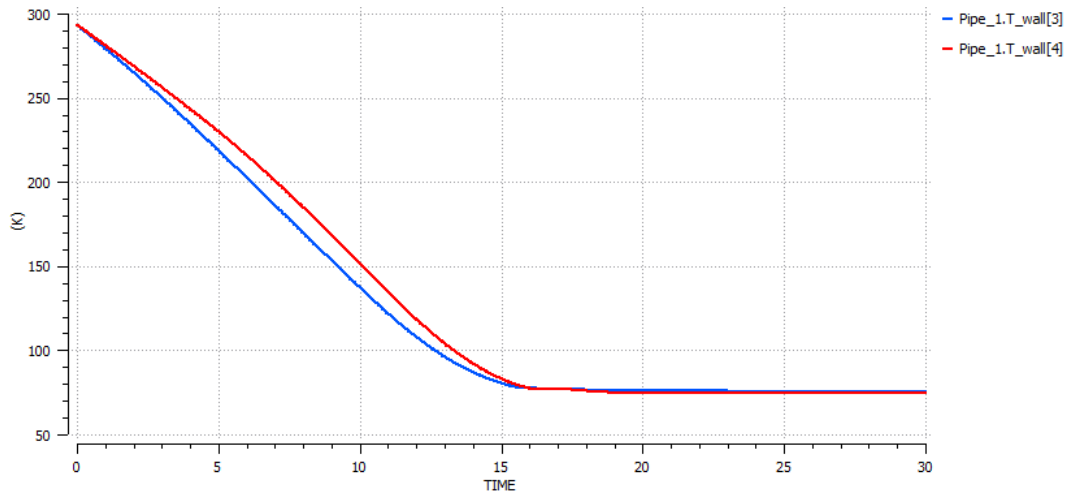

Figure 4.65. $T_{wall} = f(t)$ history under $0-g$ or $1-g$ condition, flow rate of $20\frac{g}{s}$, EcosimPro.

The last observation regarding the software is that it does not consider the effect of gravity in both saturation and subcooling conditions:

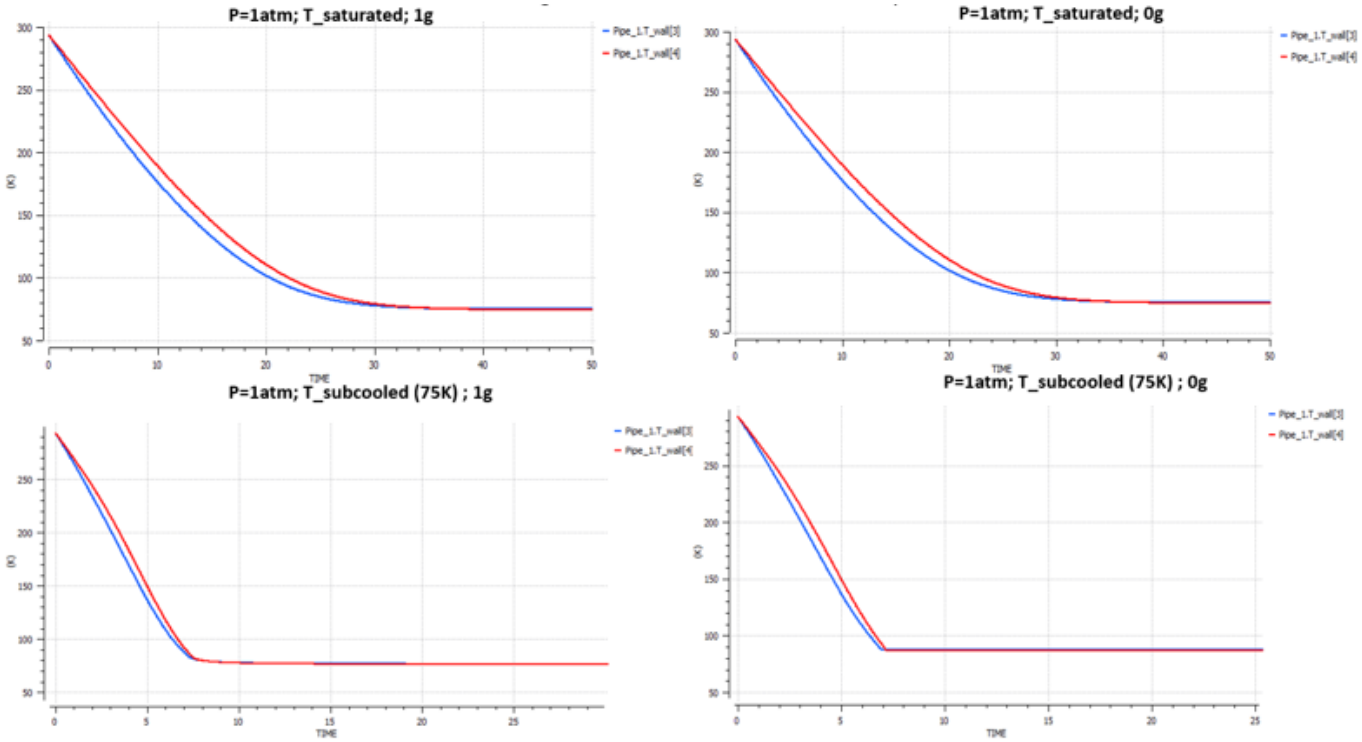

Figure 4.66. Gravitational acceleration effect: saturated v_s subcooled fluid, EcosimPro.

4.5 Test case 4

The next test case simulated in EcosimPro is the experimental analysis conducted by Jin et al. [2019], using liquid argon (LAr), and Jin et al. [2017], using liquid nitrogen (LN_2).

Although the working fluid differs, the experimental apparatus and procedure used in both studies are identical.
Figure 4.67 shows the schematic of the test setup and sensor locations used in the experiment.

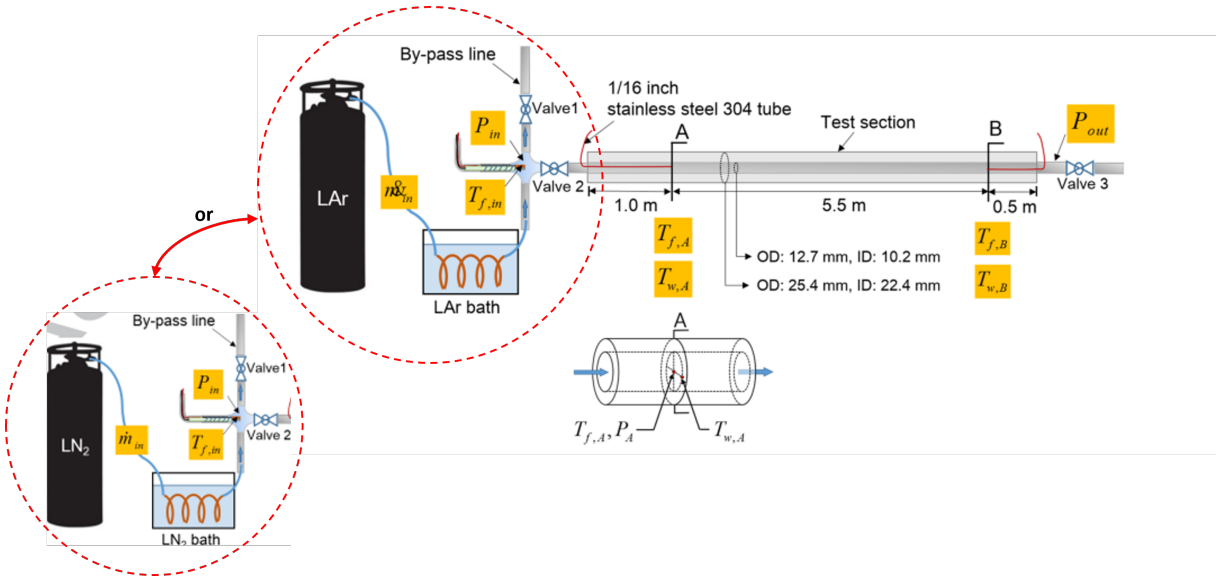

Figure 4.67. Schematic of the test setup and sensor locations.

The liquid working fluid that flows into the test section is subcooled in a LAr or LN_2 bath by saturated fluid at atmospheric pressure. The fluid is then vented to the atmosphere after cooling the test section. The line chill-down process begins when the inlet fluid is in a subcooled state, with valve 2 and valve 3 fully open and valve 1 closed. The chill-down technique employed is the full flush flow technique.

The information available from the paper related to the test section used in the experiment is presented in the following table.

L $[m]$	inner tube OD $[mm]$	inner tube ID $[mm]$	outer tube OD $[mm]$	outer tube ID $[mm]$	material $[-]$	working fluid $[-]$	p_{out} $[Pa]$
7	12.7	10.2	25.4	22.4	stainless steel 304	LAr or LN_2	0.07

Table 4.4. Case 4 experimental conditions

Two temperature sensors were used to measure the wall temperature T_{wall} and fluid temperature T_{fl} at Location A (1m away from the inlet) and Location B (6.5m away from the inlet) of the test section (Fig. 4.67). These two locations correspond to cells 10 and 65 of the EcosimPro pipe model, which has 69 nodes in total.
The paper provides the boundary conditions used in the experimental tests that were simulated in the software:

- Ambient/room temperature is $T_{out} = T_{amb} = 293$K, which is the initial wall temperature.
- Inlet fluid temperature is $T_{in} = T_{sub} = 92$K for LAr and $T_{in} = T_{sub} = 81 - 83$K for LN_2.
- Inlet driving pressure ranges from 236.7 to 505.5KPa for LAr and from 216.8 to 480.3KPa for LN_2.

The average mass flux is also given, but the valve area is unknown. In order to match the mass flow rate value with the given value in the paper, the valve area is set to $A_{valve,in} = 3.5 \cdot 10^{-6} m^2$.
Furthermore, although the inlet flow was subcooled for the experiment, it was decided to work in saturated conditions in the software since it handles saturated fluids well:
$p_{in} = p_{sat} \rightarrow T_{in} = T_{sat}$ (Antoine's equation).

4.5.1 Liquid Argon

Tuning case

Experimental conditions:

- $p_{in} = 382.6\text{KPa} \rightarrow T_{sat} = 102.15\text{K}$;
- Avg. mass flux $G = 60\frac{kg}{m^2 s}$.

Simulation results:

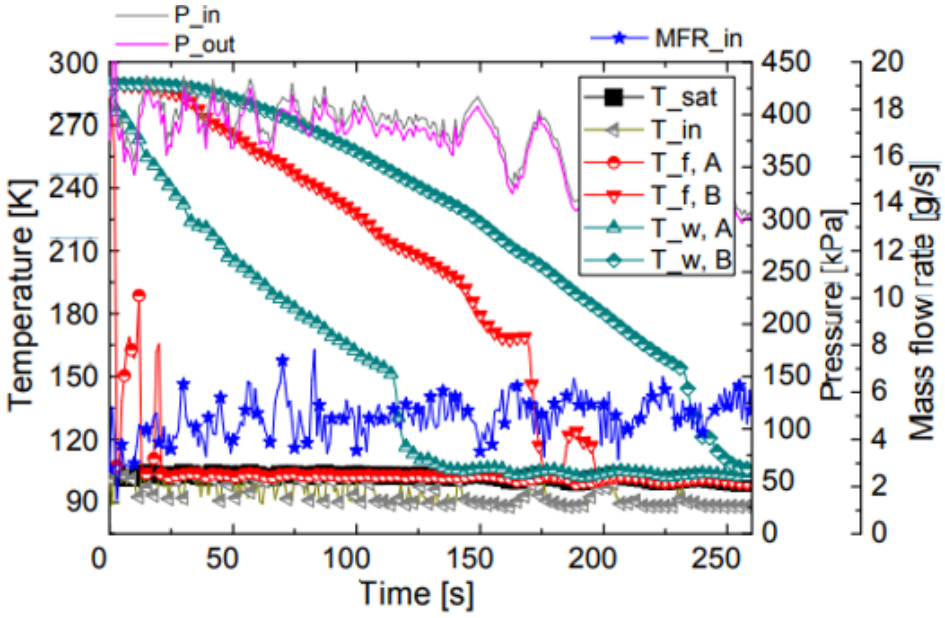

Figure 4.68. Time history of temperature, pressure and mass flow rate, experimental case.

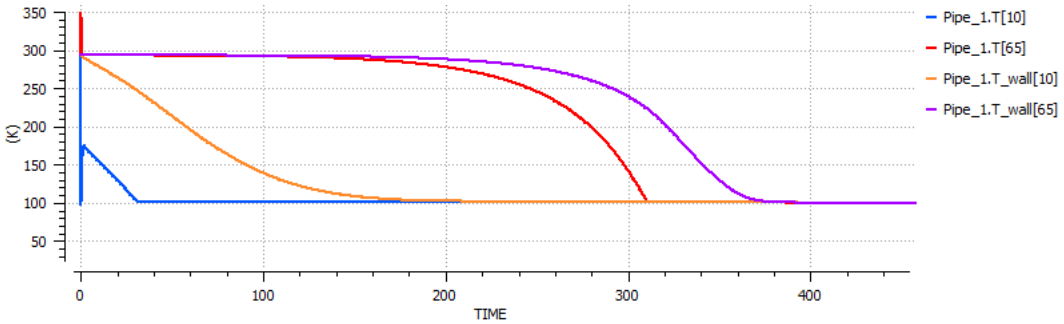

Figure 4.69. T_{fl} and T_{wall} time history, tuning case, in EcosimPro.

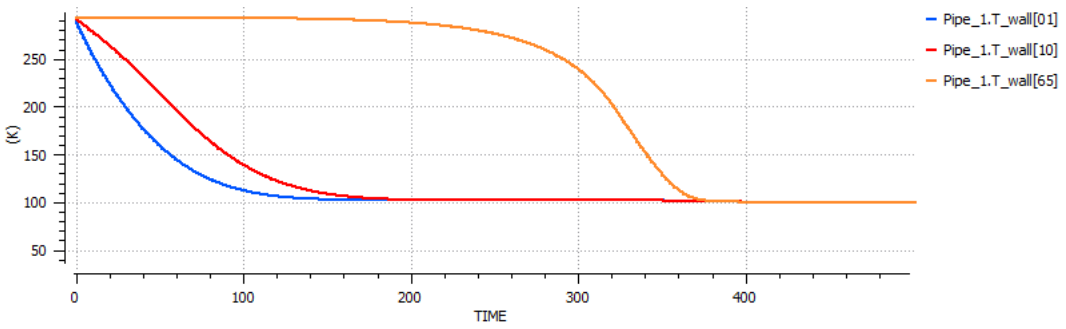

Figure 4.70. $T_{wall} = f(t)$ history, tuning case, in EcosimPro.

Comparison between experimental cases and simulations

Table 4.5 shows the experimental cases with LAr from the paper, reproduced using the software. The experimental conditions are given, which include the input pressure and average mass flux.

Case	avg. p_{in} [KPa]	avg. mass flux [kg/m^2 s]
1	236.7	33.2
2	259.5	38.5
3	279.0	40.8
4	296.0	44.4
5	299.4	47.2
6	307.7	45.4
7	325.1	52.4
8	340.7	54.1
9	359.0	55.6
10	361.7	56.9
11	373.7	58.6
12	382.6	60.0
13	398.7	62.7
14	412.3	64.7
15	420.2	66.5
16	446.8	70.1
17	458.4	69.3
18	505.5	79.5

Table 4.5. Experimental cases with LAr

Figures 4.71 and 4.72 show the comparison of cooling times, while Figures 4.73 and 4.74 show the comparison of fluid argon consumption during the chill-down process, between the experimental cases and EcosimPro simulations. The limitations of the software are obvious.

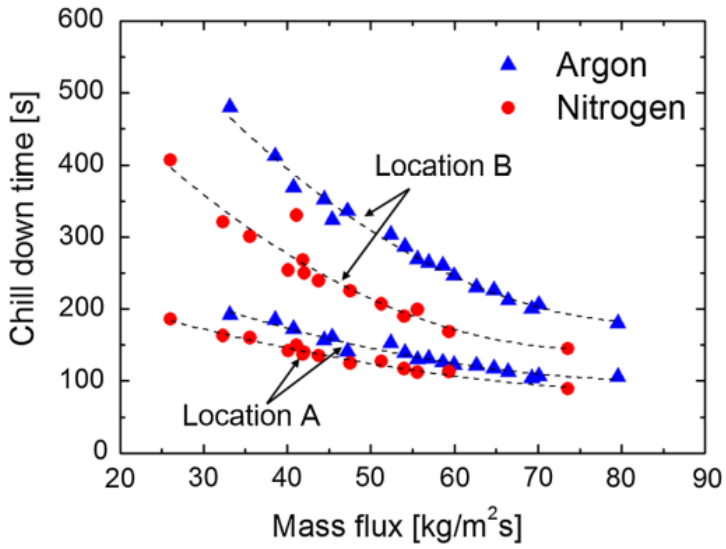

Figure 4.71. Line chill-down time of liquid argon experimental cases.

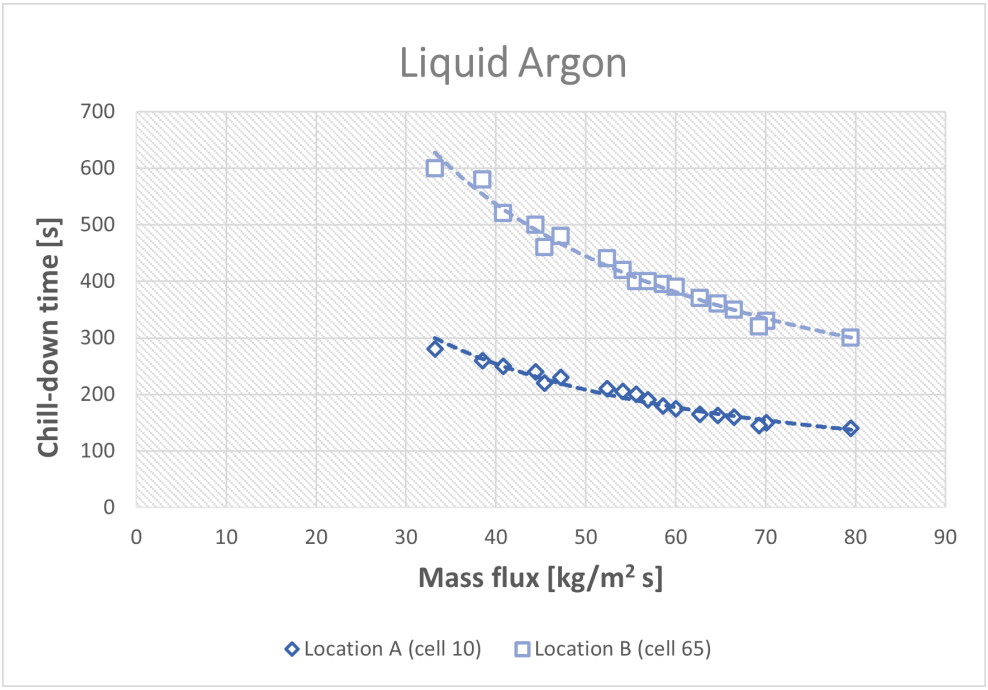

Figure 4.72. Line chill-down time of liquid argon simulated cases, EcosimPro.

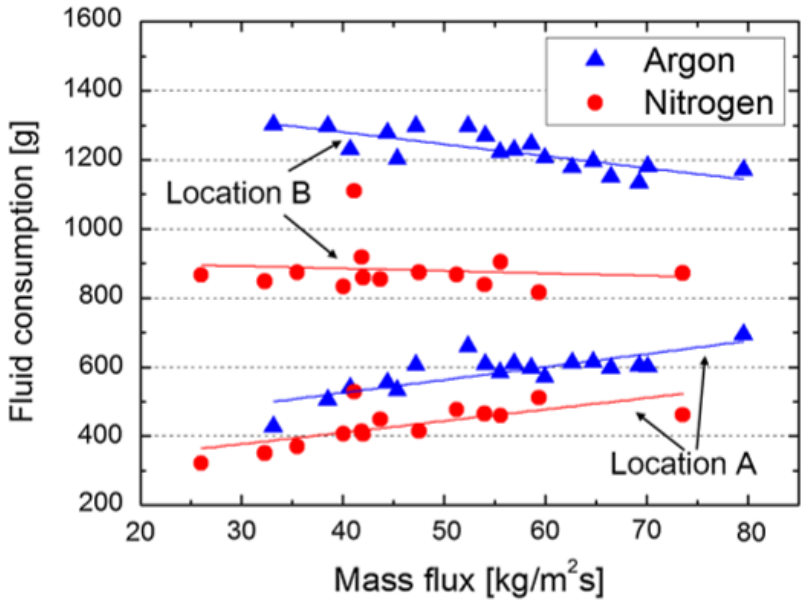

Figure 4.73. Propellant consumption during chill-down process with liquid argon, experimental cases.

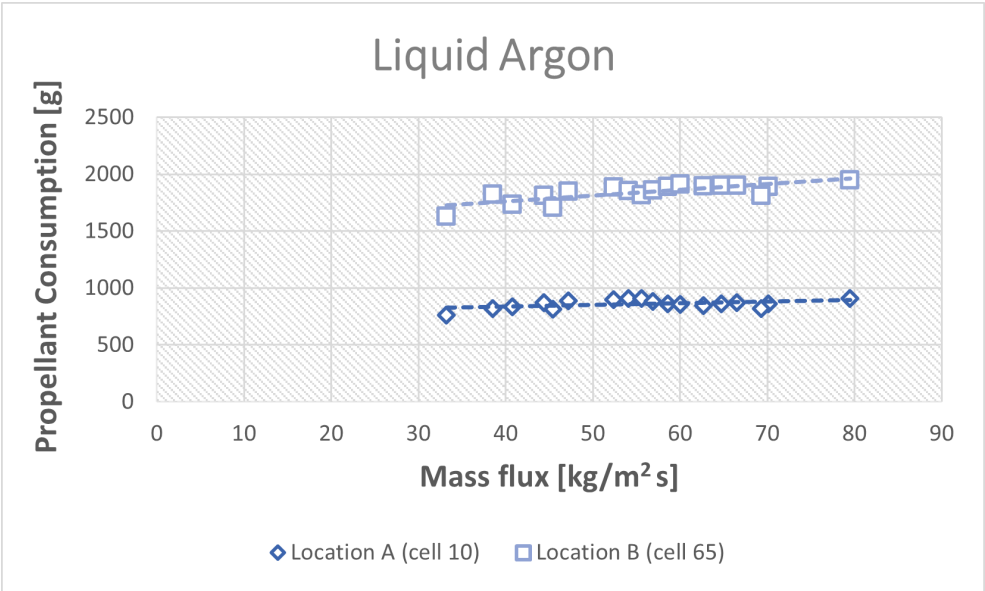

Figure 4.74. Propellant consumption during chill-down process with liquid argon, EcosimPro.

4.5.2 Liquid Nitrogen

Tuning case

Experimental conditions:

- $p_{in} = 337.9\text{KPa} \rightarrow T_{sat} = 89.252\text{K}$;
- $p_{out} = 329.9\text{KPa}$;
- Avg. mass flux $G = 47.5 \frac{kg}{m^2 s}$.

Simulation results:

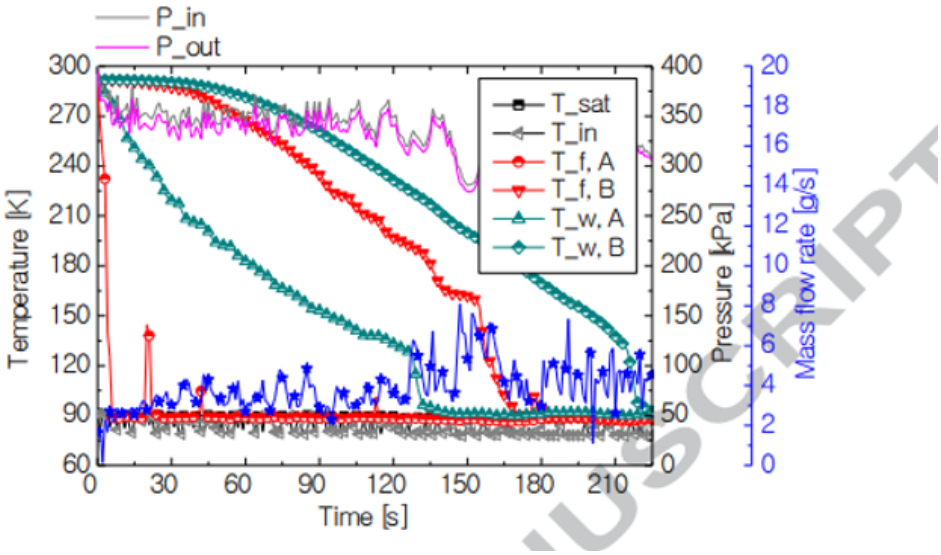

Figure 4.75. Time history of temperature, pressure and mass flow rate, experimental case.

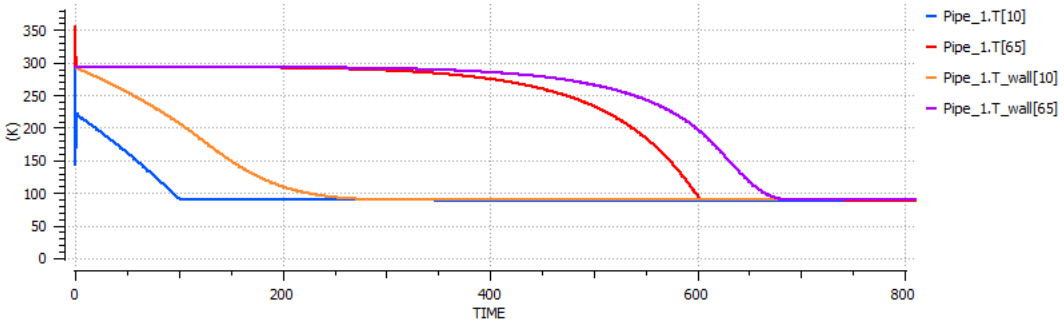

Figure 4.76. T_{fl} and T_{wall} time history, tuning case, in EcosimPro.

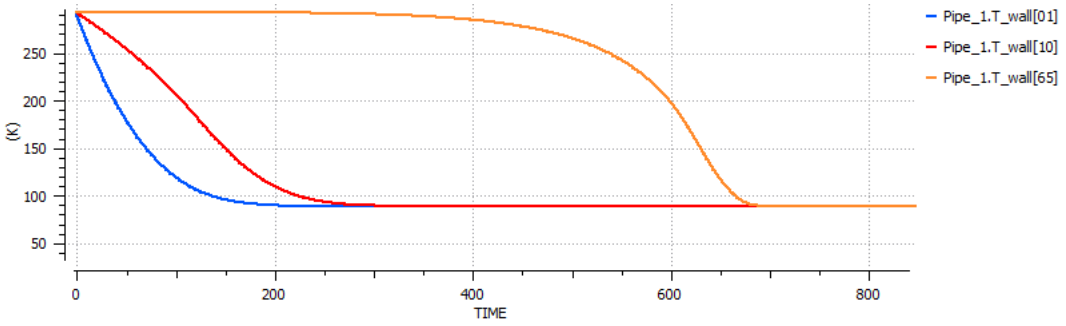

Figure 4.77. $T_{wall} = f(t)$ history, tuning case, in EcosimPro.

Comparison between experimental cases and simulations

Table 4.9 shows the experimental conditions for each of the experimental cases with LN_2 from the paper, reproduced using the software. It includes the average values of the inlet pressure (p_{in}), outlet pressure (p_{out}), and mass flux.

Case	avg. p_{in} [KPa]	avg. p_{out} [KPa]	avg. mass flux [kg/m^2 s]
1	480.3	469.3	73.6
2	426.6	416.9	59.4
3	387.7	379.1	54.0
4	372.6	363.8	55.6
5	359.7	351.2	51.3
6	337.9	329.9	47.5
7	328.6	320.7	43.8
8	307.7	300.6	42.1
9	301.3	294.5	40.1
10	290.7	283.4	41.9
11	263.1	256.8	35.5
12	252.0	246.1	41.1
13	250.0	244.3	32.3
14	216.8	212.1	26.0

Table 4.6. Experimental cases with LN_2

Figures 4.78 and 4.79 show the comparison of cooling times, while Figures 4.80 and 4.81 show the comparison of fluid nitrogen consumption during the chill-down process, between the experimental cases and EcosimPro simulations.

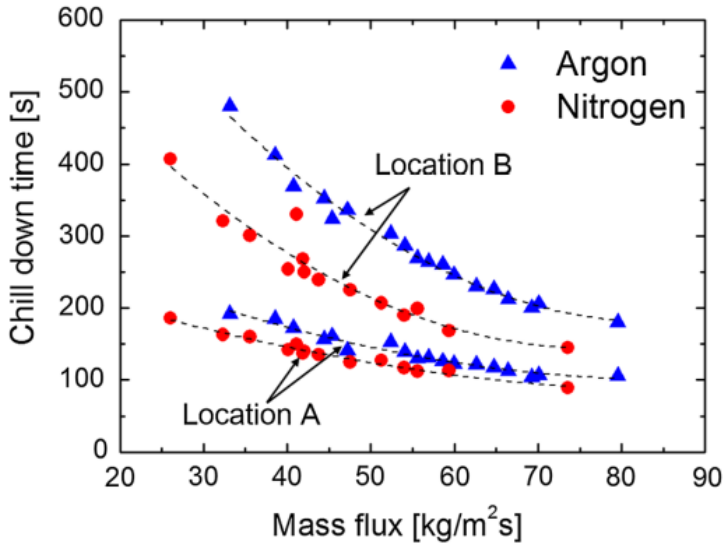

Figure 4.78. Line chill-down time of liquid nitrogen experimental cases.

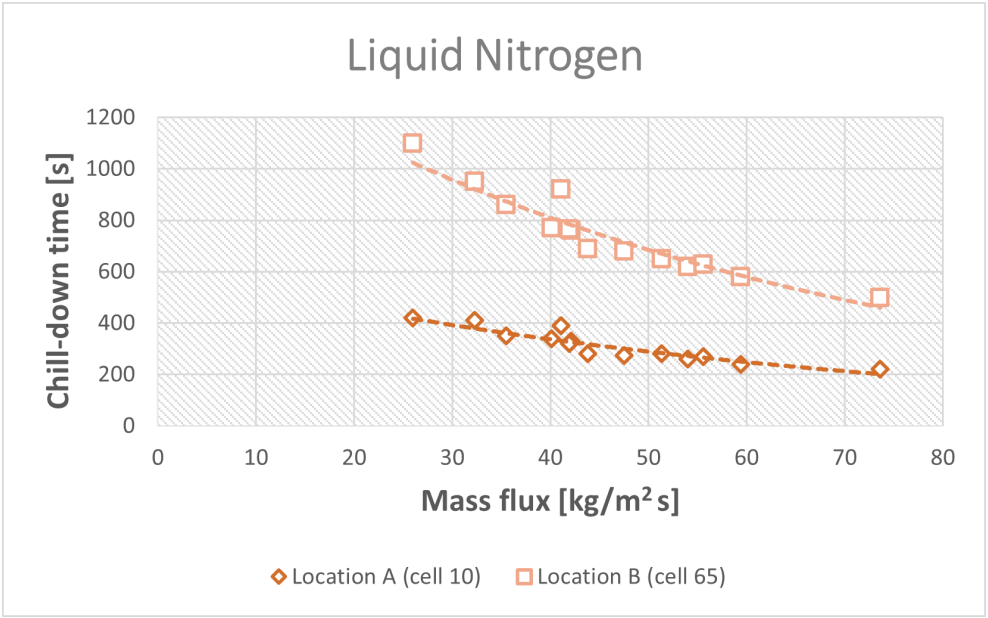

Figure 4.79. Line chill-down time of liquid nitrogen simulated cases, EcosimPro.

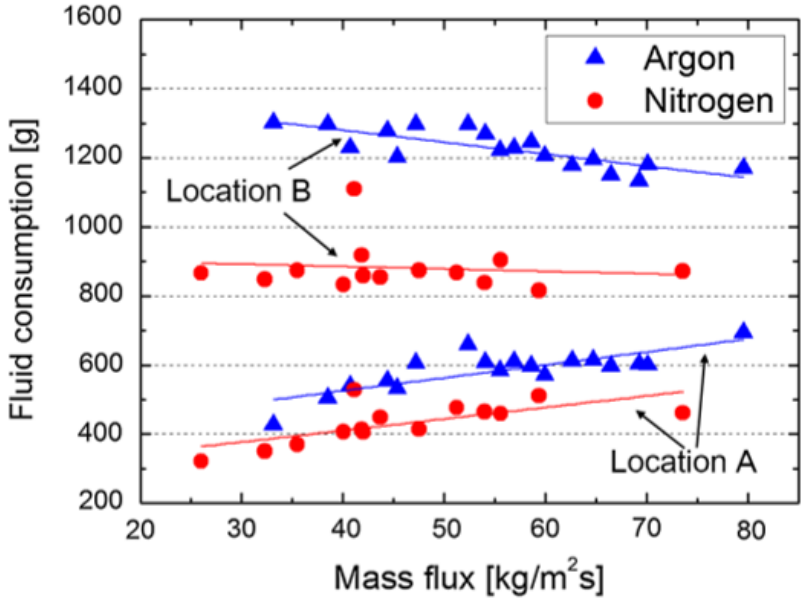

Figure 4.80. Propellant consumption during chill-down process with liquid nitrogen, experimental cases.

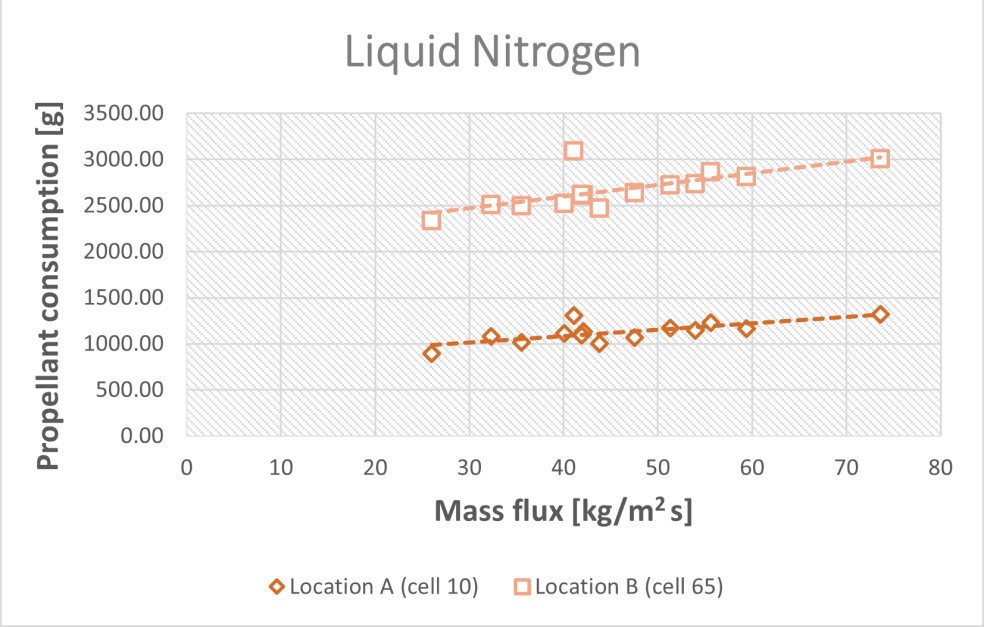

Figure 4.81. Propellant consumption during chill-down process with liquid nitrogen, EcosimPro.

The table below (tab.4.7) displays the percentage of relative errors in chill-down time and propellant consumption for both LAr and LN_2, as observed in the experimental analysis from the paper and the simulated results in EcosimPro.

Argon		**Nitrogen**	
Location A	Location B	Location A	Location B
$Err_{chilldown_{time}}$ 22.7%	$Err_{chilldown_{time}}$ 14.18%	$Err_{chilldown_{time}}$ 6.38%	$Err_{chilldown_{time}}$ 6.01%
$Err_{propellant_{consumption}}$ 19.18%	$Err_{propellant_{consumption}}$ 8.9%	$Err_{propellant_{consumption}}$ 29.55%	$Err_{propellant_{consumption}}$ 35.81%

Table 4.7. Relative errors

As can be readily observed, the errors are substantial, indicating a need for the development of a new pipe model to accurately estimate the characteristic parameters of the chill-down process.

4.6 Test case 5

In the next test case simulated using EcosimPro, the experimental analysis conducted by Jin et al. [2016] is considered.
The experiments described in this paper involve cryogenic chill-down on a stainless steel horizontal pipe with 12.7mm outer diameter (OD), 1.25mm wall thickness (t_{wall}), and 7m length (L) using liquid nitrogen (LN_2). The pipe is vacuum insulated during the experiment to minimize the heat leak from room temperature. The temperature and pressure profiles of the chill-down line are obtained 5.5m downstream from the pipe inlet. The experiments are conducted under a mass flux range of approximately $19kg/m^2s$ to $49kg/m^2s$.
The experimental apparatus for cryogenic line chill-down is schematically illustrated in figure 4.82. It mainly consists of an LN_2 supply tank, a subcooler, a bypass line, and a test section. The detailed information of the test section and the location of the sensor are depicted in figure 4.83. The specifications of experimental tests are listed in table 4.8.

The subcooler is characterized by a copper tube coil and is submerged in an LN_2 bath which is approximately 77K at atmospheric pressure. The chill-down process is considered to have started when the entire line upstream of the test section has already been cooled, and the valve 3 is closed while the valves 1 (Main Propellant valve) and 2 (Discharge Valve) are left open.

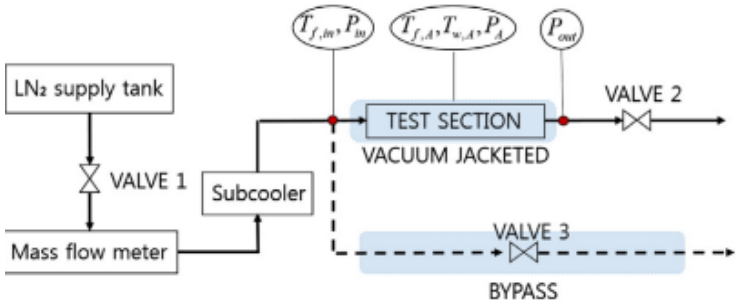

Figure 4.82. Schematic diagram of experimental apparatus for cryogenic line chill-down.

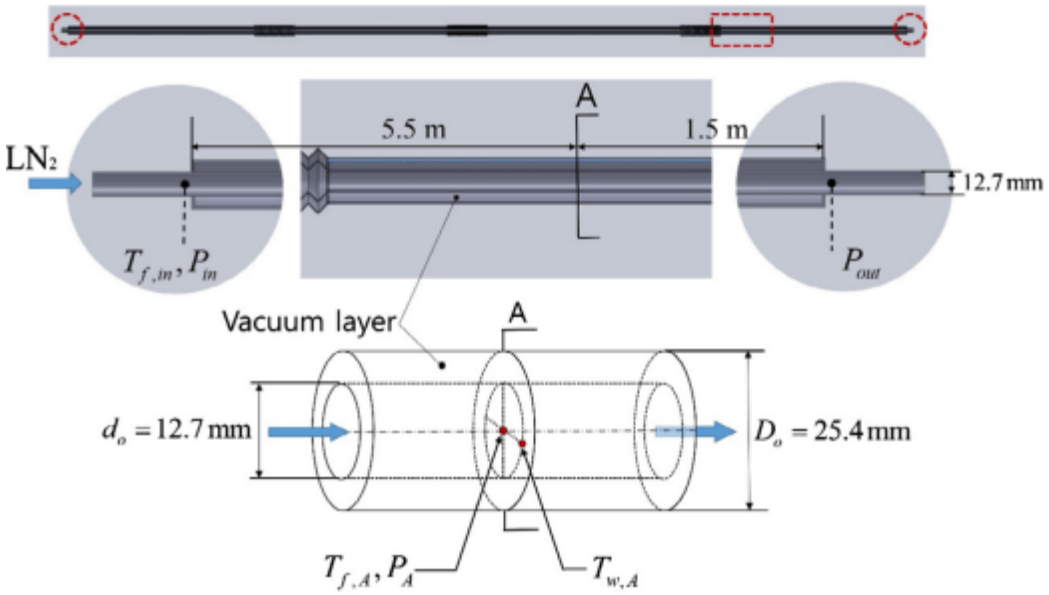

Figure 4.83. View of test section.

L $[m]$	inner pipe OD $[mm]$	inner pipe t_{wall} $[mm]$	outer pipe OD $[mm]$	outer pipe t_{wall} $[mm]$	material $[-]$	working fluid $[-]$	p_{out} $[mTorr]$
7	12.7	1.25	25.4	1.50	stainless steel 304	LN_2	vacuum (< 0.5)

Table 4.8. Case 5 experimental conditions

The experimental analysis comprises a total of six different conditions, as follows:

Case	avg. p_{in} [KPa]	avg. p_{out} [KPa]	pressure drop Δp [KPa]	avg. $\dot{m}$ [g/s]
1	176.4	174.8	1.6	1.6
2	254.9	252.5	2.4	2.5
3	293.1	290.6	2.5	3.6
4	315.5	313.0	2.5	3.7
5	382.5	379.6	2.9	4.0
6	433.1	429.5	3.6	4.0

Table 4.9. Experimental conditions with LN_2

Temperature conditions:

- The ambient temperature is $T_{out} = T_{amb} = 293$K, which is the initial wall temperature.
- The inlet fluid LN_2 temperature is $T_{in} = 77$K.

The temperature sensor A is placed at the reference section of the pipe, corresponding to node 54 in EcosimPro, where 69 cells have been set up.
The chill-down process is simulated using the full flush flow method.

However, the paper does not provide information on the stroke of the valve used in the experiments. For the purpose of matching the experimental mass flow rate values with the simulated ones and enabling a comparison of chill-down times, a valve stroke area of $A_0 = 0.1 \cdot A_{in} = 1.2668 \cdot 10^{-5} m^2$ ($Stroke_{Valve} = 0.1$) is assumed and kept constant for all tests.

4.6.1 Experiment 1: $p_{in} = 176.4KPa$, $p_{out} = 174.8KPa$, $\dot{m} = 1.6g/s$

With these input conditions, the software produces a mass flow rate value of $6.48g/s$, which is higher than the desired value of $\dot{m} = 1.6g/s$. To adjust the flow rate to the desired value while keeping the stroke fixed, the pressure drop Δp is reduced, which in turn slows down the flow and reduces the mass flow rate. The new pressure drop is $\Delta p_{new} = 0.1KPa$, which is underestimated by the software.

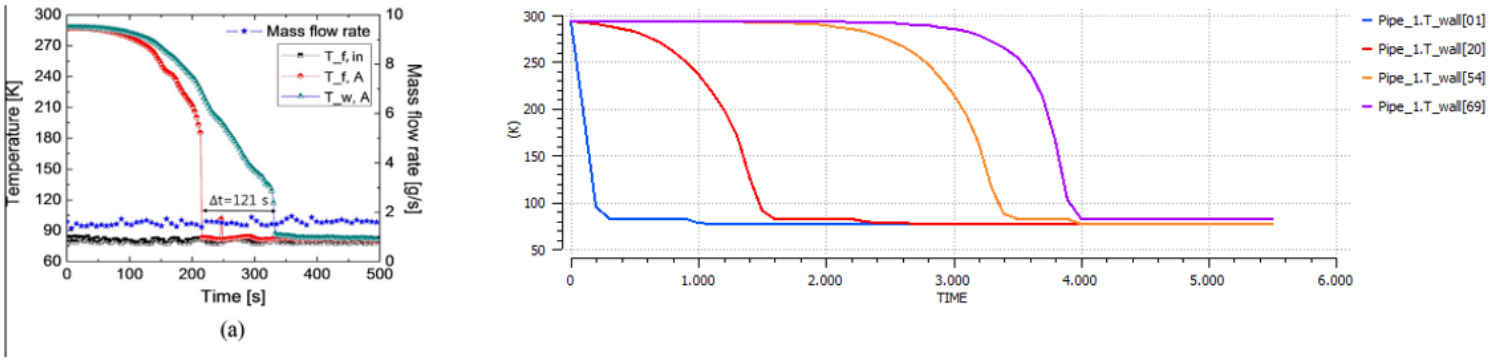

Experimental (paper) (350s)

EcosimPro (4000s)

Figure 4.84. Comparison on $\Delta T_{cooling}$ between the experimental case and EcosimPro.

4.6.2 Experiment 2: $p_{in} = 254.9KPa$, $p_{out} = 252.5KPa$, $\dot{m} = 2.5g/s$

- $\Delta p_{exp} = 2.4KPa \rightarrow \dot{m} = 7.95g/s$; $\Delta p_{new} = 0.25KPa \rightarrow \dot{m} = 2.56g/s$.

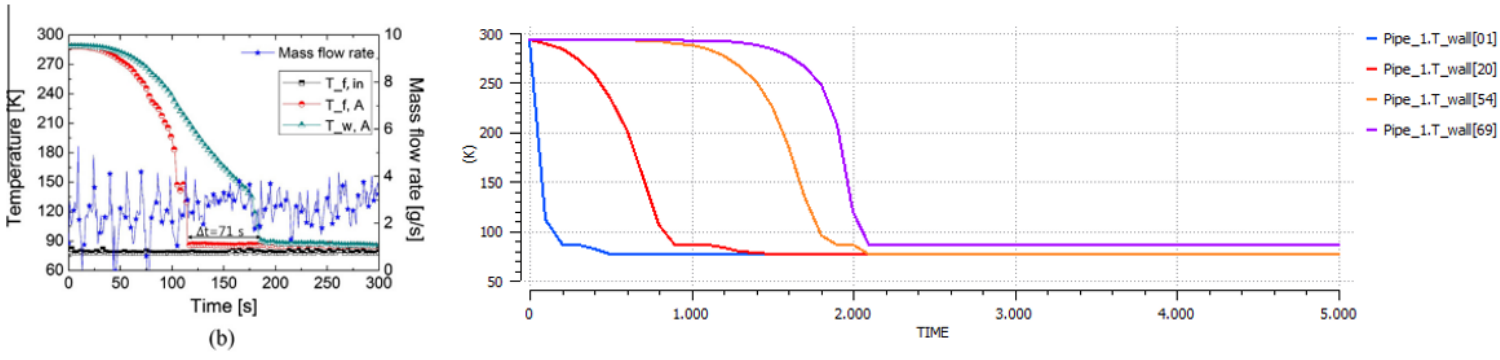

Experimental (paper) (185s)

EcosimPro (2100s)

Figure 4.85. Comparison on $\Delta T_{cooling}$ between the experimental case and EcosimPro.

4.6.3 Experiment 3: $p_{in} = 293.1KPa$, $p_{out} = 290.6KPa$, $\dot{m} = 3.6g/s$

- $\Delta p_{exp} = 2.5KPa \rightarrow \dot{m} = 8.12g/s$; $\Delta p_{new} = 0.5KPa \rightarrow \dot{m} = 3.63g/s$.

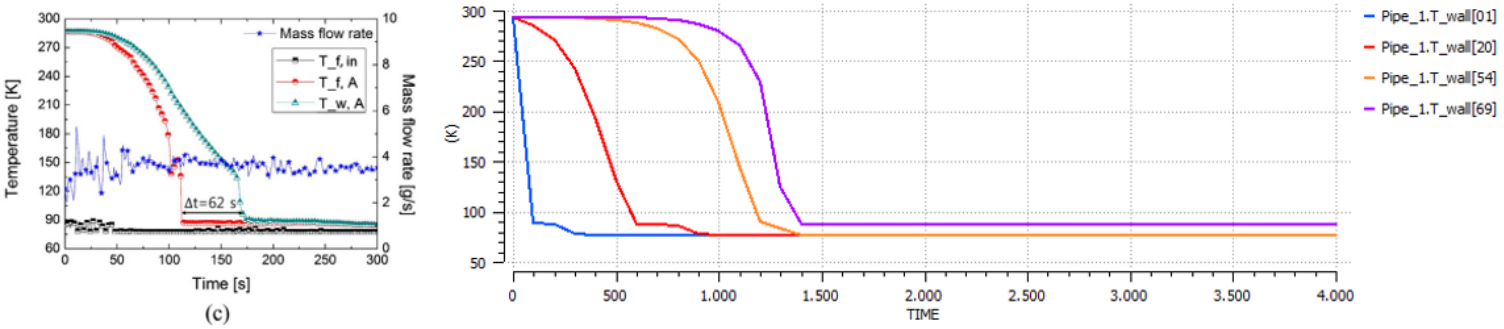

Experimental (paper) (175s)

EcosimPro (1400s)

Figure 4.86. Comparison on $\Delta T_{cooling}$ between the experimental case and EcosimPro.

4.6.4 Experiment 4: $p_{in} = 315.5KPa$, $p_{out} = 313.0KPa$, $\dot{m} = 3.7g/s$

- $\Delta p_{exp} = 2.5KPa \rightarrow \dot{m} = 8.12g/s$; $\Delta p_{new} = 0.55KPa \rightarrow \dot{m} = 3.79g/s$.

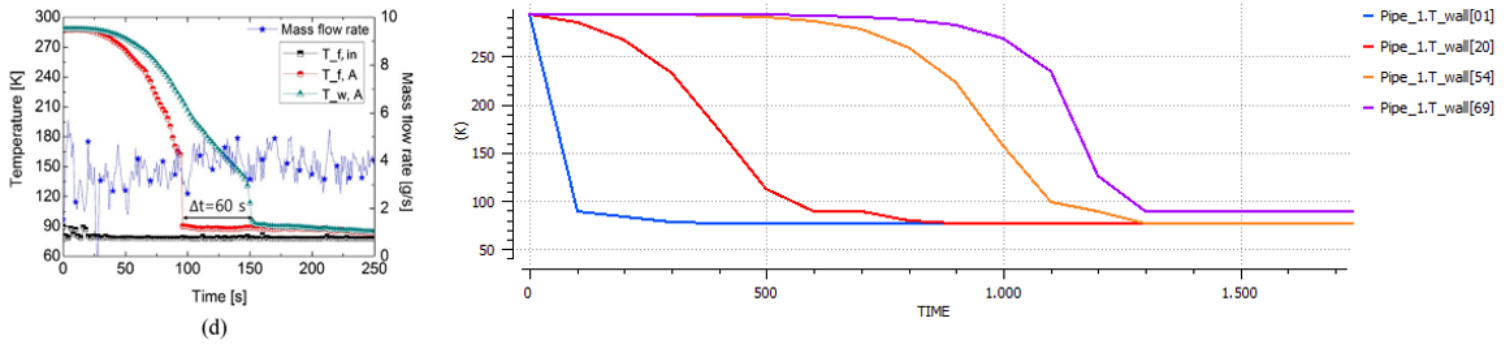

Experimental (paper) (150s)

EcosimPro (1300s)

Figure 4.87. Comparison on $\Delta T_{cooling}$ between the experimental case and EcosimPro.

4.6.5 Experiment 5: $p_{in} = 382.5KPa$, $p_{out} = 379.6KPa$, $\dot{m} = 4.0g/s$

- $\Delta p_{exp} = 2.9KPa \rightarrow \dot{m} = 8.75g/s$; $\Delta p_{new} = 0.65KPa \rightarrow \dot{m} = 4.12g/s$.

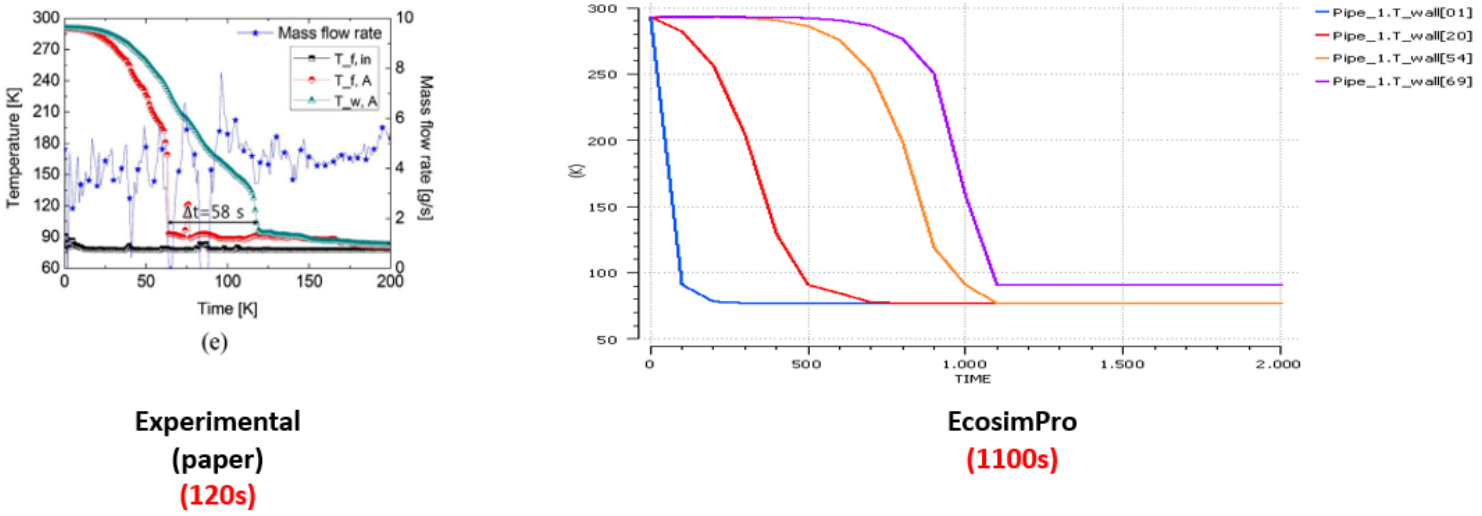

Figure 4.88. Comparison on $\Delta T_{cooling}$ between the experimental case and EcosimPro.

4.6.6 Experiment 6: $p_{in} = 433.1KPa$, $p_{out} = 429.5KPa$, $\dot{m} = 4.0g/s$

- $\Delta p_{exp} = 3.6KPa \rightarrow \dot{m} = 9.76g/s$; $\Delta p_{new} = 0.65KPa \rightarrow \dot{m} = 4.12g/s$.

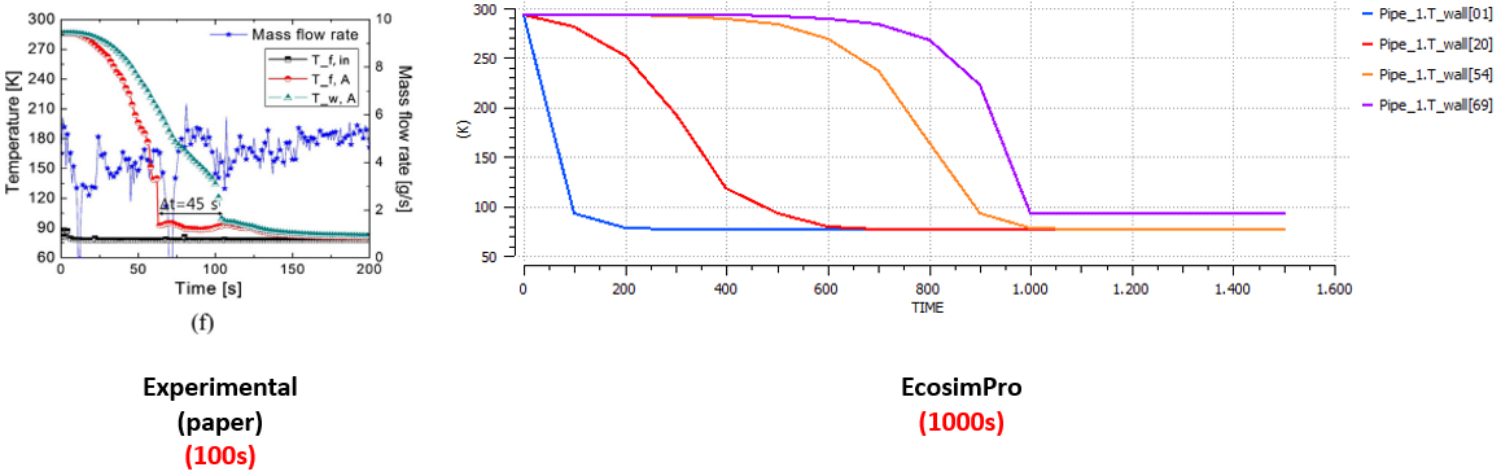

Figure 4.89. Comparison on $\Delta T_{cooling}$ between the experimental case and EcosimPro.

The comparison between the experimental and simulated results shows a significant discrepancy in the cooling times. However, it should be noted that Test Case 5 cannot be used to evaluate the accuracy of the model due to the lack of information about the boundary conditions of the LN_2 at the test section inlet when the cooling process actually begins (as depicted by the red circle in fig. 4.82). In fact, the chill-down process is considered started when the whole line upstream of the test section has already been cooled, but there are not sufficient information to establish the new boundary conditions of the LN_2.
This can be observed from the experimental graphs in the paper, such as fig. 4.89, where the mass flow rate shows a mainly constant trend throughout the experiment. In contrast, during a typical cryogenic chill-down test, the mass flow rate first experiences a transient phase of approximately increasing magnitude before reaching a steady state with constant trend, as shown in fig. 4.90.

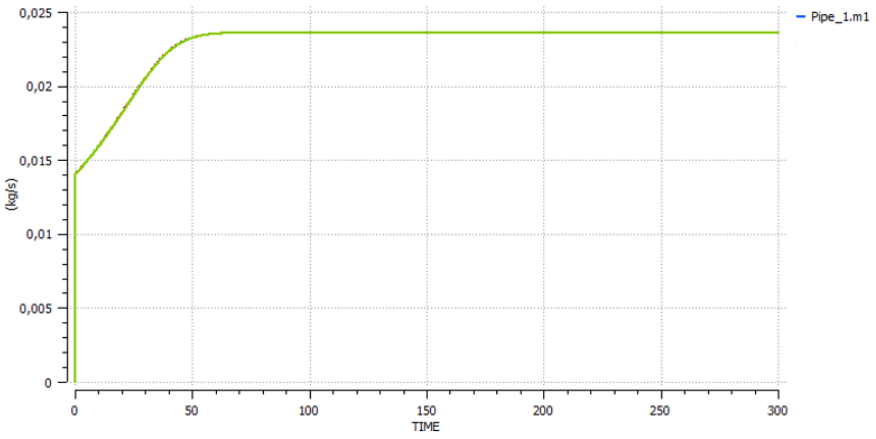

Figure 4.90. Classic mass flow rate $\dot{m}$ trend in a cryogenic chill-down process.

4.7 Test case 6

The last test case simulated in EcosimPro is based on the experimental analysis conducted by Ramé et al. [2014], which involved performing chill-down tests on a warm cryogenic line with liquid hydrogen.
The experimental setup used for these tests is shown in Figure 4.91.

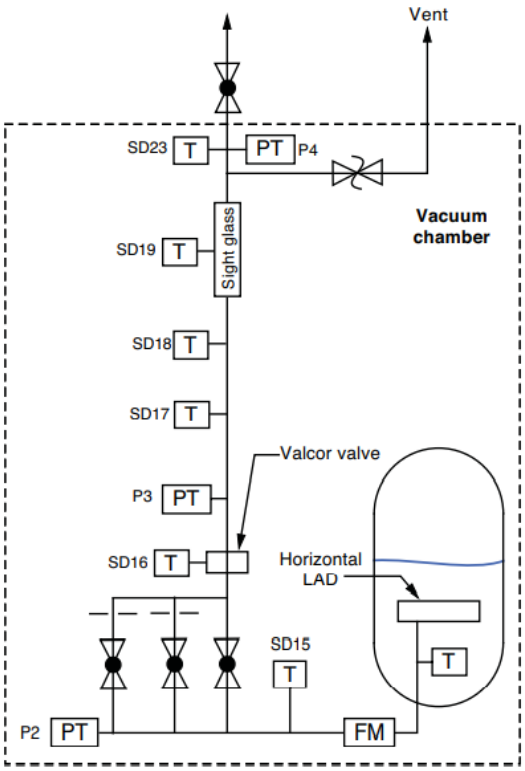

Figure 4.91. Schematic of the chill-down equipment showing the test section line.

The experimental conditions obtained from the paper are reported in the following table:

L $[m]$	OD $[mm]$	material $[-]$	working fluid $[-]$	mass flow rate $[lb/min]$	chill-down technique	p_{out} $[atm]$
2.26	12.7	stainless steel 304	LH_2	$\cong 2$	trickle and pulsed	0.1

Table 4.10. Case 6 experimental conditions

A sight glass section was installed in the flow line about 1.86m downstream of the line inlet to allow observation of the flow near the downstream end of the line (as shown in Figure 4.91). Temperature and pressure were measured at instrumentation stations corresponding to nodes 21-22 in EcosimPro, using a silicon diode temperature transducer (SD23) and a pressure transducer (P4). The chill-down techniques simulated in EcosimPro were the trickle with bypass and the pulsed method.

The experimental conditions used in the simulation are as follows:

- Ambient temperature $T_{out} = T_{amb} = 265$K, which is the initial wall temperature.

- Inlet fluid LH_2 temperature $T_{in} = T_{sat} = 20\text{K}$, indicating that the fluid is in saturated conditions (EcosimPro works well with saturated LH_2).
- Inlet driving pressure $T_{in,sat} = 20\text{K} \rightarrow p_{in} = p_{sat} = 90717\text{Pa}$.

However, the wall thickness of the test pipe t_{wall} was not provided in the paper, so it was assumed in order to match the experimental chill-down times.

4.7.1 Trickle chill-down test

Two flow strategies, namely trickle with bypass and pulse, were used for line chill-down. In both cases, the mass flow rate of hydrogen was approximately $\dot{m} \cong 2lb/min = 0.01512kg/s$. During the trickle flow set, hydrogen was continuously injected into the chill-down test section. In contrast, during the pulse test, LH_2 flowed for n_{ON} seconds, followed by n_{OFF} seconds of zero flow.
During the trickle chill-down test, a reduced mass flow rate initially flows through the inlet valve with bypass ($Valve_{in}$ in fig. 4.4, valve stroke is fixed equal to 10% of the pipe area) for the first 20 seconds, after which the valve is fully opened (valve stroke equal to 100% of the pipe area, $A_{Valve_{in}} = A_{pipe}$) until the end of the chill-down process. The discharge valve ($Valve_{out}$ in fig. 4.4) is kept open continuously during the trickle test. From the experimental graph, it can be deduced that there is a reduced flow rate for the first 20 seconds.

The pipe wall thickness typically varies between $1 - 3$ mm. However, by selecting t_{wall} in this range with the given OD, the chill-down times obtained from the simulations are too low (approximately 20 seconds) compared to the available experimental results (approximately 150 seconds). Similarly, with these same conditions, the mass flow rate values are too low (approximately $1.13lb/min$).
Therefore:

- To increase the chill-down time, it is necessary to increase the wall thickness.
$$\uparrow t_{wall} \Rightarrow \uparrow \Delta t_{cooling}$$
- To increase the mass flow rate, it is necessary to increase the flux passage area, i.e. the inner diameter ID. This is because ρ and V are respectively fixed with the fluid and with Δp.
$$\uparrow ID \rightarrow \uparrow A \Rightarrow \uparrow \dot{m} = \rho \cdot V \cdot A$$

To perfectly match the chill-down time of approximately 150 seconds and the mass flow rate of approximately $2lb/min = 0.015kg/s$ of the available experimental trickle test, the following values are fixed:

$$t_{wall} = 20\text{mm}$$
$$ID = 12.2\text{mm}$$

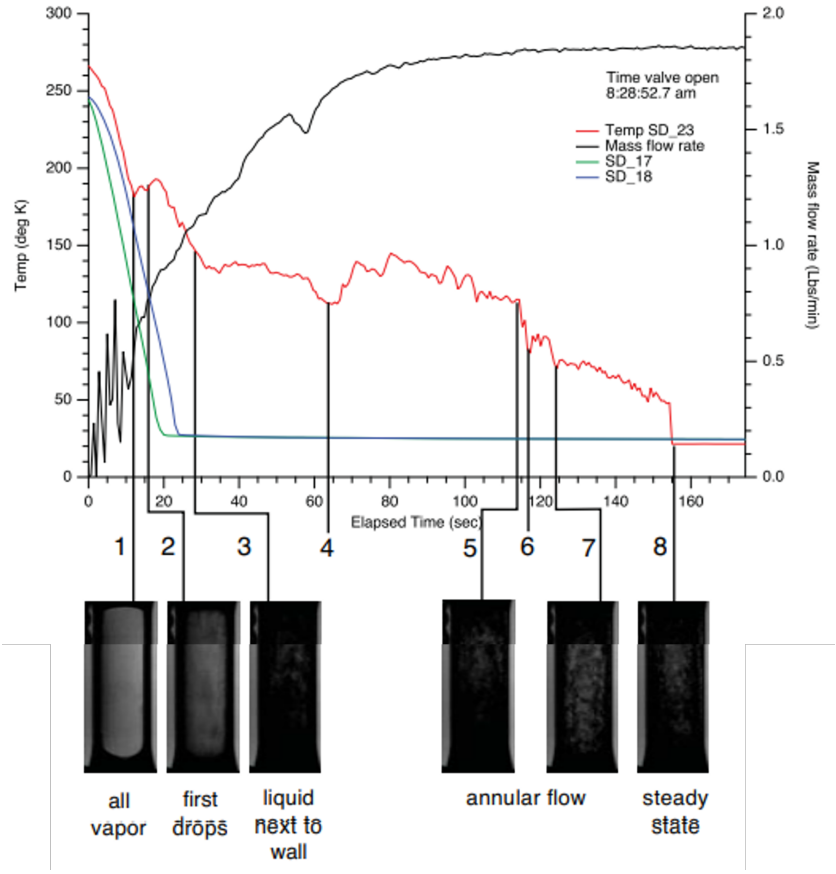

Figure 4.92. Time history of wall temperature (red line) and mass flow rate (black line) of a medium trickle flow test, experimental case.

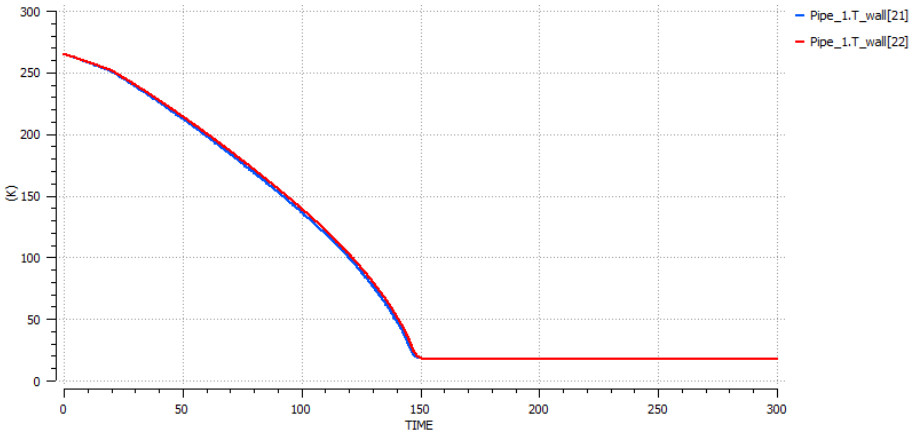

Figure 4.93. $T_{wall} = f(t)$ history of a medium trickle flow test, EcosimPro.

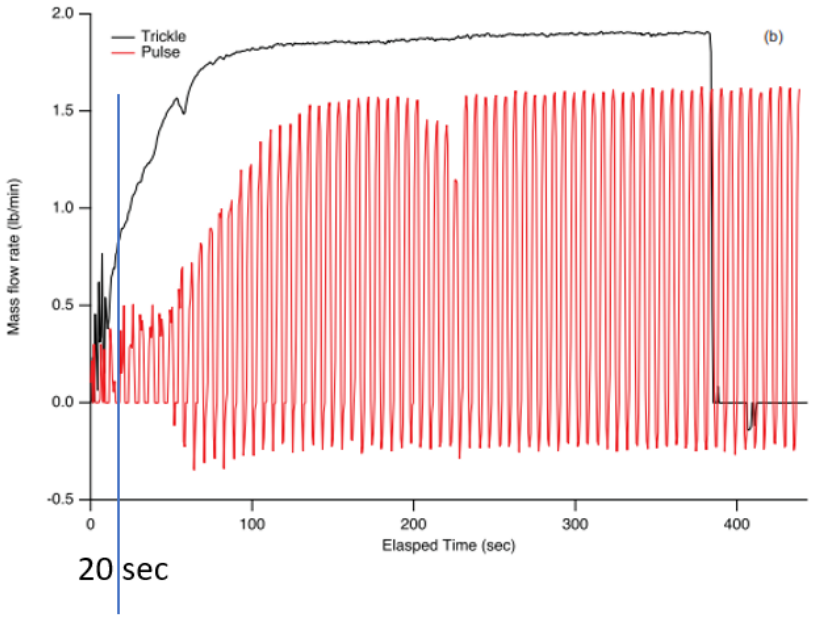

Figure 4.94. Time history of mass flow rate for medium trickle flow test (black line), experimental case.

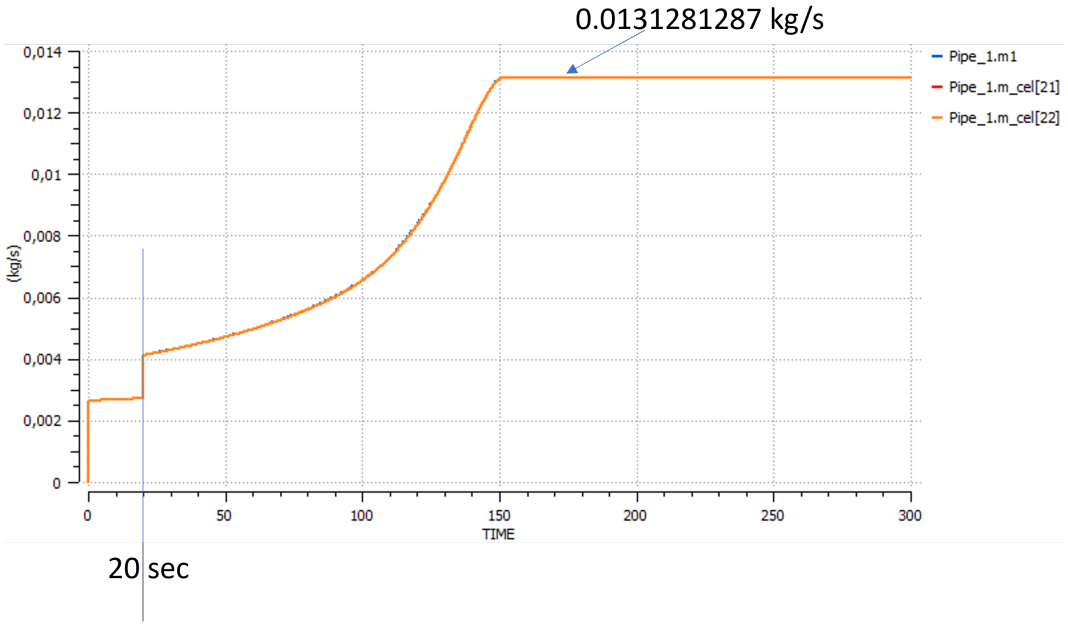

Figure 4.95. Mass flow rate $\dot{m}$ history for medium trickle flow test, EcosimPro.

4.7.2 Pulse chill-down test

The paper experimented with a second chill-down strategy known as the pulsed technique, specifically a 3-3 pulse test (i.e. 3 seconds on and 3 seconds off of LH_2 flow). After perfectly tuning the simulated trickle test to match the experimental one by forcing the physical dimensions of the pipe, the simulation was used to test whether EcosimPro could accurately simulate the pulse methodology.
The pipe model used to simulate the full flush flow and the trickle method (fig. 4.4) in the software environment is different for the pulse strategy. The new tube model, shown in figure 4.96, includes a control on the inlet flow valve to regulate the number of seconds n_{ON}/n_{OFF} in which the valve is open/closed. The outflow valve remains permanently open.

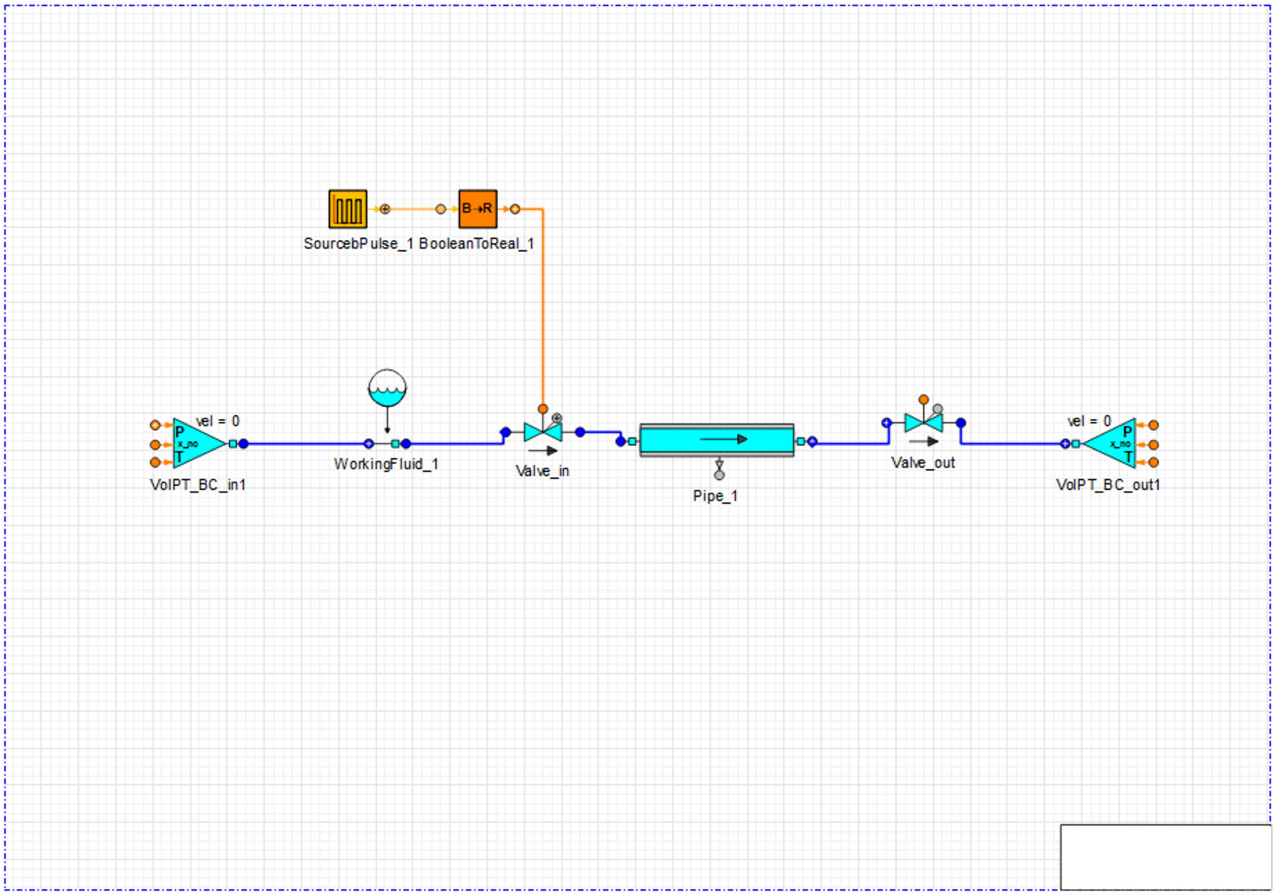

Figure 4.96. Experimental setup for pulse chill-down tests in EcosimPro.

The temperature and pressure boundary conditions applied are the same as those used in the trickle test.

The simulation results are compared with the experimental results from the paper in the following figures:

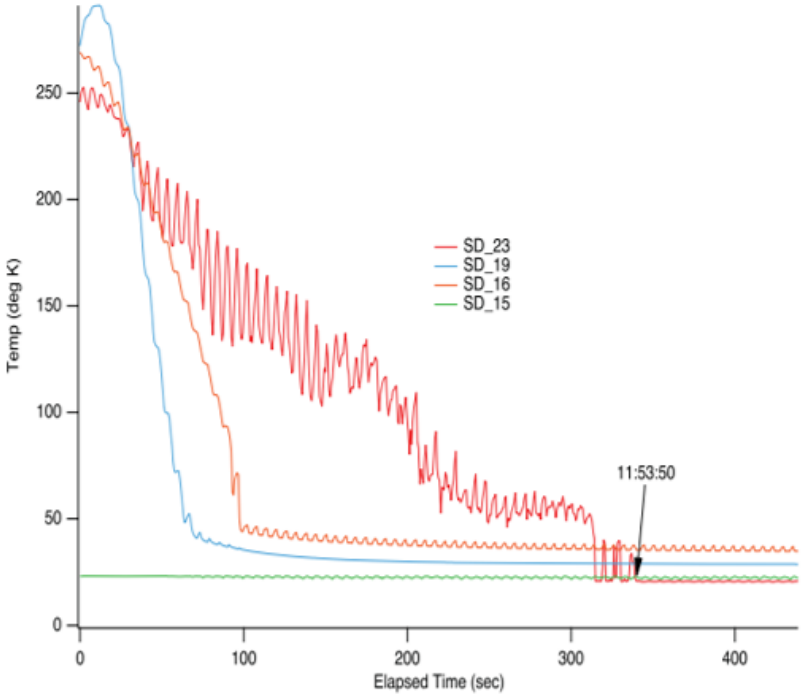

Figure 4.97. Time history of wall temperature (red line) of a medium flow 3-3 pulse test, experimental case.

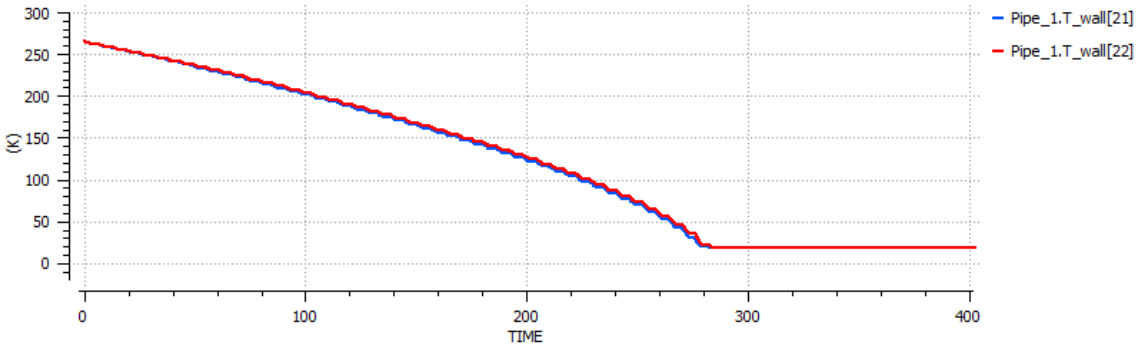

Figure 4.98. $T_{wall} = f(t)$ history of a medium flow 3-3 pulse test, EcosimPro.

It can be seen that by adjusting the physical dimensions of the model, EcosimPro is able to simulate the chill-down time well ($\cong 300s$), although it does not capture the correct trend of the curve, i.e., the real behavior of the fluid flow in all its phases.

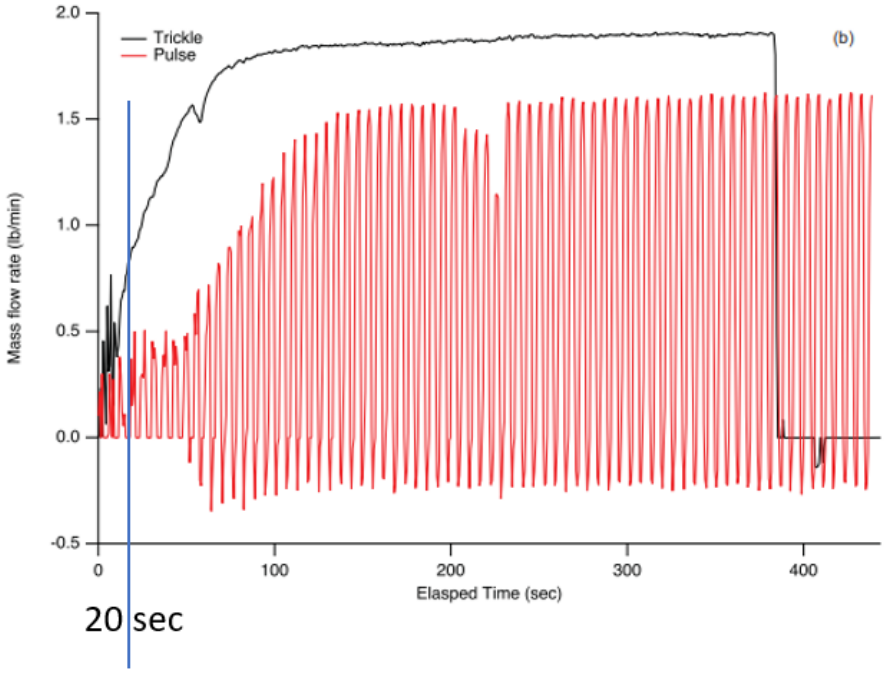

Figure 4.99. Time history of mass flow rate for medium flow 3-3 pulse test (red line), experimental case.

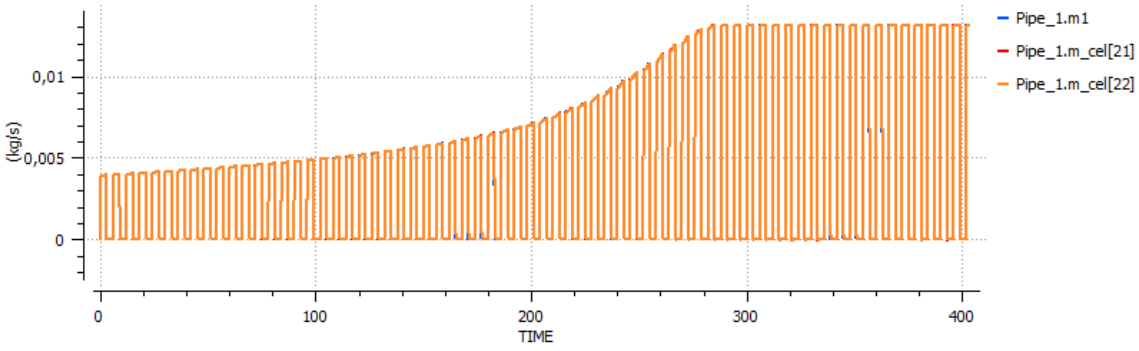

Figure 4.100. Mass flow rate $\dot{m}$ history for medium flow 3-3 pulse test, EcosimPro.

4.7.3 Conclusions about test case 6

The following results and differences have emerged between the simulations and experiments regarding the propellant consumption:

EcosimPro		**Experimental Paper**	
Trickle	Pulse	Trickle	Pulse
m_{LH_2}	m_{LH_2}	m_{LH_2}	m_{LH_2}
3.947 kg	1.32 kg	5 kg	1.5 kg

Table 4.11. Propellant consumption m results

Overall, EcosimPro underestimates the propellant consumption, with values of 3.95 kg and 1.32 kg for the trickle and pulse tests, respectively, compared to 5 kg and 1.5 kg in the experimental analysis. However, Table 4.11 shows that the reduction in fluid mass for cooling in the pulse test compared to the trickle test is about 67 % in EcosimPro ($m_{consumption_{Pulse}} = 33\% \cdot m_{consumption_{Trickle}}$), which is consistent with the 70 % reduction in propellant consumption observed in the experimental results. In fact, the cumulative mass spent in pulse flow is only 30 % of that in trickle flow due to the off-time during pulsing, as shown in figure 4.101.
The chill-down time in the pulse test is also accurately matched by the software.

In conclusion, with the initial forcing of the pipe dimensions, EcosimPro is able to simulate well the cooling time $\Delta t_{cooling}$ and the propellant consumption m of the pulsed chill-down technique. However, it is worth noting that the software is not able to capture the real physical behavior of the flow, as evidenced by the trend discrepancies between the simulated and experimental curves.

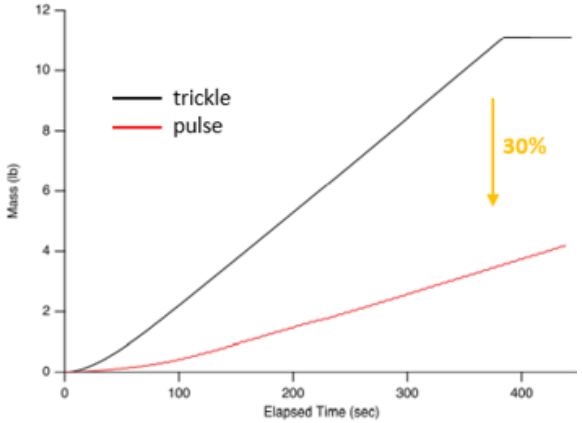

Figure 4.101. Time history of mass for trickle and pulse tests, experimental cases.

Moreover, in agreement with the experimental analysis, the pulse technique is found to require lower propellant consumption than the trickle method, at the cost of longer chill-down times.

Chapter 5

Analysis and optimization of *full flush flow* chill-down process of the cryogenic LOx transfer line

The goal of this new chapter is to use EcosimPro software to optimize and analyze the chill-down process for the transfer line of the M10 engine's cryogenic oxidant, liquid oxygen LO_2. This engine is powered by a combination of liquid methane and liquid oxygen and serves as the new upper stage of AVIO's Vega-E launcher.
In particular, the objective is to ensure the chill-down of the entire complex feed line within a certain target time, fixed by requirement, deriving from mission analysis needs, with the lowest propellant consumption. Thus the aim of this section is to realize the best trade-off between chill-down time $\Delta t_{cooling}$ (xxx s), which is a preset value, and propellant consumption $m_{consumption}$ (kg), which must be calculated, performing an open loop optimization of full flush flow chill-down technique. Therefore the Main Propellant Valve MPV is completely open and the propellant employed in the process is vented into the environment through the discharge valves, for both the main compartment, which sends the fluid in the combustion chamber, and the bearing housing.

The input data will not be reported, or they will be appropriately non-dimensionalized, due to Avio's company privacy reasons.

The assigned boundary conditions are as follows:

- The inlet driving pressure, p_{in}, is a fixed value of A bar. This pressure level is within the typical pressure range of tanks that require feeding systems by turbopumps. P_{in} corresponds to the pressure of the liquid oxygen (LO_2) in the storage tank.
- The ambient pressure is $p_{amb} = 1$ bar.

- The ambient temperature is $T_{amb} = 25°\text{C} = 298.15$ K.
- The inlet subcooled temperature of fluid is at most 3 degrees subcooled, due to EcosimPro limitations.

The cryogenic fluid used as an oxidizer is liquid oxygen LO_2, and its saturation temperature is determined from the given inlet pressure p_{in} using Antoine's equation.

$$p_{in} = A \text{ bar} \rightarrow T_{sat} = B \text{ K}$$

The inlet fluid temperature is chosen to be in subcooled conditions to reduce chill-down times, and it is set to be equal to the saturation temperature at the given pressure minus 2 degrees for subcooling, in accordance with software limits.

$$T_{in,sub} = T_{sat} - 2 \text{ K}$$

The first run of software will be the baseline of the analysis, in which all valves of schematic, Main Propellant Valve, Main Discharge Valve and Bearing Housing Discharge Valve, will be set completely open, i.e. the valves stroke will be selected at 1.

At the end of the full flush flow chill-down process, the Main Discharge Valve will be closed and the liquid propellant will be sent into the combustion chamber.

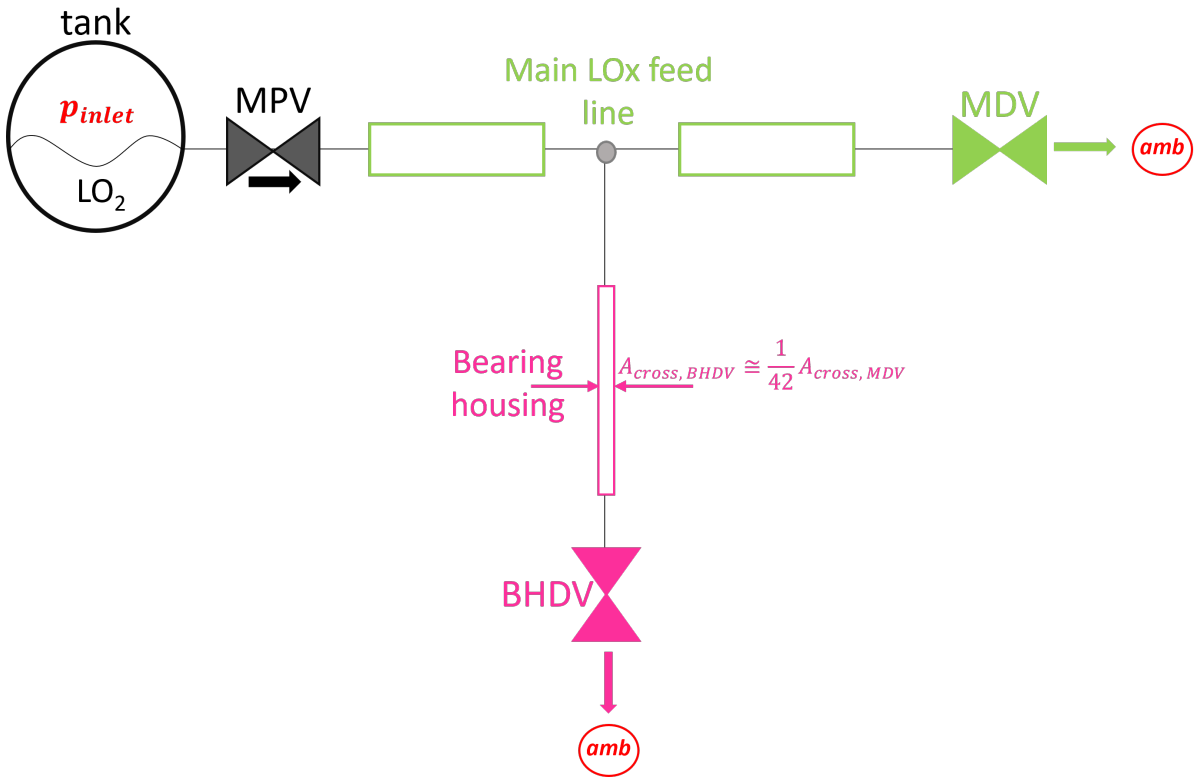

Figure 5.1. Simplified schematic of Cryogenic LOx transfer line, during chill-down.

Chill-down is necessary for both the main propellant line and the bearing housing in order for the engine to work correctly in all its parts, ensure ignition guarantees, avoid cavitation of the pumps, and lubricate the bearings. Since the propellant also serves as a lubricant for the bearings, it must be in liquid form in the dedicated compartment.

The figure 5.1 shows in a very simplified way the cryogenic oxidizer transfer line, in which substantially there are two feed lines downstream of the oxidizer storage tank, the main propellant one (green path), where the liquid oxygen destined to the thrust chamber flows, and the bearing housing one (magenta path), where the cryogenic fluid employed for the cooling of bearing housing flows. It shall be noted that the main transfer line is characterized by much larger pipes than the bearing transfer line, so this leads to longer chill-down times for the bearing housing, since a reduced mass flow rate flows through the ducts, in comparison to the ducts of the main line, therefore the heat exchanges are reduced. Additionally, the chill-down time required to cool the bearing housing is longer because there is a larger mass that needs to be cooled.

5.1 Baseline: Saturated LO_2

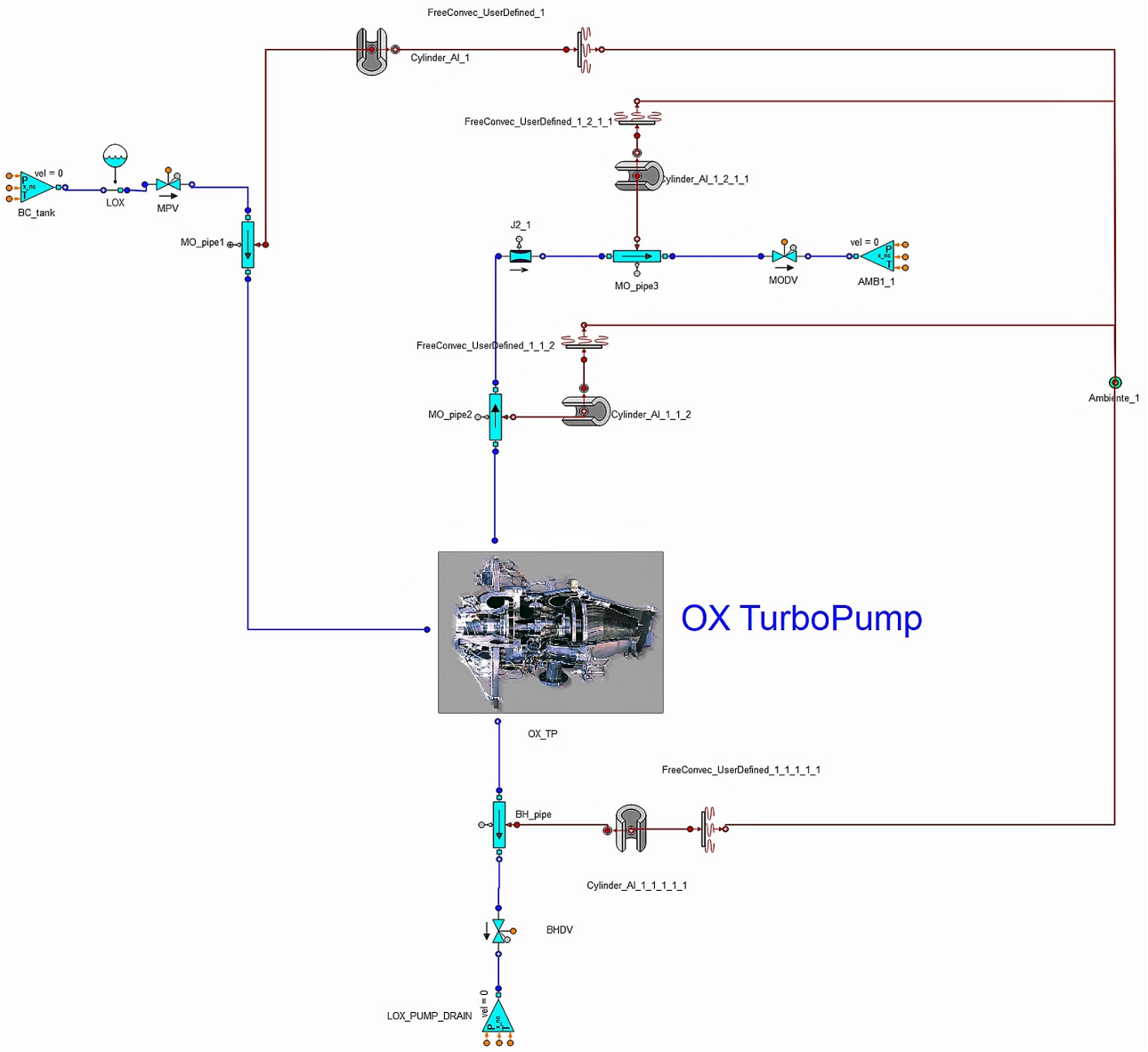

Figure 5.2. EcosimPro schematic model of Cryogenic LOx transfer line, open loop chill-down design.

The figure 5.2 displays in a simplified way the schematic used in EcosimPro to simulate the open loop chill-down process of cryogenic LOx feeding system.
The initial run of the transfer line model serves as the baseline for the analysis and optimization work.

For this baseline, the liquid oxygen will be assumed to be in a state of saturation, at the given inlet pressure.

The boundary conditions are as follows:

- $p_{amb} = 1$ bar; $T_{amb} = 298.15$ K
- $p_{in} = p_{tank}$; $T_{in,fl} = T_{sat,fl}$
- All valves completely open: $Stroke_{MPV} = Stroke_{MDV} = Stroke_{BHDV} = 1$

Based on these conditions, the graphs indicate that the chill-down process, so the liquid state of fluid, is not reached in both the main propellant feed line and the bearing housing. This is evident from the quality factor *.x* (fig. 5.3), which represents the vapor fraction in the injected liquid propellant mass, remaining constantly equal to 1 over time. As a result, it is not possible to calculate the chill-down time $\Delta t_{cooling}$ or propellant consumption $m_{consumption}$.

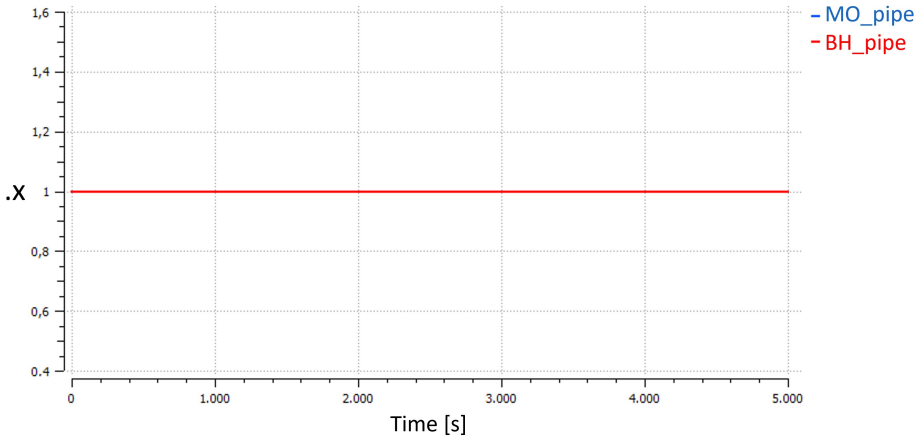

Figure 5.3. Quality factor .x history for Main Oxidizer pipe and Bearing Housing pipe.

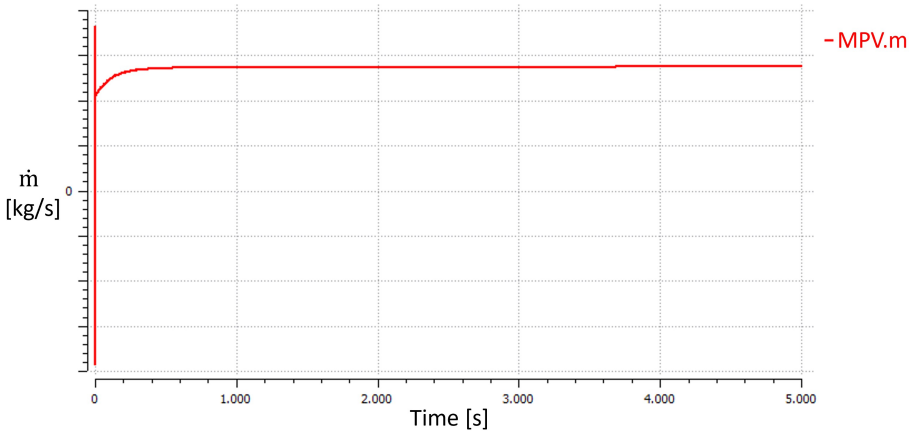

Figure 5.4. Mass flow rate $\dot{m}$ history for Main Propellant Valve.

The propellant consumption represented by the area under the curve in fig. 5.4 until steady-state is reached, is not truthful and accurate, but it is underestimated because the chill-down process is not achieved. This is due to the fact that the liquid propellant remains in a saturated state, and does not reach the necessary subcooled state for chill-down.

5.2 Baseline: Subcooled LO_2

To ensure chill-down and achieve the liquid state for the stored oxygen, it is necessary to bring the liquid oxygen LO_2 in the tank to a subcooled state. Specifically, the subcooling temperature chosen for the oxidizer is two degrees below its saturation temperature at the given inlet pressure. This is because it has been observed that EcosimPro does not function properly with subcooled conditions.

Therefore, the new boundary conditions are as follows:

- $p_{amb} = 1$ bar; $T_{amb} = 298.15$ K
- $p_{in} = p_{tank}$; $T_{in,fl} = T_{sat,fl} - 2$ K$= T_{sub,fl}$
- All valves completely open: $Stroke_{MPV} = Stroke_{MDV} = Stroke_{BHDV} = 1$

These conditions form the new baseline for the analysis.

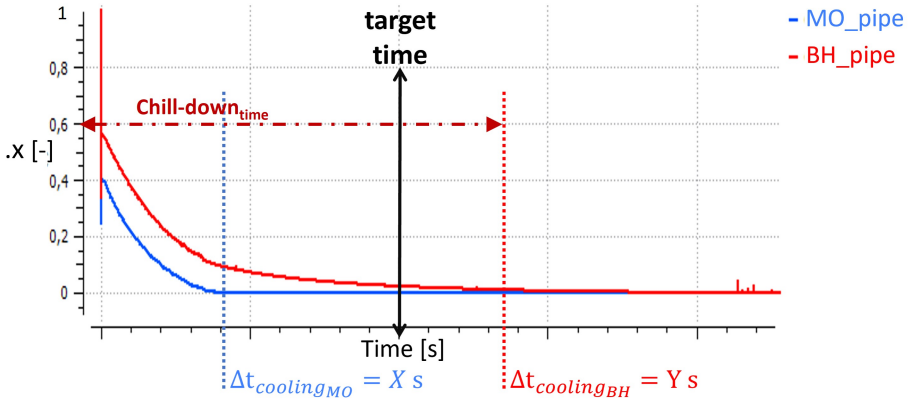

Figure 5.5. Quality factor .x history for Main Oxidizer pipe and Bearing Housing pipe, subcooled conditions.

Based on the results obtained, it is possible to evaluate $\Delta t_{cooling}$ for both transfer lines (fig. 5.5). Specifically, the chill-down time for the main oxidizer feed line is calculated to be $\Delta t_{cooling_{MO}} = X$ s, while the chill-down time for the bearing housing feed line is calculated to be $\Delta t_{cooling_{BH}} = Y$ s, with $Y = 3.18X$. Although the transfer line for the bearing housing undergoes chill-down, it requires a significantly longer time compared to the main transfer line. This is due to the larger pipes diameter of the main feed line, which allows for a higher mass flow rate and more efficient heat exchanges.
Having a different $\Delta t_{cooling}$ between the two transfer lines can negatively impact the performance of the propulsion system. This is because even after reaching a steady liquid state in the main feed line, oxidizer injection must continue in both lines to achieve chill-down also in the bearing compartment. This results in a significant amount of propellant loss, due to the much larger pipes in the main feed line, leading to an increase in propellant consumption.
Moreover, apart from the longer chill-down time for the bearing transfer line, the results also indicate that the required time for achieving chill-down exceeds the 35 % target time requirement (without considering that EcosimPro already underestimates chill-down times when simulates with liquid oxygen, whereas in chapter 4 it was observed that the software overestimates chill-down times for tests with liquid argon LAr and liquid nitrogen LN_2). This is not an ideal situation since it leads to additional propellant consumption and reduces engine performance. Therefore, it is crucial to optimize the transfer line design to achieve chill-down for both transfer lines at the same time, and to match the target time requirement.

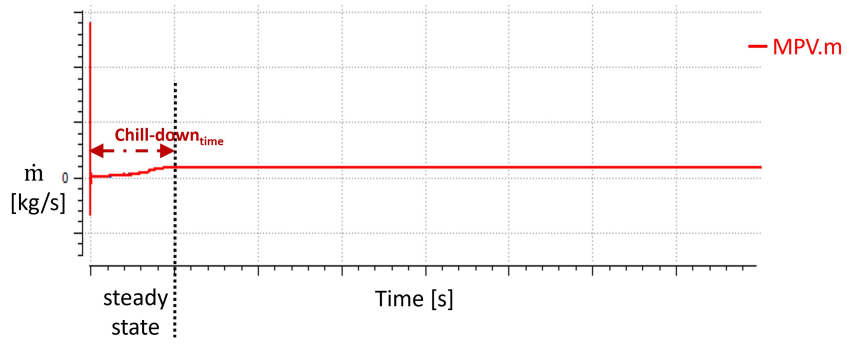

Figure 5.6. Mass flow rate $\dot{m}$ history for Main Propellant Valve, subcooled conditions.

From the graph in Figure 5.6, it is possible to determine the propellant consumption, which is the mass flow that flows through the MPV from the beginning of the cooling process up to the point of steady state achievement:

$$m_{consumption} = C \text{ kg}$$

To evaluate $\Delta t_{cooling}$ has been considered the quality factor $.x$ over time and not the wall and fluid temperatures history, $T_{wall} = f(t)$ or $T_{fluid} = f(t)$.
The quality factor over time is a more appropriate parameter to use for evaluating the chill-down time in this case because the temperature graphs (fig. 5.7) do not reach steady-state conditions and therefore do not accurately reflect the chill-down process. This is because given the nature of EcosimPro as a lumped parameter model, the analysis of quality .x, which derives from an energy balance, is more suitable than temperature, which is affected by the specific type of model used for the evaluation of h. Therefore, the EcosimPro model used for the heat transfer coefficient to simulate the thermal exchanges of the pipes is inaccurate.
Thus, the quality $.x$ provides a more accurate indication of the chill-down process and can be used to evaluate the time required to achieve the liquid state.

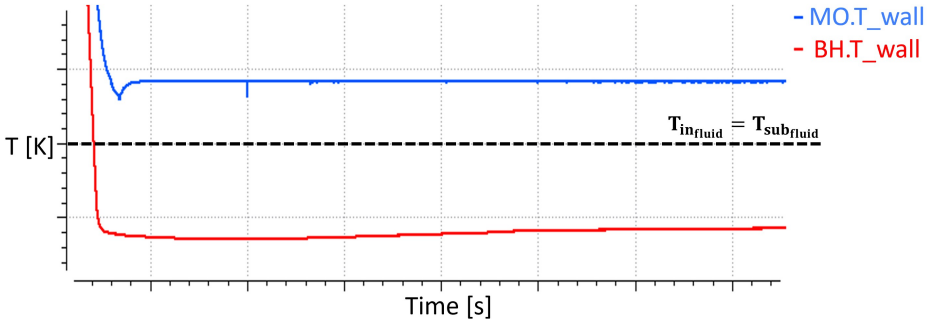

Figure 5.7. T_{wall} history for Main Oxidizer pipe and Bearing Housing pipe, non-steady state detail.

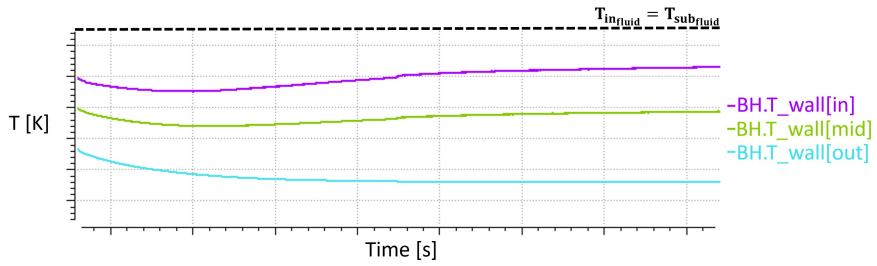

Figure 5.8. T_{wall} history for Bearing Housing pipe in three different sections (inlet, middle, outlet of the pipe), non-steady state detail.

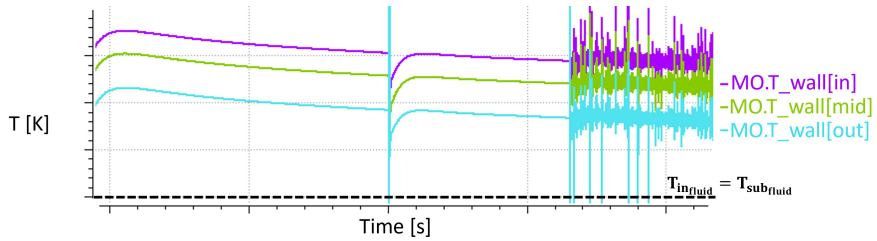

Figure 5.9. T_{wall} history for Main Oxidizer pipe in three different sections (inlet, middle, outlet of the pipe), non-steady state detail.

The plots in figures 5.8, 5.9 not only show the non-steady state condition but also the different temperature range of the walls for the MO feed line and BH feed line, both between the two lines and with respect to the inlet LO_2 temperature ($T_{in_{fl}} = T_{sub,fl}$). This is because the propellant transfer line is a complex system of tubes, valves, pipes, and other components, so there are other parts of the engine that wrap around the lines and heat them. This complex motor structure, with various components and systems surrounding the transfer lines, leads to heat transfer between the components and the transfer lines, resulting in different wall temperature ranges for the MO feed line and BH feed line (fig. 5.10).

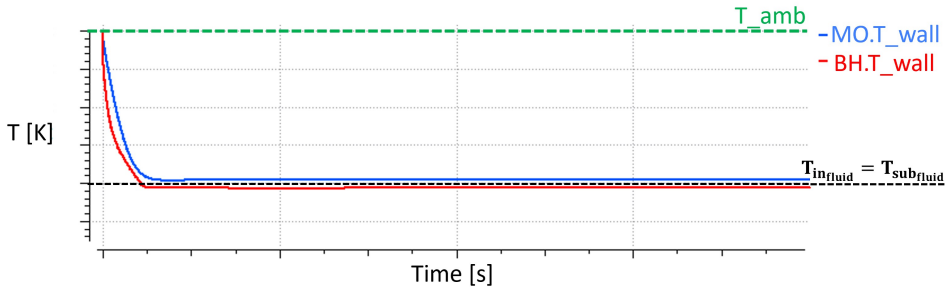

Figure 5.10. T_{wall} history for Main Oxidizer pipe and Bearing Housing pipe, different wall temperatures detail.

To confirm that the quality *.x* is a more convenient parameter to evaluate the chill-down process compared to temperature, it has been observed that the mass flow rate $\dot{m}_{MPV}$ graph reaches steady-state at the same time as the quality of BO_{pipe} reaches the final liquid steady-state, indicating that the entire oxidant transfer line has achieved chill-down. This suggests that using the quality .x parameter can provide a more accurate indication of the chill-down process than temperature.

Furthermore, the figure 5.10 demonstrates that when considering the temperature curves instead of the .x parameter to evaluate the process, the chill-down is achieved first for the BH feed line and then for the MO feed line. This is a significant error and inconsistency, as it is well-known that the Main feed line, characterized by larger pipes and lines, shall reach chill-down first followed by the Bearing Housing feed line, which consists of ducts approximately 42.5 times smaller than MO pipes in size.

From the baseline results, it was found that even with all valves completely open, the chill-down process could not be achieved within the target time. Therefore, the only variable that can be adjusted is the inlet fluid temperature $T_{in,fl}$, while keeping other boundary conditions fixed, such as the inlet driving pressure, environmental conditions, and the design and size of the oxidizer feeding system. Lowering the inlet fluid temperature, i.e., increasing the subcooling of the stored fluid, can reduce the chill-down time and achieve chill-down faster, but this ideal solution cannot be realized and simulated with the current version of pipe model, due to the limitations of the EcosimPro software in subcooling conditions, leading to inaccurate estimations. However this issue will have to be investigated when the new component will be developed.
Hence, it is accepted that achieving chill-down within the target time is currently neither feasible nor simulatable. However, it is possible to investigate the required modification in the transfer system design to achieve optimization on propellant consumption.
Thus the optimization will focus on the fraction of propellant consumption by finding the optimal configuration of valve strokes that provides the best balance between $\Delta t_{cooling}$ and $m_{consumption}$.

5.3 Open loop optimization of *full flush flow* chill-down technique

After establishing the baseline for the analysis, the objective is to optimize the chill-down process using the *full flush flow* technique with an open loop approach. The aim is to achieve chill-down almost simultaneously for both the lines, MO_{line} and BO_{line}, to reduce propellant loss, while keeping chill-down times not too long (although they will still be beyond the target time[1]).

[1]It will be possible to return to the correct target time by appropriately choosing the subcooling level of fluid.

Given the fixed boundary conditions, pipe sizing, and inlet subcooling temperature, the parameters to adjust are the strokes of the discharge valves, namely $Stroke_{MDV}$ and $Stroke_{BHDV}$ ($Stroke_{MPV}$ remains fixed at 1 since the chill-down method is *full flush flow*). To reduce propellant consumption, the chill-down of the MO feed line, where a large mass flow rate continuously flows, needs to be delayed to match its $\Delta t_{cooling}$ with that of the BH feed line. Different combinations of $Stroke_{MODV}$ and $Stroke_{BHDV}$ have been tested and simulated in EcosimPro.
The results obtained in terms of $\Delta t_{cooling}$ and $m_{consumption}$ have been summarized in Figure 5.11.

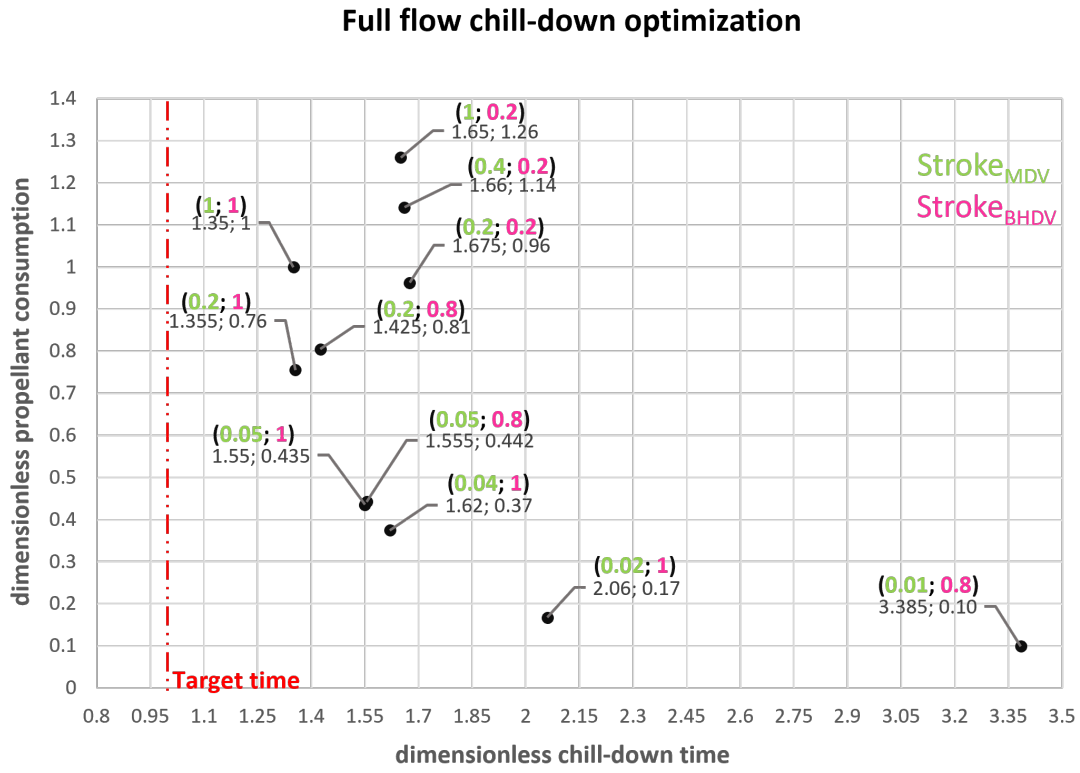

Figure 5.11. Dimensionless $\Delta t_{cooling}$ and $m_{consumption}$ required by $Stroke_{MODV}$ and $Stroke_{BHDV}$ combinations.

The dimensionless graph in figure 5.11 presents the required propellant consumption and chill-down time for different combinations of strokes valves, where the chill-down time is normalized to the target time and the consumption is normalized to $m_{consumption}$ of the baseline configuration ($Stroke_{MDV} = 1$; $Stroke_{BHDV} = 1$).

The optimal configuration, shown in figure 5.12, achieves the best compromise between a reasonable chill-down time and reduced propellant consumption. This configuration uses strokes valves (0.02;1), reducing the mass flow rate through MO_{pipe} and maintaining full mass flow rate through BH_{pipe}. This configuration results in an 83 % reduction in consumption compared to the baseline, with a chill-down time approximately twice the target time:

$$m_{consumption} = 0.17 \cdot m_{consumption_{baseline}} \; ; \; \Delta t_{cooling} = 2.06 \cdot \Delta t_{target_{time}}$$

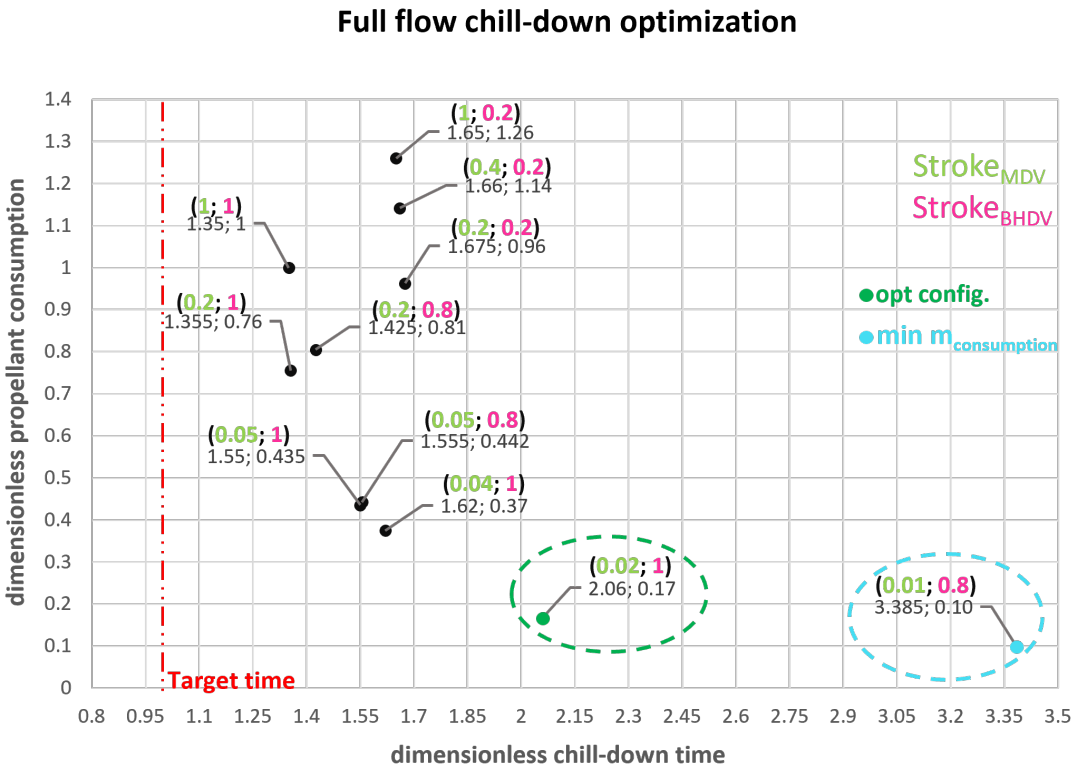

Figure 5.12. Dimensionless $\Delta t_{cooling}$ and $m_{consumption}$ required by strokes valves combinations, focus on the optimal configuration and minimum $m_{consumption}$ configuration.

Figure 5.12 also displays the configuration with the minimum $m_{consumption}$, which requires the couple of strokes valves (0.01; 0.8). This combination of values significantly reduces the consumption loss by 90 % compared to the baseline configuration, but it leads to a very long $\Delta t_{cooling}$, almost three and a half times the target time, and thus hardly reducible within the limits of the target time by only subcooling the propellant:

$$m_{consumption} = 0.10 \cdot m_{consumption_{baseline}} \; ; \; \Delta t_{cooling} = 3.385 \cdot \Delta t_{target_{time}}$$

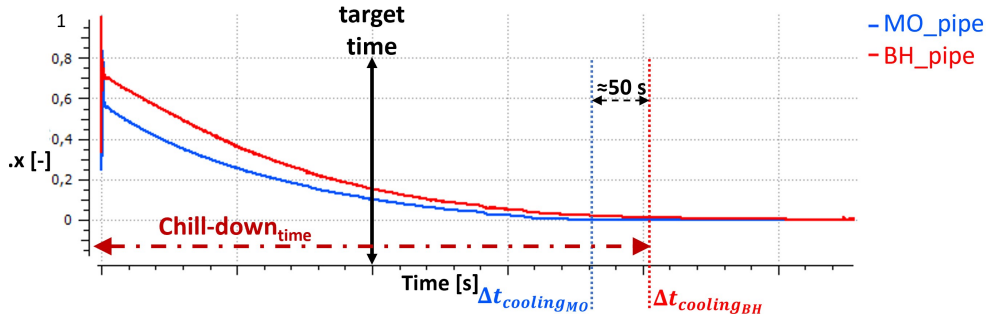

Figure 5.13. Quality factor .x history for MO pipe and BH pipe, optimal configuration.

The figure 5.13 shows the $.x$ parameter over time for the MO feed line and BH feed line for the chosen optimal strokes valves configuration. Compared to the baseline configuration (fig. 5.5), the chill-down process of MO_{pipe} has been delayed to match its $\Delta t_{cooling}$ with that of BH_{pipe} and reduce the propellant loss. There is a difference of almost 50 seconds in $\Delta t_{cooling}$ between the two feed lines.
The chill-down time of the entire LO_2 transfer line system coincides with $\Delta t_{cooling_{BH}}$.

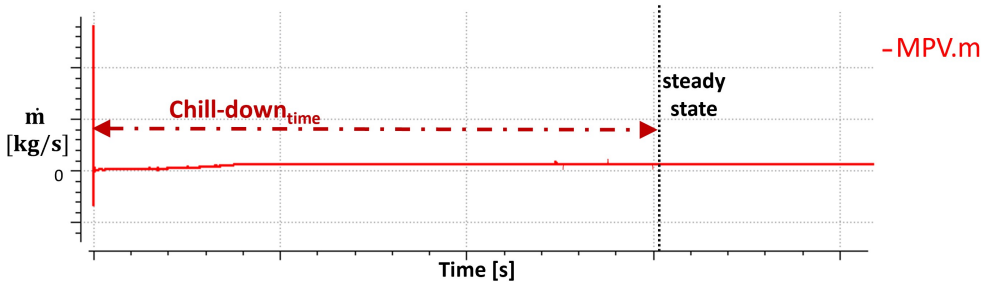

Figure 5.14. Mass flow rate $\dot{m}$ history for MPV, optimal configuration.

The figure 5.15 shows the evolution of quality $.x$ over time for MO and BH feed lines in the minimum consumption configuration (strokes valves [0.01;0.8]). As previously stated, this configuration requires almost three and a half times the target chill-down time, resulting in a longer duration of the process.

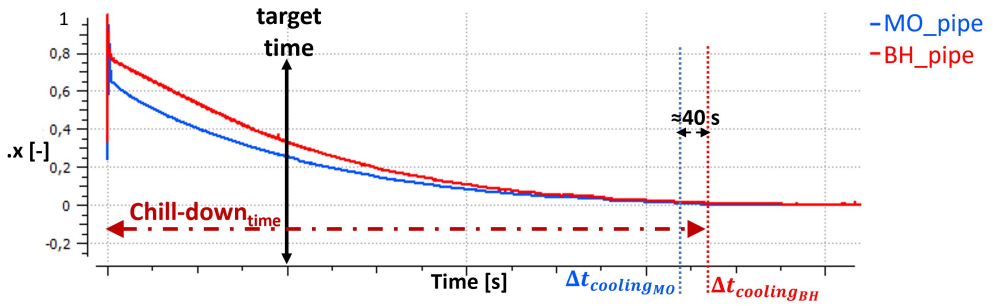

Figure 5.15. Quality factor .x history for MO pipe and BH pipe, minimum $m_{consumption}$ configuration.

The figure 5.16 shows the mass flow rate variation of the MPV up to the steady state. This configuration allows for a significant reduction in propellant consumption (90 % less than the baseline configuration), but it leads to a very long chill-down time.

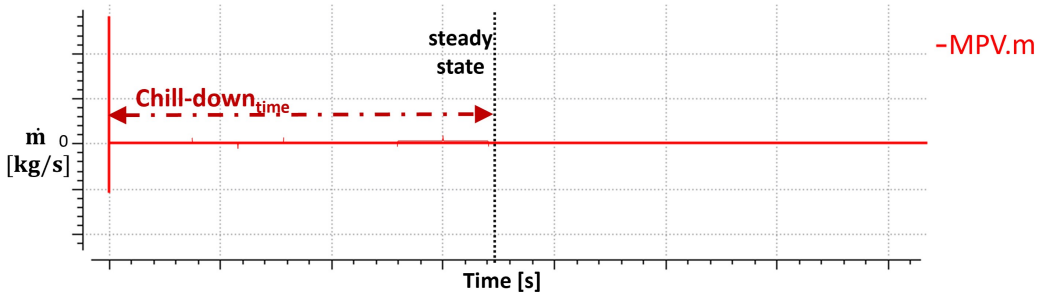

Figure 5.16. Mass flow rate $\dot{m}$ history for MPV, minimum $m_{consumption}$ configuration.

Chapter 6

Closed loop optimization of *full flush flow* chill-down technique for the cryogenic LOx transfer line

In this new chapter of the thesis, the main objective is to optimize the chill-down process of the cryogenic LO_x transfer line using a closed loop approach in EcosimPro. The traditional open loop approach results in the loss of the propellant used for the chill-down process, which is vented towards the environment. However, in a closed loop approach, the mass flow injected through the feeding lines is re-entered into the circuit and re-used for a specific purpose, instead of being vented and lost. This approach is necessary when there are strict requirements on the mass budget, as the mass flow employed for chill-down and engine operation decreases the payload that can be inserted into orbit. It is also preferred for performance reasons, as it is desirable to use the stored propellant in the tank for producing thrust instead of cooling the transfer lines. Additionally, the closed loop approach, if it has been well designed, is desirable for economic reasons as it reduces the costs, weight, and complexity associated with increasing the total required $\dot{m}$.

6.1 Closed loop optimization of *full flush flow* chill-down technique

The proposed approach involves reusing and recirculating the propellant downstream of the MO transfer line by employing it as pressurizing gas for the cryogenic propellant storage tank, instead of venting it into the environment. The Bearing Housing continues to discharge into environment.

However, since the fluid used for chill-down downstream of the MO pipes exists in a biphasic state, as a mixture of liquid and vapor phase, it needs to be converted into a monophasic flow of only vapor state before it can be used as pressurizing gas. To achieve this, the biphasic flow is collected downstream of the main line in a collection tank and is forced to flow through a heater that raises its temperature and pressure levels, converting it into all gas and allowing it to go back upstream into the circuit. The heater, collection tank, and required power have been carefully sized to ensure the complete vaporization of the mass flow, bringing it to its saturation point at the local pressure downstream of the line. This allows it to be recirculated back into the circuit by increasing the pressure level necessary to overcome the pressure drop along the circuit. To prevent any back-streaming of the propellant, non-return valves have been added to the EcosimPro closed loop model, including a $Valve_{NRV_1}$ located upstream of the collection tank and heater to impede the propellant from flowing in the opposite direction and heating the MO pipes instead of cooling them.

The chill-down method used in the process is always a *full flush flow*, which means that the stroke of the main propellant valve ($Stroke_{MPV}$) is set to 1.

6.1.1 Closed loop chill-down of MO feed line

The simplified schematic that shows the closed loop chill-down idea of MO feed line is represented in the following figure:

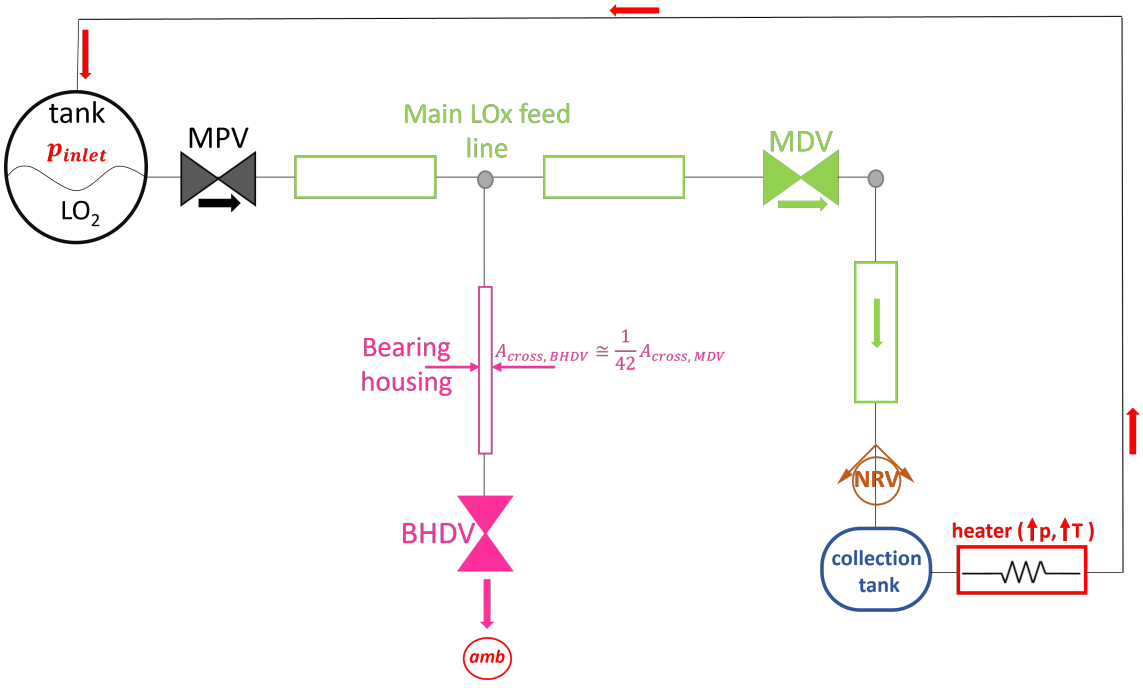

Figure 6.1. Simplified schematic of closed loop chill-down of Main Oxidizer transfer line.

In essence, as previously explained, while the BH feed line continues to vent into the environment and lose its fraction of injected propellant, the propellant used in the MO feed line is collected in a dedicated tank. It is then vaporized and pressurized by a heater that is correctly sized in terms of required power. A Non Return Valve has been added in the schematic upstream of the heater to prevent back-stream of the flux.
The fluid pressure level ensured by the heater outlet is exactly the same as the inlet fluid driving pressure, adding it to the pressure drop of the fluid along the path from the outlet of the heater to the return in the storage tank:

$$p_{fl_{out,heater}} = p_{in} + \Delta p_{loss}$$

However, the analysis of the closed loop proposal shows two significant issues in Ecosim-Pro.

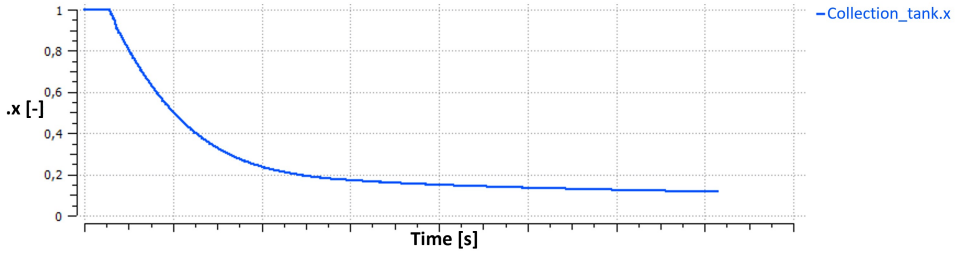

Figure 6.2. Quality factor .x history of the collection tank during a closed loop chill-down simulation.

The first one is that from the graph in figure 6.2, it turns out that the collection tank begins the chill-down instead of the MO pipes. This is because the mass flux flows in the opposite direction, meaning it turns in reverse, from the tank to the heater, through the recirculation circuit (red path in fig. 6.4). This happens because Ecosimpro does not consider the effect of gravitational acceleration in the pressure contribution:

$$p_{tot} = p_{in,fl} = p_{static} + \tfrac{1}{2}\rho \cdot v^2 + \cancel{\rho \cdot g \cdot h}$$

This is what really happens in microgravity conditions (remember that the engine must perform several re-ignitions, therefore as many chill-down processes even in $0 - g$ conditions).
Therefore, both in the software and in the physical reality of the phenomenon, there are two possible paths completely equal for the fluid in which it can flow, the MO (green) path and the recirculation (red) path. The stored propellant flows where less energy content is required, meaning where the fluid encounters less hydraulic resistance. Instead of cooling the MO transfer line, the propellant flows through the red path, characterized by less structural complexity of lines and pipes.

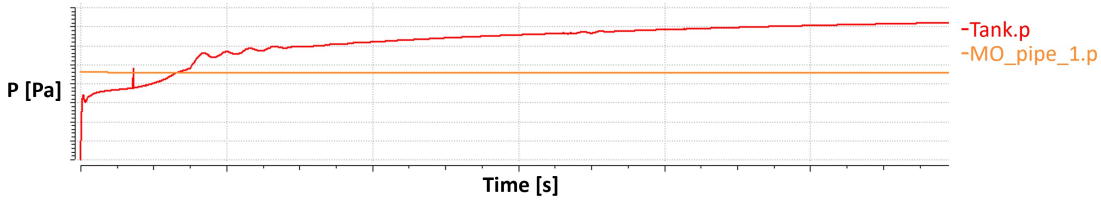

Figure 6.3. Pressure level over time during a closed loop chill-down for storage tank and $MO_{pipe,1}$.

The second significant issue that has been evidenced by the software is that after a few seconds of the beginning of the simulation, the pressure level in the first pipe of MO_{line} overcomes the pressure p_{in} in the propellant tank, i.e., $p_{MO_{pipe_1}} > p_{in}$ (fig. 6.3). This is translated into a back-flow that goes again into the storage tank. Before the process and the propellant injection begin, the pipes are all in conditions of $p_{amb} = 1$ bar, and the tank is pressurized to the p_{in} level, so $p_{tank} = p_{in} > p_{MO_{pipe_1}}$, and the mass flow rate flows in the correct direction. Right after the oxidizer injection begins, the tank loses pressure (because there is the propellant that flows in the pipes), and the pipes downstream of the tank increase their pressure level because there is $\dot{m}$ that flows inside them. This is translated into a back-stream of the flux.

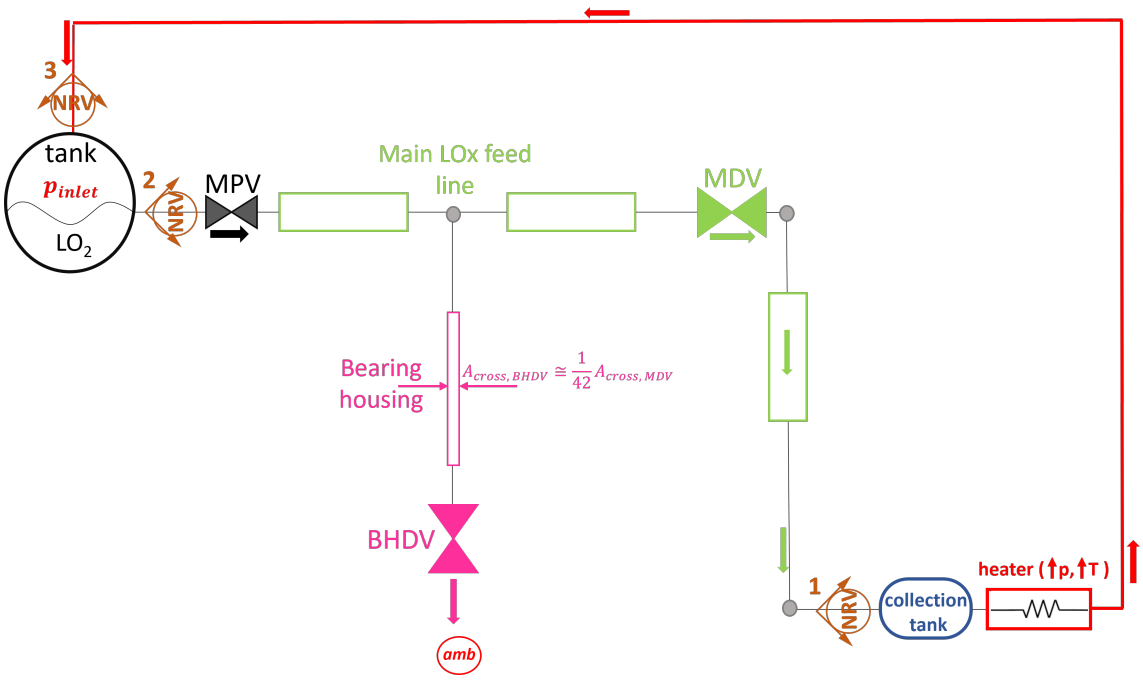

Figure 6.4. Simplified schematic of closed loop chill-down of Main Oxidizer transfer line, addition of NRVs.

The solutions adopted for these two problems are the addition of different check-valves (NRVs) in the EcosimPro model of the transfer system (fig. 6.4). In particular, NRV_3 is added to prevent the propellant from flowing clockwise along the recirculation path, while NRV_2 is added to prevent the propellant from flowing back to the tank. Additionally, NRV_1 is installed to prevent the monophasic flux downstream of the heater from flowing back.

The results of the simulation with the new closed loop chill-down configuration reveal that the BH feed line experiences chill-down before the MO feed line, which is unrealistic given that the main pipes are larger than the BH pipes.

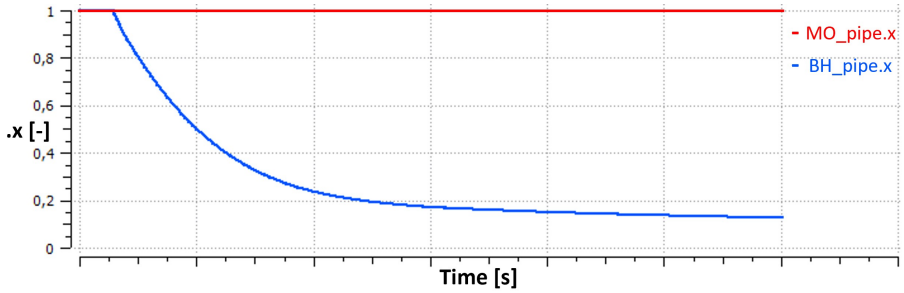

Figure 6.5. Quality factor .x history for MO and BH pipes, closed loop configuration with NRVs.

This occurrence is attributed to the fact that the propellant tends to flow in the BH_{pipes} rather than the MO_{pipes} due to a higher pressure drop Δp between the upstream and downstream of the BH feed line, as it discharges its mass flux in the environment. Consequently, it is essential to develop and design a closed loop chill-down model for both the MO and BH transfer lines.

6.1.2 Closed loop chill-down of both MO and BH feed lines

In this paragraph, the goal is to implement a complete closed loop chill-down process for the entire cryogenic LO_x transfer line. The schematic used for simulating this process in EcosimPro is displayed in the figures 6.6 and 6.7.

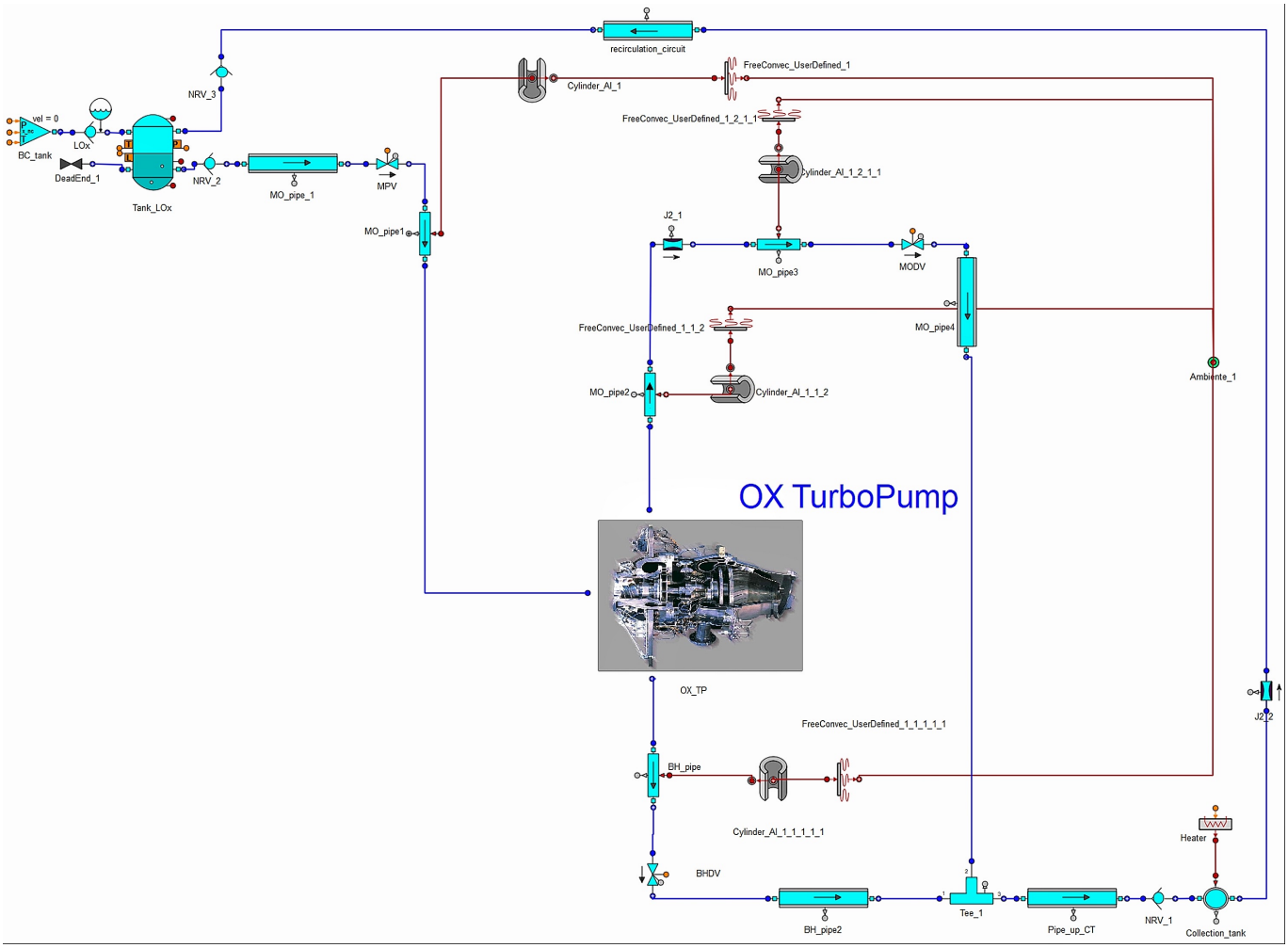

Figure 6.6. EcosimPro schematic model of Cryogenic LOx transfer line, closed loop chill-down design.

With this new configuration, both the mass flow rate through the MO feed line and the BH pipes are recirculated using a collection tank with a heater and NRVs to prevent any flux returns. After setting the boundary conditions for the inlet pressure, initial ambient conditions, inlet fluid temperature, fully open valve strokes ($Stroke_{MPV} = Stroke_{MODV} = Stroke_{BHDV} = 1$), and the required heater power, the simulation results are shown in the figures below.

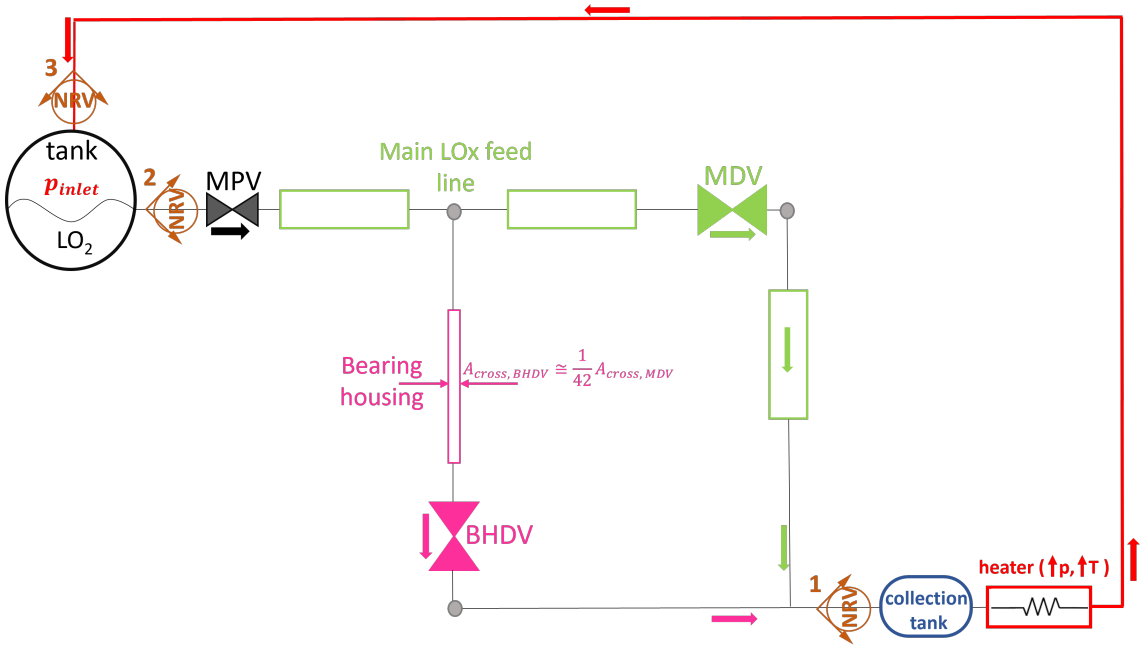

Figure 6.7. Simplified schematic of closed loop chill-down of both Main Oxidizer and Bearing Housing transfer lines, addition of NRVs.

First of all, the results show that initially, only the MO feed line undergoes the chill-down process, as seen in the graph of figure 6.8. This is due to the insufficient mass flow rate in the BH_{pipes}, as depicted in figure 6.9. In order to ensure the cooling of the BH pipes, the stroke of the MPDV should be reduced to force the flow to pass through the bearing housing, even though this will result in a further increase in chill-down times, which are already too long for a closed-loop approach.

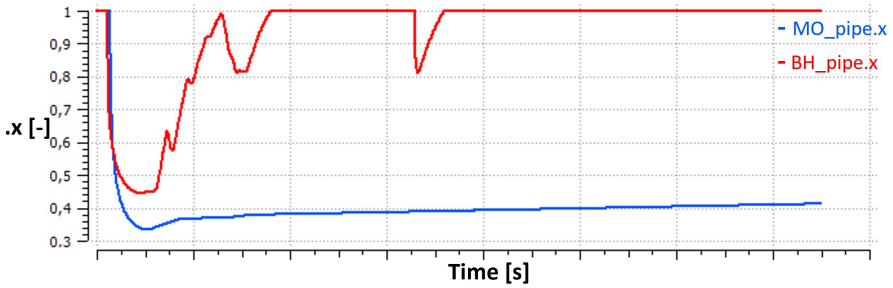

Figure 6.8. Quality factor .x history of both MO and BH feed lines.

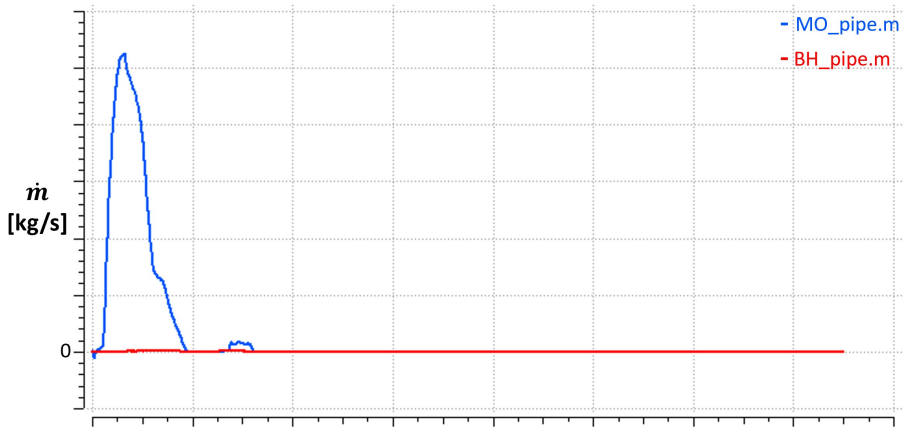

Figure 6.9. Mass flow rate $\dot{m}$ over time for MO and BH feed lines.

The simulation results show that this closed loop design cannot achieve the complete chill-down process for both MO and BH feed lines. At the initial instant $t = t_0$, $p_{tank} = p_{in} > p_{MO_{pipe_1}}$, causing the cryogenic fluid to enter the circuit pipes. However, after a short time from the injection start, the tank loses pressure, and the downstream pipes increase their pressure level (figures 6.10 and 6.11) due to the certain $\dot{m}$ flowing through the MPV. As a result, $p_{in} < p_{MO_{pipe_1}}$, causing the check valve NRV_2 to close and subsequently the MPV. Thereafter, there is no more propellant mass flowing in the fluidic lines. The graphs in figures 6.12 and 6.13 show that, with that quantity of $\dot{m}$ which initially enters in the lines, the heater is unable to re-pressurize the tank sufficiently to enable NRV_2 to reopen, which is necessary to ensure the re-opening of the main valve of propellant MPV, through which the propellant flows. A check valve opens when:

$$p_{upstream} > p_{downstream}$$

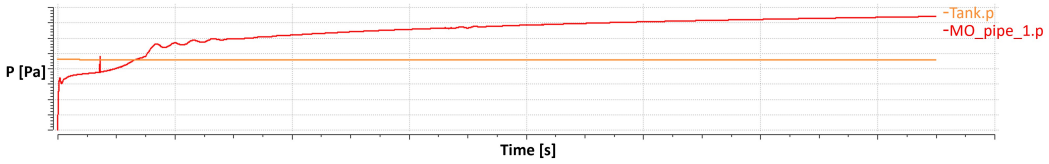

Figure 6.10. Pressure level over time for LO_2 tank and MO_{pipe_1}.

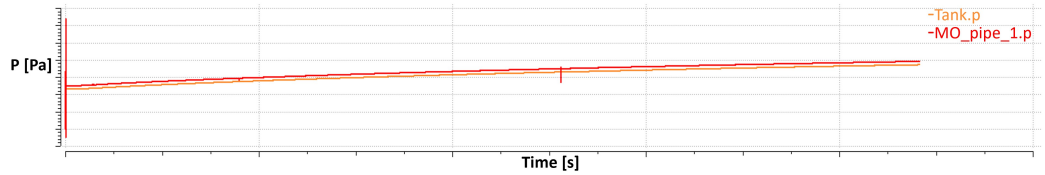

Figure 6.11. Pressure level over time for LO_2 tank and MO_{pipe_1}.

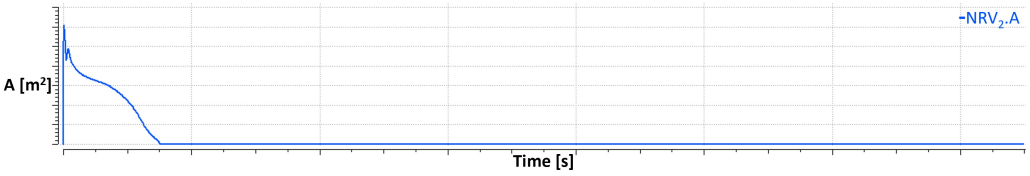

Figure 6.12. Opening area over time of NRV_2.

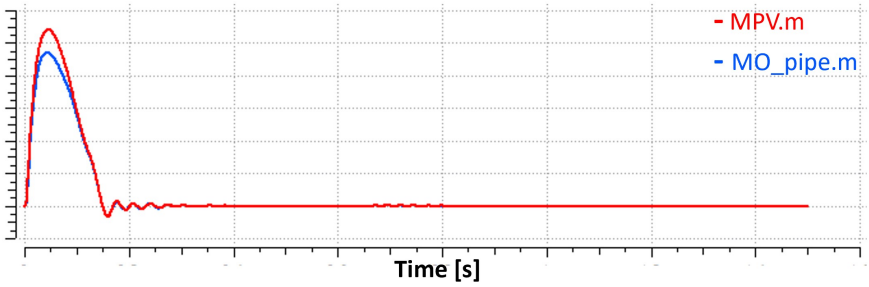

Figure 6.13. Mass flow rate $\dot{m}$ over time for MPV tank and MO_{pipe_1}.

Based on the simulation results, it appears that the current closed loop approach using a collection tank and heater is not sufficient to achieve the desired chill-down process for both the MO and BH transfer lines. The issue is that the tank loses pressure quickly, and the heater is not able to re-pressurize the tank enough to allow the check valve NRV_2 to reopen and continue the flow of propellant through the system.

One potential solution to this issue is to add an electric pump downstream of the heater to pressurize the vapor flux and bring it to a higher pressure level than that of the pipes, which would allow for the reopening of the main valve of the propellant MPV.

$$p_{tank} > p_{MO_{pipe_1}} \rightarrow \text{MPV, } NRV_2 \text{ open}$$

However, this solution may be too expensive, complex, and heavy when considering the benefits of propellant savings and mass budget reduction.

Another feasible option is to implement a partial closed loop system, acknowledging that not all of the propellant injected into the lines can be recovered. In this solution, the previous closed loop method with heater is combined with appropriate venting phases. Orifices are strategically placed along the fluid path to expel a certain amount of propellant into the environment every t seconds. This is done to maintain a tank pressure level of $p_{tank} = p_{in} > p_{MO_{pipe_1}}$, prevent flow stall in the lines, and allow the transfer line to be reopened. A semi-pulsed semi-closed loop chill-down strategy is performed.
However, implementing this solution in EcosimPro may not be possible due to software convergence issues with the check-valves, which would require excessively long computational times.

Therefore, it may be necessary to explore alternative approaches to achieve the desired chill-down process for both the MO and BH transfer lines while balancing the cost and complexity of the system with the benefits of propellant savings and mass budget reduction.

6.1.3 Closed loop chill-down with electric pump

The final proposed solution for achieving closed loop chill-down is shown in the following EcosimPro schematic.

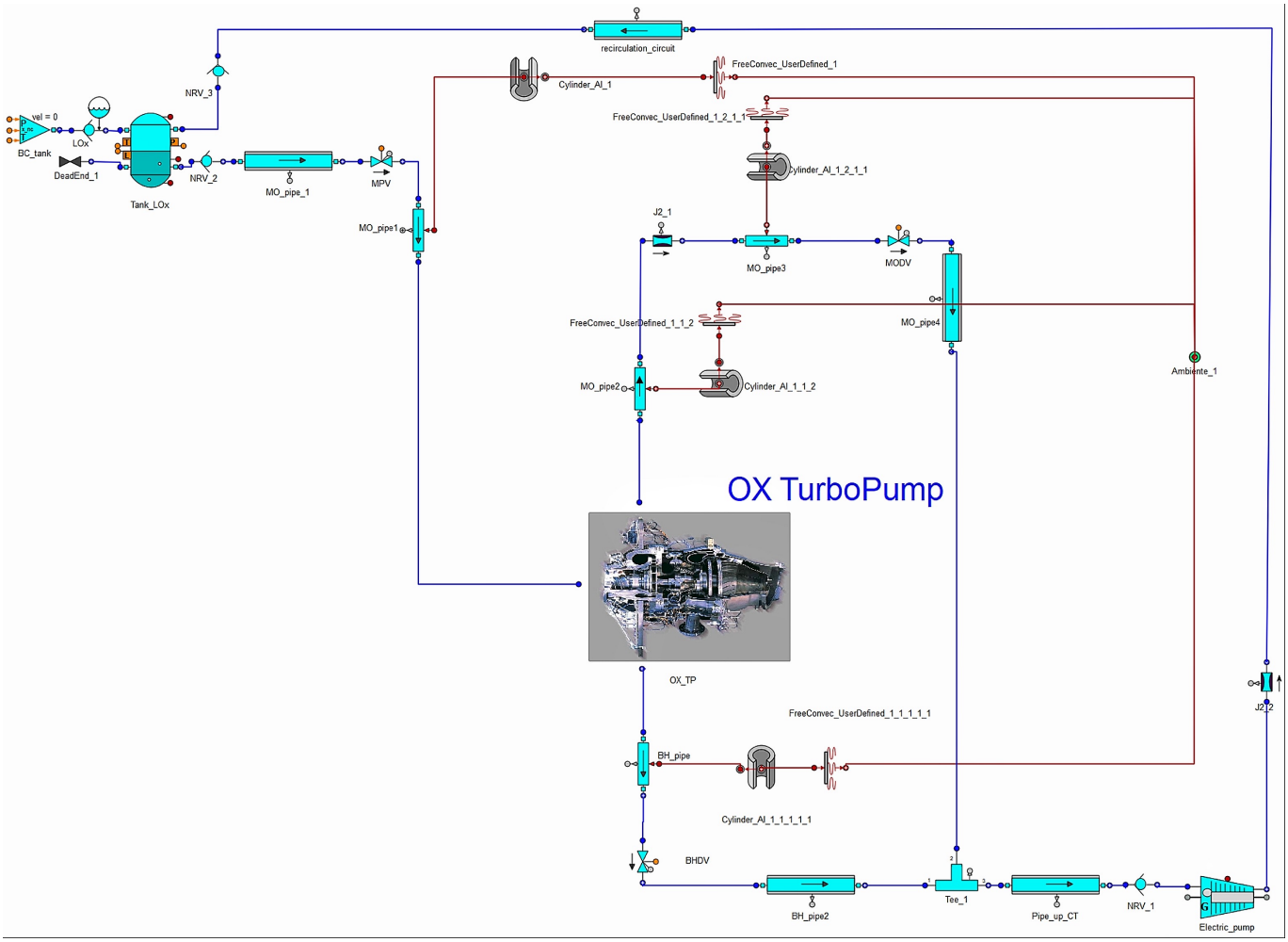

Figure 6.14. EcosimPro schematic model of Cryogenic LOx transfer line, closed loop chill-down design with Electric Pump.

The original approach using a heater with a collection tank has been replaced, because too heavy and redundant, with a new model using only an electric pump, which will work with biphasic flow.
The compression ratio β required by the pump has been estimated to pressurize the flux downstream of the entire circuit without exceeding the tank's pressure limit.

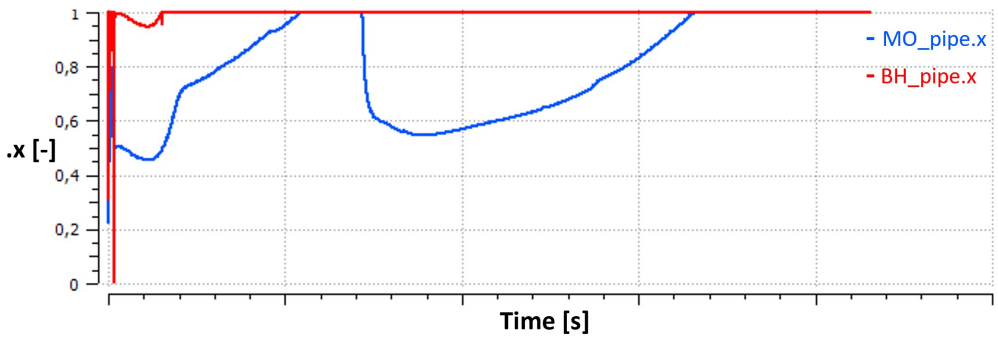

Figure 6.15. Quality factor .x over time for MO and BH pipes.

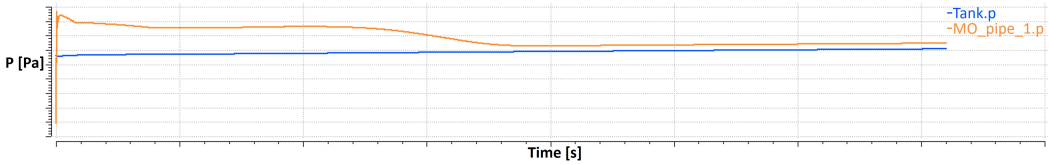

Figure 6.16. Pressure level over time for LO_2 tank and MO_{pipe_1}.

However, simulation results indicate that this new approach cannot achieve chill-down with only the EP, as the issue of $p_{tank} < p_{MO_{pipe_1}}$ still exists (as seen in fig. 6.16). Additionally, the BH transfer line does not undergo chill-down, so the MPDV stroke needs to be reduced (fig. 6.15).

To solve the issue of p_{in} being at a lower pressure level in $MO_{pipe,1}$ and allowing the propellant flux to flow inside both MO and BH lines, a pump with a compression ratio β too high would be needed, which could burst the storage tank. Oversizing the propellant tank could be a solution, but this would result in increased weight and complexity, nullifying the advantage of propellant recovery.

However, this alternative solution will not be considered as the engine design, including the propellant tanks sizing, has already been determined by the Vega E project of Avio S.p.A.. Therefore, a new feasible approach must be devised and implemented. But this requires time, not available within the end of this thesis project, and advanced and updated simulation tools, such as a new pipe model in EcosimPro, to accurately simulate the chill-down process, including subcooled conditions of cryogenic fluids.

Chapter 7

Conclusions & Future Work

This experimental thesis was conducted at Avio S.p.A. Company, with the aim of analyzing and optimizing chill-down processes in cryogenic liquid propellant rocket engines, employing the EcosimPro simulation tool with the ESPSS library.

Physical phenomena involved in chill-down processes are detailed, highlighting requirements to be fulfilled to ensure correct propulsion subsystem operation. In particular, proper operation of the turbopumps, ignition, and pumps cavitation avoidance are discussed.
Moreover, the behavior of cryogenic fluids in propellant transfer lines during chill-down, as well as the parameters that most influence it (such as inlet driving pressure, gravity or microgravity conditions, injected mass flow rate etc.), and possible chill-down techniques are deeply investigated.

A preliminary trade-off is conducted to select suitable methodologies for application on VEGA-E upper stage, which resulted in the identification of three possible techniques: Full Flush Flow, Trickle Flow, and Pulsed method. This is achieved with the help of the creation of a decision matrix.

Then, several experimental test cases, available in literature, are reproduced and analyzed to validate and identify weakness points in EcosimPro components necessary to study chill-down processes. As outcome of validation process, strong numerical instability and unacceptable error budget is obtained as consequence of wrong subcooled and microgravity conditions simulation.
As consequence, the necessity to develop a new custom pipe component is justified.

The second part of the thesis is first devoted to analyzing and optimizing the full flush flow chill-down process with an open loop approach, and subsequently to designing closed loop chill-down circuits for the cryogenic oxidizer transfer line in both cases of the VEGA-E program.
In the first section of this second part, the objective was to achieve the chill-down of the entire LOx feed line within a certain target time, set by requirement, by identifying the

optimal circuit configuration with the lowest propellant consumption. Various possible configurations are examined, and software limitations are highlighted.

Subsequently, the possibility of totally or partially recovering the propellant employed for chill-down purposes is studied, considering the option to introduce heat-exchangers, non-return valves, catch tank and/or electrical pumps. All the architectures presented have shown that the application of these methods for the cryogenic oxidant transfer line of VEGA-E upper stage is not possible for several detailed reasons, such as too large power consumption, complexness, excessive oversizing of tanks etc.
Nevertheless, the study highlighted the possibility of designing a partial closed loop.

In conclusion, this thesis work has highlighted the need for the development of a new custom pipe in EcosimPro to accurately simulate phenomena involved during chill-down processes. This is essential to have realistic propellant consumption and accurate chill-down time estimations, so as to have a correct evaluation of the launcher mass budget and consequently payload that can be put into orbit.
Moreover, after analyzing possible design ideas, the thesis has proposed a viable solution for achieving a partially closed loop chill-down of cryogenic oxidant transfer line in the VEGA-E program.
Further research and development in this area will be necessary to effectively implement and actualize this idea, while also optimizing propellant consumption and reducing the overall system's costs.

Bibliography

Lingxue Jin, Hyokjin Cho, and Sangkwon Jeong. *Experimental investigation on line chill-down process by liquid argon*. Elsevier, 2019. doi: 10.1016/j.cryogenics.2018.11.003.

Lingxue Jin, Changgi Park, Hyokjin Cho, Cheonkyu Lee, and Sangkwon Jeong. *Experimental Investigation on Chill-down Process of Cryogenic Flow Line*. Cryogenics, 79: 96–105, 08 2016. doi: 10.1016/j.cryogenics.2016.08.006.

Gagan Agrawal, Deepak Agarwal, and S. Sunil Kumar. Mathematical modeling of cryogenic feedline chilldown process. Proceedings of the 22nd National and 11th International ISHMT-ASME Heat and Mass Transfer Conference December 28-31, 2013, IIT Kharagpur, India, 12 2014.

Kun Yuan, Yan Ji, and J.N.Chung. *Numerical modeling of cryogenic chill-down process in terrestrial gravity and microgravity*. International Journal of Heat and Fluid Flow, 2008.

J. A. Brennan, E. G. Brentari, R. V. Smith, and W. G. Steward. *An Experimental Report on COOLDOWN OF CRYOGENIC TRANSFER LINES to National Aeronautical and Space Administration*. 1966.

A.K.Shukla, Arunkumar Sridharan, and M.D. Atrey. *Investigation of transient chill-down phenomena in tubes using liquid nitrogen*. IOP Conference Series: Materials Science and Engineering, 278, 2017. doi: 10.1088/1757-899X/278/1/012035.

Lingxue Jin, Hyokjin Cho, Cheonkyu Lee, and Sangkwon Jeong. *Experimental research and numerical simulation on cryogenic line chill-down process*. Elsevier, 2017. doi: https://doi.org/10.1016/j.cryogenics.2017.11.003.

Enrique Ramé, Jason Hartwig, and John McQuillen. *Flow Visualization of Liquid Hydrogen Line Chill Down Tests*. 52nd Aerospace Sciences Meeting, 01 2014. doi: 10.2514/6.2014-1074.

Jelliffe Jackson, Jun Liao, James Klausner, and Renwei Mei. *Transient Heat Transfer During Cryogenic Chilldown*. Proceedings of the ASME Summer Heat Transfer Conference, 2, 01 2005. doi: 10.1115/HT2005-72145.

J. C. Burke, W. R. Byrnes, A. H. Post, and F. E. Ruccia. Pressurized cooldown of cryogenic transfer lines. In K. D. Timmerhaus, editor, Advances in Cryogenic Engineering, pages 378–394, Boston, MA, 1960. Springer US. ISBN 978-1-4757-0540-9.

Acknowledgements

Con l'avvicinarsi del termine di questa faticosa ma soddisfacente impresa, si addentra nel crepuscolo il mio cammino accademico, caratterizzato da un variegato mosaico di sfide e gioie che hanno arricchito e insaporito i miei anni di studio. A conclusione di questa tesi, che ha visto investito tutto il mio impegno e passione, desidero ringraziare chi ha avuto un ruolo cardine nella sua realizzazione.

Inizio con esprimere la mia più sincera gratitudine al Prof. Lorenzo Casalino per aver accettato di supervisionare il mio lavoro di tesi. È stato un grande onore e motivo di orgoglio per me poter lavorare con un tale esperto del settore, e sono profondamente grata per questa opportunità che mi ha concesso. Durante questi mesi, il Prof. Casalino ha condiviso con me la sua vasta conoscenza e il suo rigore critico, offrendomi preziosi consigli e insegnamenti che mi hanno permesso di portare a termine questo lavoro. Sono inoltre molto grata per il tempo, la pazienza e l'impegno che con estrema umiltà ha dedicato alla mia tesi. I suoi contributi sono stati fondamentali per il successo di questo progetto e per la mia crescita personale e professionale. Custodirò con cura i suoi consigli e insegnamenti nel mio bagaglio culturale e di vita, che mi seguirà ovunque il mio cammino mi porterà.

Desidero esprimere la mia profonda gratitudine a chi mi ha affiancato quotidianamente, supportato, spronato e anche rialzato dai miei momenti di sconforto e profondo stress durante tutto il percorso di questa tesi. In particolare, vorrei ringraziare il mio relatore aziendale, Riccardo Pellicanò, per aver creduto nelle mie capacità sin dall'inizio e per aver riposto in me fiducia nell'assegnarmi un progetto di notevole spessore che lo vedeva coinvolto in prima persona. Grazie per il tuo tempo, la tua dedizione e la tua passione nel fornirmi feedback costruttivi e preziosi per il miglioramento del mio lavoro e del mio profilo professionale. La tua esperienza, la tua energia e la tua competenza nel campo di studio mi hanno ispirato e mi hanno fatto sentire parte di una comunità aziendale stimolante e accogliente. Vorrei ringraziarti anche per la relazione sincera e autentica che abbiamo instaurato, che ha permesso di creare nel tempo un rapporto di amicizia che porterò nel cuore. Infine, ti sono immensamente grata per avermi dato l'opportunità di entrare a far parte della famiglia di Avio S.p.A., che è diventata la mia seconda casa e la mia famiglia lontano dalle radici. Grazie di cuore.

Desidero esprimere il mio commosso e autentico ringraziamento ai miei genitori, che sono il mio porto sicuro durante le tempeste della vita, la mia forza e la mia luce nei

momenti di difficoltà e la mia gioia nei successi raggiunti. I vostri occhi colmi di orgoglio per ogni mio traguardo conseguito, indipendentemente dalla sua grandezza, mi spingono a volgere lo sguardo sempre oltre e in alto. Siete stati costantemente presenti in ogni aspetto della mia vita, mostrando sempre un profondo interesse e un grande sostegno. Grazie per avermi dato ogni mezzo possibile per realizzare i miei obiettivi, sacrificandovi silenziosamente per alleggerire il mio carico, anche quando la distanza fisica sembrava insormontabile. Siete sempre ad un palmo dal mio cuore, in ogni città, continente, o pianeta.

Vorrei ringraziare di tutto cuore e manifestare la mia riconoscenza a mio fratello Felice. Tu sei da sempre il mio angelo custode, una guida affettuosa che mi protegge silenziosamente in ogni momento. La tua presenza si manifesta in mille sfumature diverse di amore e premura, e le attenzioni che mi dedichi mi arricchiscono l'anima e mi confortano il cuore. Ti ringrazio e ti ammiro in particolare per la tua pazienza nel sopportare il mio carattere burrascoso, per la tua calma nel gestire la mia altalena quotidiana di emozioni, per la tua diplomazia e serietà nell'affrontare la vita, motivo di profonda ispirazione per me. Ti stimo come poche persone nella vita, sei un esempio di fratello e uomo.

Desidero poi ringraziare la mia grande famiglia, il cuore pulsante della mia vita, il tesoro più prezioso che ho. Ogni giorno siete lo stimolo a non mollare mai e a tentare di andare sempre un passo oltre i miei limiti, conscia di avere la ricchezza più grande al mondo, la consapevolezza che se anche qualora cadessi, avrei comunque un materasso di salvataggio che mi attutirebbe la caduta in qualsiasi momento e luogo. Siete la mia possibilità di applicare il "reach for the stars" senza esitazioni, e di rischiare senza avere paura delle conseguenze, gioiose o amare che siano.

Vorrei inoltre ringraziare i miei colleghi universitari, in particolar modo Gianmaria, Davide e Matteo, per l'impegno, la collaborazione e la condivisione di idee che hanno dimostrato durante questi anni di studio. Il vostro sostegno e la vostra disponibilità sono stati fondamentali per raggiungere i miei e i nostri obiettivi accademici. Vi ringrazio per l'amicizia e il supporto che si è consolidato nel tempo, per aver condiviso le gioie e i dolori di questo intenso percorso.

Desidero poi esprimere la mia sincera gratitudine ai miei colleghi in Avio. Ringrazio tutti voi per avermi accolto sin dall'inizio, per la disponibilità e l'apertura che avete avuto nel permettermi di integrarmi facilmente col team. Vi sono grata per aver sempre considerato le mie opinioni e ricercato i miei consigli, nonostante la mia acerba esperienza lavorativa. Grazie per aver costruito intorno a me un ambiente di lavoro positivo e accogliente, dove ho avuto la possibilità di crescere non solo come professionista, ma anche come individuo. Siete il mio luogo felice fuori dalle mura di casa.

Ringrazio infine tutte le persone, sia amici che parenti, che sono state al mio fianco, fisicamente e non, con piccoli o grandi gesti, con attenzioni silenziose o dichiarate. Grazie per avermi sostenuto e aver accettato la mia personalità complessa, supportandomi anche nelle difficoltà, interiori ed esterne. Sappiate che vi tengo tutti nel mio cuore e apprezzo il vostro sostegno più di quanto possiate immaginare.

Infine, ringrazio me stessa,

per la determinazione, la tenacia e la forza di volontà,

i reali motori della mia vita.

"Space is for exploration, for curiosity, for wonder. It's not just for the science, it's for the spirit."- Naomi Kurahara